SELECTIVE RING OPENING OF NAPHTHENES PRESENT IN HEAVY GAS OIL DERIVED FROM ATHABASCA BITUMEN

A Thesis Submitted to the College of Graduate Studies and Research

In Partial Fulfillment of the Requirements for the

Degree of Doctor of Philosophy

In the Department of Chemical Engineering

University of Saskatchewan

Saskatoon

By

Chandra Mouli Kotikalapudi

COPYRIGHT

ABSTRACT

Removal of polynuclear aromatics from diesel fuel has become a focus of intense research due to the stringent environmental legislation associated with clean fuels. In this work, selective ring opening of model compound decalin over the set of catalysts comprising of 1) Ir-Pt supported on mesoporous Zr-MCM-41, large and medium pore zeolites like HY and H-Beta and 2) Ni-Mo/carbide on HY, H-Beta, Al-SBA-15, γ-alumina and silica alumina were studied. All the catalysts were extensively characterized by BET surface area measurement, CO-chemisorption, XRD, FTIR, TPR and TPD of ammonia. Ring opening of decalin was studied on these catalysts in a trickle-bed reactor in a temperature range of 200- 400 °C, pressure range of 2-7 MPa and LHSV of 1 to 3 h^{-1}. 31.7 and 65.0 wt.% of RO yield and selectivity were observed on Ir-Pt/HY catalyst at 220 °C, whereas 34.0 and 40.0 wt.% of ring opening yield and selectivity were observed on Ni-Mo carbide/HY catalyst at 240 °C. From the model compound studies, Ir-Pt/HY, Ni-Mo carbide/HY and Ni-Mo carbide/H-Beta were selected for study of hydrotreated light gas oil in a trickle bed reactor. Ni-Mo carbide/HY performed better over other catalysts and increased the cetane index of hydrotreated light gas oil by 12 units at 325 °C. A first order kinetic model was fitted for the hydrotreated light gas oil study. 89, 111 and 42 KJ/gmol of activation energies was observed for dearomatization, aromatization and naphthenes cracking steps, respectively. The thermodynamic equilibrium calculations reveal that the selectivity of ring opening products of decalin can be maximized by favoring the formation of unsaturated compounds at higher operating temperatures. Energetics of dealkylation and ring opening reactions of naphthenes in gas phase and on

the surface of Brønsted acid sites were calculated using quantum chemical simulations. In gas phase, ratio of Arrhenius activation energies for forward and reverse reactions of RO and dealkylation reactions are 1.92 and 1.82 respectively. Deakylation on different level clusters revealed that surface reaction is the rate controlling.

ACKNOWLEDGEMENT

I would like to take this opportunity to express my profound gratitude to my supervisors, Dr. Ajay Kumar Dalai and Dr. Zbigniew Ring for their immense contributions, support and guidance throughout my Ph.D program. Special thanks also go to Dr. Jagannathan Govindakhannan and Dr. Sundaramurthy Vedachalam for their valuable suggestions and help: they were ever ready to give me a helping hand whenever I was faced with a difficult problem. My appreciation also goes to the members of my committee: Dr. Ding-Yu Peng, Dr. Mehdi Nemati, Dr. Gordon Hill and Dr. Stephen Foley for their directions, contributions and precious time. I would also like to thank Dr. Aaron Phoenix for valuable suggestions regarding thermodynamics. Technical assistances from Mr. T. B. Wellentiny, Mr. Richard Blondin and Mr. Dragan Cekvic are also highly acknowledged. Financial assistances from national centre for upgrading technology (NCUT), University of Saskatchewan are gratefully acknowledged. I would like to also thank the people working in Catalysis and Chemical Reaction Engineering Laboratory for their support.

DEDICATION

This work is dedicated to my wife Lakshmi, my daughter Srindhi, my parents Sreeramamurthy and Padmavathi, and all my family members.

TABLE OF CONTENTS **Page #**

LIST OF FIGURES **Page #**

LIST OF TABLES **Page#**

NOMENCLATURE

n_i	Mole number of the chemical species i
A_k	Total number of atoms of element k
N_E	Total number of elements
λ_k	Lagrangian multipliers for each element k
a_{ik}	Number of atoms with respect to species i and element k
n_C	Number of center points
F	Number of factors
$\Delta H_f{}^0$	Standard enthalpy change of formation (kcal/mol)
$\Delta S_f{}^0$	Standard entropy change of formation (kcal/mol-K)
$\Delta G^0{}_{f_i}$	Standard Gibbs free energy change of formation (kcal/mol)
G^t	Total Gibbs free energy (kcal/mol)
A_k	Total number of atoms of element k from initial composition
N_S	Total number of chemical species
N_E	Total number of elements
N'	Total number of experimental runs
c^0	Concentration ($kmol/m^3$)
C_{Ab}	Bulk concentration ($kmol/m^3$)
C_{As}	Concentration of A at the catalyst surface (mol/m^3)
C_m	Ratio of reaction rate to the external diffusion rate
C_{WP}	Weisz-Prater parameter

D	Density at 15°C (g/mL)
D_{AB}	Bulk or Knudsen diffusivity of *A* in *B*
D_e	Effective diffusivity (m^2/s)
d_p	Diameter of the catalyst particle (m)
F_{calc}	Model predicted values
F_{exp}	Experimental values
h	Planck's constant = 6.626068 X 10^{-34} (Js)
$I\Psi I^2$	Probability distribution of the particle
k(T)	Rate constant at temperature T
k_1	Rate constant for 1st order reaction, $(mol/m^3)^{n-1}(m/s)$
$k_1, k_2 k_3$	Rate constants
k_B	Boltzmann constant = 1.3806504 X 10^{-23} (J/K)
k_c	Mass transfer coefficient (m/s)
L	Length of the reactor (m)
n	Reaction order
R	Gas constant = 8.31441 (J/mol -K)
R	Radius of catalyst particle (m)
r_A	Reaction rate per unit mass of catalyst (kmol/kg-s)
S_a	Catalyst surface area (m^2/kg catalyst)
T_{10}	10% distillation temperature (°C) determined
T_{10N}	T_{10} - 215 (°C)
T_{50}	50% distillation temperature (°C)
T_{50N}	T_{50} – 260 (°C)

T_{90}	90% distillation temperature (°C)
T_{90N}	T_{90} - 310 (°C)
T_s	Temperature at the surface of the catalyst (°C)
V	Potential field in which the particle is moving.
ΔG^0	Gibbs free energy of activation (kcal/mol)
η	Effectiveness factor
ξ	Tortuosity
ρ_b	Bulk density of the catalyst bed (kg/m^3)
ρ_c	Catalyst density (kg/m^3)
σ	Construction factor,
Ψ	Wave function
Φ_p	Pellet porosity

ABBREVIATIONS

1T	H(OH)Al(OH)
5T	$OH_3Si(OH_3Si)Al(OH_3Si)OHSiH_3$
ASTM	American Society for Testing and Materials
BET	Brunauer Emmett Teller theory
CCC	Central composite circumscribed
CHNS	Carbon, hydrogen, nitrogen and sulphur analyzer
CN	Cetane number
CP	Cracking products
CPE	Chemical and phase equilibrium problem
CUS	Coordinately unsaturated
DBT	Density functional theory
DH	Dehydrogenated products
DRIFTS	Diffuse reflectance infrared Fourier transform spectroscopy
DTA	Differential thermal analyzer
FID	Flame ionization detector
GC-MS	Gas chromatography-Mass aspectroscopy
HF	Hartree-Fock theory
HGO	Heavy gas oil
HLGO	Hydrotreated LGO

IBP	Initial boiling point
ICP-MS	Inductively coupled plasma mass spectroscopy
IRC	Intrinsic reaction coordinate
LGO	Light Gas oil
LHSV	Liquid hourly space velocity
LP	Linear programming problem
MP2	Møller–Plesset 2nd level theory
NMR	Nuclear magnetic resonance
RC	Ring contraction products
RO	Ring opening products
RSM	Response surface method
SS	Sum of squares
TCD	Thermal conductivity detector
TEM	Transmission electron microscopy
TG	Thermo gravimetry
TPD	Temperature programmed desorption
TPR	Temperature programmed reduction
TRO	Two ring opening products
XRD	X-ray diffraction
ZPE	Zero-point energy

1 INTRODUCTION

Global oil resources appear to be sufficient to meet demand up to 2030 as projected in world energy outlook by the International Energy Agency (IEA) in 2007. Global demand for oil is increased over the last 40 years by 150% and by 20% in the past two decades to the current 80 million barrels per day. It is projected to grow 1.3 to 1.4% per annum in the next 30 years and reach 116 to 118 million barrels per day by 2030 (Kjärstad, 2009). This demand for oil comes at a time when there is a gradual decline in supply from relatively cheap conventional crude and discoveries are not being replaced with new ones (Laherrere, 2003). Figure 1.1 shows the conventional global oil reserves that is ultimately recoverable and the projected world oil production from 2005 to 2050 (Kjärstad, 2009). As shown in Figure 1.1, in the period 2005 to 2030, 70% of the current available reserves will be consumed where the cumulative oil production will reach to 860 billion bbls. However, the world has over twice as much supply of unconventional oil as compared to conventional oil and it is estimated that there are 8-9 trillion barrels of heavy oil and bitumen in place worldwide, of which potentially 900 billion bbls of oil are commercially exploitable with today's technology (Davis, 2002). Oil sands production constitutes both raw bitumen and upgraded synthetic crude oil while the conventional portion includes light and heavy. By 2015 the growth in oil sands expansion will exceed by 2 to 3 times of conventional oil production. According to Canada's National Energy Board (CNEB, 2006), at the end of 2004, Alberta oil sands contain 315 billion bbls of an ultimately recoverable bitumen resources. By assuming 315 bbls recoverable out of 1600 billion bbls oil originally in place (OOIP) gives a recovery factor of 20%. There are currently extensive activities within Canada's oil sands industry with some C$125

billions capital expenditure in publicly announced projects by 2015. CNEB projects production to increase from current 1.1 Mbbl/d (2005) to between 1.9 and 4.4 Mbbl/d in 2015 with a base case of 3 Mbbl/d (CNEB, 2006).

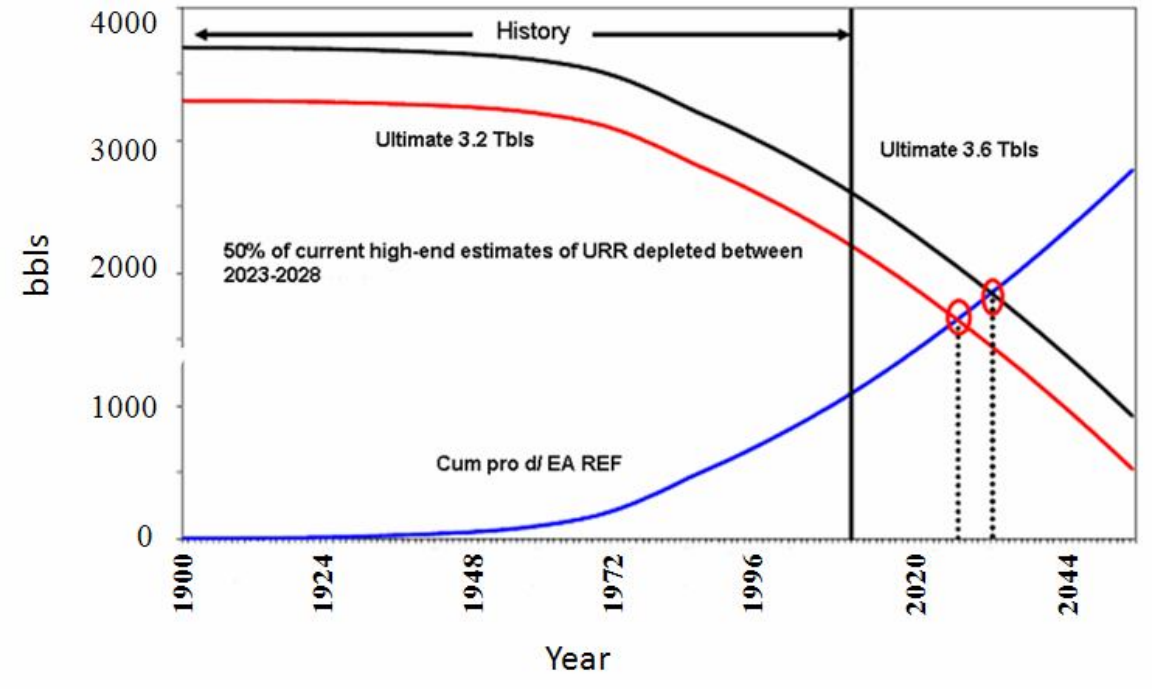

2.1: Depletion of conventional global oil reserves assuming 3.3 and 3.7 Tbls ultimately recoverable as of 1st January 2006 and demand according to IEA 2006 (Kjärstad, 2009).

Suncor and Syncrude expansions are two of the largest projects, which will take combined production up from 385 kbls/d in 2005 to around 910 kbls/d in 2015. Currently, half of Canada's total crude oil output is making up by oil sands production and by 2015 it is expected to account for three quarters of all Western Canadian production (Canadian Association of Petroleum Producers, 2004-2015 Crude oil forecast).

Programs such as Kyoto protocol demand new technologies to produce high quality liquid fuels with maximum combustion efficiency and minimum emissions. The

new Environment Protection Agency (EPA) regulations limit sulfur content in diesel fuel to 15 ppm. Additional specifications for minimum cetane index at 40, and maximum aromatics content at 15 vol.% are also be imposed. In the coming years, US and Canadian refineries will have to cope up with the low quality feed stocks due to the worldwide increase in crude oil demand and decreased production of light crudes from mature regions such as the US and North Sea and heavy oil supplies increased from Canada and Venezuela. The heavy gas oil (HGO), bottom cut from Synthetic Crude Oil (SCO) (about 38 vol %) contains more than 90% of cyclic hydrocarbons which causes processing problems, particularly in fluid catalytic cracking (FCC) units, as this constitutes approximately 80% of the US conversion capacity (NCUT news letter, 2004). This has led to its limited acceptance in a conventional FCC refinery intake. In addition to the poor HGO quality, SCO also yields poor quality middle distillate (potentially jet and diesel fuel blending components). These potential motor fuel components have low cetane numbers and poor ignition qualities. Heavy gas oil (HGO) quality as FCC feedstock is one of the most severe problems faced by the upgrading industry (NCUT news letter, 2004). Therefore, in order to upgrade HGO quality as FCC feedstock, new hydrotreating technology is needed, particularly in the development of more active catalysts and novel catalytic processes that are capable of doing selective ring opening (SRO) of at least one of the naphthenic rings. The upgrading process involves (i) decreasing the sulfur and nitrogen content; (ii) reducing the aromatic content, and increasing the cetane number by opening the rings of naphthenes. Cobalt- or nickel-promoted MoS_2 catalysts, supported on Al_2O_3 have been widely used in industry for hydrotreating gas oils, primarily for hydrodesulphurization (HDS) and

hydrodenitrogenation (HDN). However, the cetane number (CN) due to hydrogenation of aromatics to naphthenes may not always be high, as the CN of naphthenes is low. This is a problem particularly in upgrading highly aromatic fractions such as heavy gas oil (HGO) derived from bitumen.

The present gas oil upgrading technology employing hydrotreating in which aromatics converted to naphthenes is not efficient as the cetane number of the naphthenes is low. Further, the high density of naphthenes gives reduced volume of the distillate fuel blend relative to a composition containing similar concentration of paraffins instead of naphthenes with same carbon number. Aromatic saturation (ASAT) and hydrocracking are the currently available methods to remove polyaromatics from gas oils, but are not able to improve the cetane number. Aromatic saturation cannot achieve the required cetane number even though it maintains the high molecular weight. Hydrocracking on the other hand increases the cetane number significantly but the molecular weight decreases greatly. So, in order to obtain a fuel with higher cetane number, the best alternative is SRO of polynuclear aromatics present in gas oils to paraffins. In the SRO process, only internal C-C bonds of naphthenic rings are broken without losing the carbon number. Complete saturation of multiring aromatics to multiring naphthenes prior to SRO is important. Metal and acid site promoted hydrocracking and dealkylation reactions must be avoided to minimize losses in middle distillate yield. SRO of both five- and six-membered naphthene rings is an essential reaction. Controlling the interconversion of six- and five-membered rings via an acid-catalyzed ring-contraction step is also of special importance, since selective conversion of six-membered naphthene rings to five-membered naphthene rings greatly influences ring-opening rates and selectivities.

2 LITERATURE REVIEW

This chapter presents a review on upgrading of light and heavy gas oil derived from Athabasca Bitumen. Particular emphasis is placed on the concepts of history and necessity of hydrogenation of aromatics and selective ring opening of naphthenes derived from Athabasca bitumen. The concepts of hydrogenation and selective ring opening mechanisms, catalysts and their catalysis as well as kinetic modeling of hydrogenation and ring opening are also discussed in this chapter.

2.1 Introduction

Bitumen is a thick black viscous liquid present in oil sands. Bitumen is substantially heavier than other crudes with an API gravity of around 13. Bitumen contains more contaminants (sulfur, nitrogen, clays and other minerals, asphaltenes, resins and metals) than light crudes. In 1967, SUNCOR Energy first started production of bitumen derived oil with a production capacity of 32000 bbls/day. Syncrude started production in 1978 with 109,000 bbls/day capacity. By 2004, Canadian oil sands production reached 1 million bbls/day (Stringham Greg, 2006).

Canadian association of petroleum producers estimated that the oil sands production will increase from 2.5 million bbls/day in 2005 to 4.9 million bbls/day in 2020 as shown in Figure 2.1.1. Currently, oil sands facilities account for about 5% of Canada's GHG emissions and less than 0.01% of global emissions. Environmental concerns and regulations require severe upgrading of gas oils to clean-burning transportation fuels and call for new technologies to produce high quality liquid fuels with maximum combustion efficiency and minimum emissions.

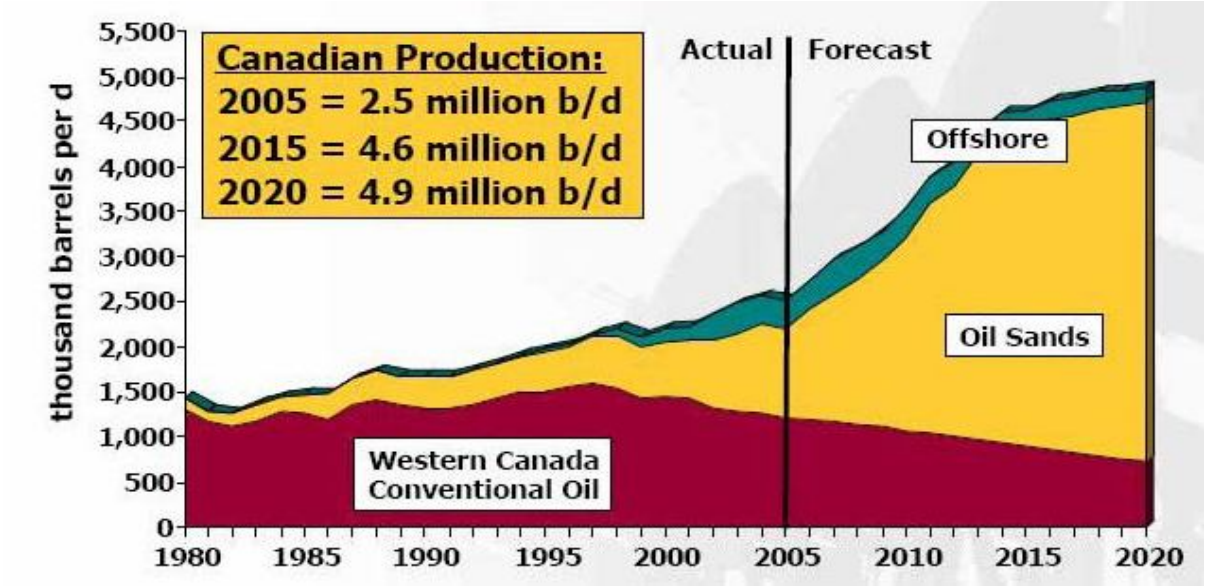

Figure 2.1.1: Conventional vs. Oil Sands Production in Western Canada: 1980-2020 (Canadian Association of Petroleum Producers, June 2006)

By June 2006, the new EPA regulations limit sulfur content to 15 ppm. Additional specifications for minimum cetane index at 43 and maximum aromatics content at 35 vol % will also be imposed. In the coming years US and Canadian refineries have to cope up with the low quality feed stocks due to the worldwide increase in crude demand and decreased production of light crudes from mature regions such as the US and North Sea and heavy oil supplies increased from Canada and Venezuela.

With 178 billion bbls (Table 2.1.1) of established bitumen reserves (recoverable in situ and mineable), the Canadian oil sands resources has been increasingly recognized as a strategic source of North American energy. Alberta bitumen production reached approximately 1 million bbls/d in 2003, accounting for 53% of Alberta's total crude oil and equivalent production. According to the Alberta Energy Utilities Board (AEUB), total bitumen production will increase to 3 million bbls/d by 2014, representing 2 million bbls/d of synthetic crude oil (SCO) and 1 million bbls/d of unprocessed crude bitumen.

Table 2.1.1: Facts about oil sands in Canada (UCDN workshop, June 2005)

Area of oil sands deposits	Six million hectares		
Current estimated reserves of oil from oil sands	178 billion barrels		
Potential reserves with improved extraction technology	300 billion barrels		
	2004	2014	2030
barrels of oil produced daily (in million barrels)	1	3	5
Annual revenues (in billion US$)	12.5	43	
Annual royalties and taxes from oil sands projects paid to Alberta (billion$)	0.873	3	
Jobs	140,000		

Compared to conventional crude oil, SCO has the valued quality attributes of low sulfur content and zero residues. However, SCO also has some major disadvantages, largely related to its high aromaticity. The heavy gas oil (HGO), bottom cut from SCO (about 38 vol %) contains more than 90% of cyclic hydrocarbons (Table 2.1.2) which causes processing problems, particularly in fluid catalytic cracking (FCC) units, this constitutes approximately 80% of the US conversion capacity. This has led to its limited acceptance in a conventional FCC refinery intake. Currently there is a 25% limitation on HGO in FCC feed. The causes for this are lower FCC conversion, potential thermal imbalance in FCC units (excessive coking), excessive yields of highly aromatic LCO, high concentration of refractory sulphur species in LCO and faster FCC catalyst consumption (excessive coking). In addition to the poor HGO quality, SCO also yields poor quality middle distillate (potentially jet and diesel fuel blending components).

Table 2.1.2: Aromaticity of Bitumen derived crude HGO (UCDN workshop, June 2005)

Composition	"paraffinic" HGO	HGO	"sour" BDC HGO
paraffins	37.9	13.6	1.8
cyclo-paraffins	44.4	45.7	35.4
Aromatics	14.5	36.1	55.4
cyclo-paraffins + aromatics	58.9	81.8	90.8
mono-aromatics	7.4	16.4	23.6
di-aromatics	3.8	10.4	13.6
tri-aromatics	1.5	3.8	5.3
tetra-aromatics	0.6	1.8	2.8
penta-aromatics	0.3	0.8	1.5
aromatic sulphur	0.5	2.4	7.8
polars	3.1	4.6	7.4

These factors have resulted in a price differential between SCO and other light crudes. Similar problems exist with other highly aromatic streams such as those from cokers and FCC units. These potential motor fuel components have low cetane numbers and poor ignition qualities. This will become a particular difficulty for refiners if higher cetane specifications are introduced worldwide in the near future. In order to accept larger volumes of bitumen-derived crudes, both the producers and refiners will have to address the quality issues and refining challenges. Therefore, in order to upgrade HGO quality as FCC feedstock, new hydrotreating technology is needed, particularly in the development of more active catalysts and novel catalytic processes that are capable of doing SRO of at least one of the naphthenic rings. The upgrading process involves (i) decreasing the sulfur and nitrogen content; (ii) reducing the content of aromatics, which also increases the cetane number; (iii) increasing the cetane number by ring opening of naphthenes. Cobalt- or nickel-promoted MoS_2 catalysts, supported on Al_2O_3 have been

widely used in industry for hydrotreating gas oils, primarily for hydrodesulfurisation (HDS) and hydrodenitrogenation (HDN). However, the CN due to hydrogenation of aromatics to naphthenes may not always be high, as the CN of naphthenes is low as shown in Table 2.1.3.

Table 2.1.3: Cetane numbers of different compounds

Compound		Cetane number
n-Paraffins		
	n-Decane	77
	n-Nonane	72
	n-Octane	64
	n-Heptane	54
	n-Hexane	45
	n-Pentane	30
	n-Butane	22
Iso-paraffins		
	2-Methylpentane	33
	2,3-Dimethylpentane	22
	2,24-Trimethylpentane	14
Cycloparaffins		
	cyclohexane	15
	Methylcyclohexane	22
	n-pPropylcyclohexane	52
	trans-Decalin	46
Olefins	1-Hexene	27
	1-Decene	56
	1-Nonene	51
Aromatics		
	Benzene	0
	Toluene	7
	Ethyl benzene	8
	ter-Butyl benzene	6
	Tetralin	13

This is a problem particularly in upgrading highly aromatic fractions such as heavy gas oil (HGO) derived from bitumen. The aromatics have poor ignition properties, and thus, a net increase of the cetane number is obtained by decreasing their concentration in the diesel fuel through hydrogenation processes. The cetane number (CN) is a very important parameter for the quality of the combustion process and thus for the amount of pollutants emitted; high CN results in lower NO_x and particulate emissions.

2.2 Chemistry and mechanism of ring opening reactions

There are three terms commonly used to describe the conversion of naphthenes to paraffins or to naphthenes containing fewer rings. They are "hydrogenolysis", "hydrodecyclization", and "ring opening". Hydrogenolysis reactions are those in which there is cleavage of a C-C bond, with addition of hydrogen at each point of cleavage. Hydrodecyclization is more specific in that a cyclic structure is cleaved in a hydrogen environment. Such reactions occur in the hydrocracking of large organic molecules, with formation of fragments that react with hydrogen in the presence of a suitable catalyst and at relatively high temperatures (McVicker, 2002). Such fragments are typically either molecules in which rings have been cleaved, or are alkyl substituents which have been cleaved, or both. The resulted products contain fewer carbon atoms than the original molecule. This of course, results in lower boiling products. "Ring opening" can simply be another way to describe hydrodecyclization. However, selective ring opening means a high inclination for cleavage of a ring bond which results in product molecules having significantly the same number of carbon atoms and one less ring than the original molecule. There are three possible ring opening path ways (McVicker, 2002). In free radical mechanism which is normally initialted by pyrolysis, it is very difficult to get the

higher selective ring opening yields due to fast competing reactions like secondary cracking and dealkylation. In the second type pathway, naphthenic molecules are activated by either direct formation of a cationic species by hydride abstraction by a Lewis acid or by protonation of an olefin intermediate formed by dehydrogenation of naphthene over a metal function. Unacceptably low yields of SRO products results in acid-catalyzed carbocation cleavage of ring C-C bonds due to the domination of the metal function by the strong acidity function where excessive side chain and product alkane cracking takes place (Weitkemp, 1994). The third possible pathway of ring opening, hydrogenolysis of alkyl substituted naphthenes can be achieved either by endocyclic or exocyclic C-C bond cleavage. The endocyclic C-C bond cleavage leads to selective ring opening.

Figure 2.2.1 outlines transformation that is likely to occur during the conversion of multi-ring aromatics to paraffins (McVicker, 2002). Complete saturation of multiring aromatics to multiring naphthenes prior to SRO is important. Metal and acid site promoted hydrocracking and dealkylation reactions must be avoided to minimize losses in middistillate yield. SRO of both five- and six-membered naphthene rings is an essential reaction. Controlling the interconversion of six- and five-membered rings via an acid-catalyzed ring-contraction step is also of special importance, since, selective conversion of six-membered naphthene rings to five-membered naphthene rings greatly influences ring-opening rates and selectivities.

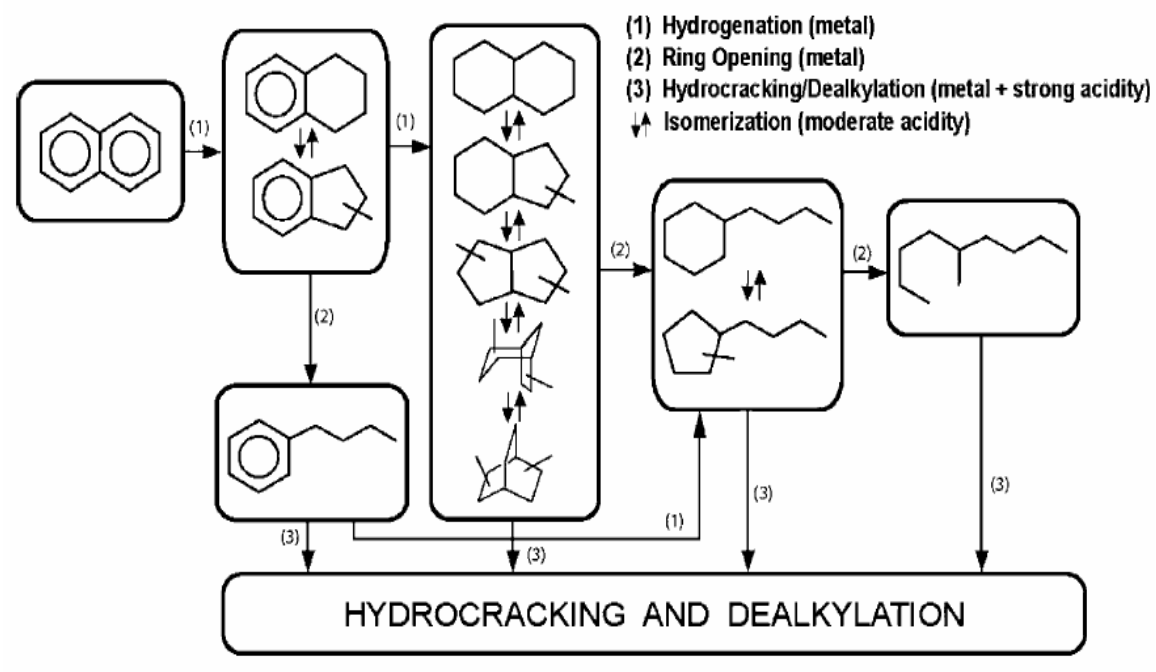

Figure 2.2.1: Key reactions during the conversions of multiring aromatics to paraffins (McVicker et. al., 2002)

The ring opening rate of alkyl substituted cyclopentanes increases with a decreasing number of secondary-secondary C-C bonds (McVicker, 2002). It was presumed that the strain in the hydrocarbon ring and the number of alkyl substituents affects the ring-opening of naphthenes. But the five and seven-membered rings possess slightly more strain than the six-membered rings (Caray, 1990). Therefore, this strain should not have a major effect on the stability of the molecule. Smaller molecules have more strain and more prone to ring opening. Therefore, complex molecules have more tendencies to open the rings (Kubicka, 2004).

2.2.1 Hydrocracking and ring opening on solid acid catalysts

Hydrocracking on solid acid catalysts takes place via carbenium intermediates initialized on Brønsted acid sites (Galperin, 1994). The reaction is carried out via protolytic cracking, protolytic dehydrogenation, hydride transfer, skeletal isomerization, β-scission and alkylation steps. Rate of β-scission is slow in cyclic hydrocarbons compared to aliphatics due to an unfavorable orientation of the p-orbital at the positively charged carbon atom and the β -bond to be broken (Weitkamp, 1984).

Kubicka et al. (2004) proposed the mechanism involved during ring opening of decalin on proton form of zeolites and is shown in Figure 2.2.2. The reaction is initiated by attack of Brønsted acid sites of catalyst on a C–C bond of decalin forming a carbanium ion. The prevailing initiation step will be protolytic dehydrogenation confirmed from formation of isomers at the beginning of the reaction exclusively. The formed carbanium ions can undergo skeletal isomerization and desorption of saturated product via hydride transfer leads to the formation of adsorbed carbenium ion. β –scission of dinaphthene carbenium ion to alkenylnaphthene carbenium ion leads to ring opening. This mechanism showed that skeletal isomerization is needed prior to the ring opening. The presence of Brønsted acid sites is essential for the accomplishment of both isomerization and ring opening of naphthenes molecules.

2.2.2 Hydrocracking and ring opening on bifunctional catalysts

Bifunctional catalysts consist of both metal and acid functions. Hydrogenation and dehydrogenation reactions are carried out on metals and cracking and isomerization are carried out on acidic sites (Mills, 1953; Weisz, 1957). Metal and acid sites are

important in bifunctional catalysts for hydrocracking and ring opening reactions as shown in Figure 2.2.2.

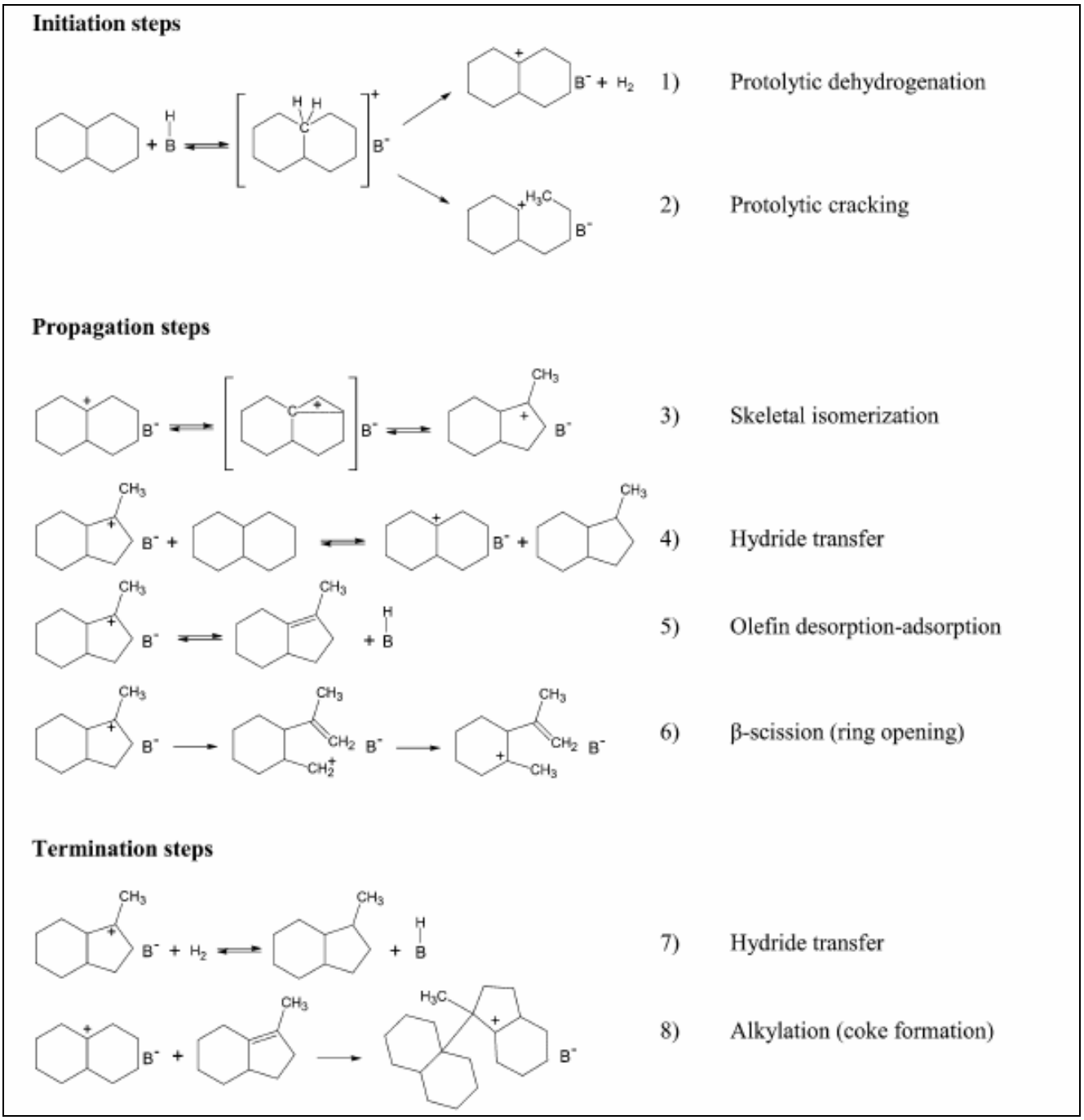

Figure 2.2.2: The mechanism of ring opening of decalin on a Brønsted acid site (Kubicka et al, 2004a)

Figure 2.2.3 shows the role of metal sites on the ring opening reactions. Hydrogenation and dehydrogenation reactions are carried out on metal sites by converting reactants to olefins (eq.1). Attack of Brønsted acid site on olefins leads to the formation of carbenium ion and subsequent skeletal isomerisation and cracking (equation 2). Then the desorbed olefin will undergo hydrogenation on a metal site (equation 3).

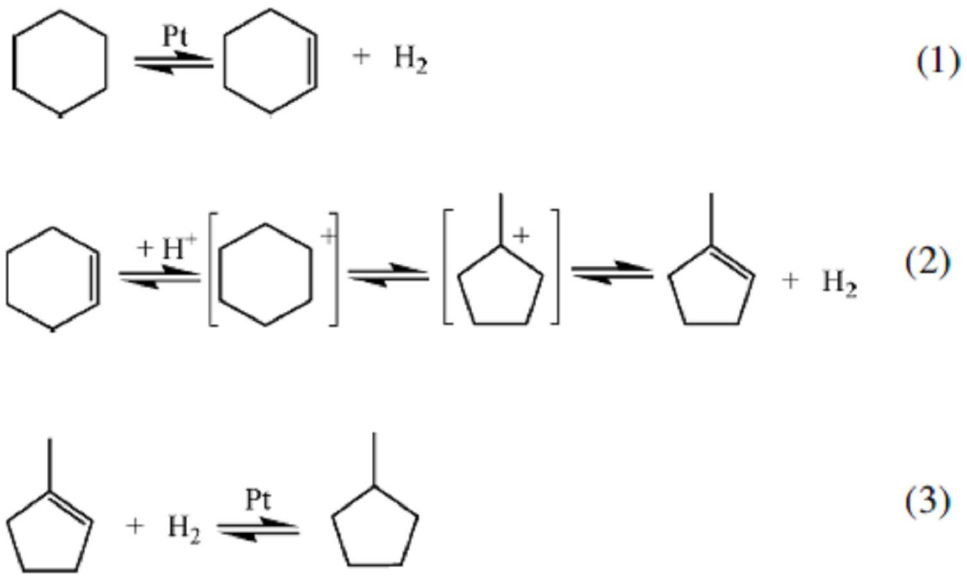

Figure 2.2.3: Hydrocracking mechanism on bifunctional catalysts (Du et al, 2005).

It was also proposed that the hydrogenation and cracking occurs at the same site due to the presence of spillover hydrogen. Spillover hydrogen provided by the metal co-catalysts migrates to the acid sites and helps in saturating the olefins at a single site. Ring opening also can be initiated by direct hydrogenolysis of a C-C bond on a metal site.

Ring opening on metal sites are supported by two well proposed mechanisms: multiplet and dicarbene mechanisms (Gault, 1981; Hayek, 1997). The two mechanisms

differ mainly in how the reaction intermediate forms on the metal surface. There are two types of multiplet mechanism: doublet and sextetdoublet. Both mechanisms compete with each other in the reaction. In the doublet mechanism, the hydrocarbons adsorb physically edge wise on two metal atoms. The doublet mechanism is thought to occur on small metal particles, and is used to explain the selective hydrogenolysis of bisecondary C–C bonds. According to this mechanism, cyclic hydrocarbon is adsorbed perpendicular to the metal surface via a bisecondary C–C bond, which then reacts with chemisorbed hydrogen in a push–pull manner to produce ring-opening products. Due to steric hindrance, the edge-wise adsorption of the tertiary–secondary or tertiary–tertiary C–C bonds is limited. In sextetdoublet mechanism the hydrocarbons adsorption is flatlying on the metal surface. In the 'sextet-doublet' mechanism, on the other hand, the cyclic molecule is physically adsorbed flat-lying on the metal surface, with the carbon atoms of the ring located over the interstices of the metal plane, e.g. Pt(1 1 1). For the five-membered ring cyclopentanes, one C–C bond has to be stretched (Figure 2.2.4), and this bond is readily attacked by neighboring, adsorbed hydrogen, leading to hydrogenolysis of the ring.

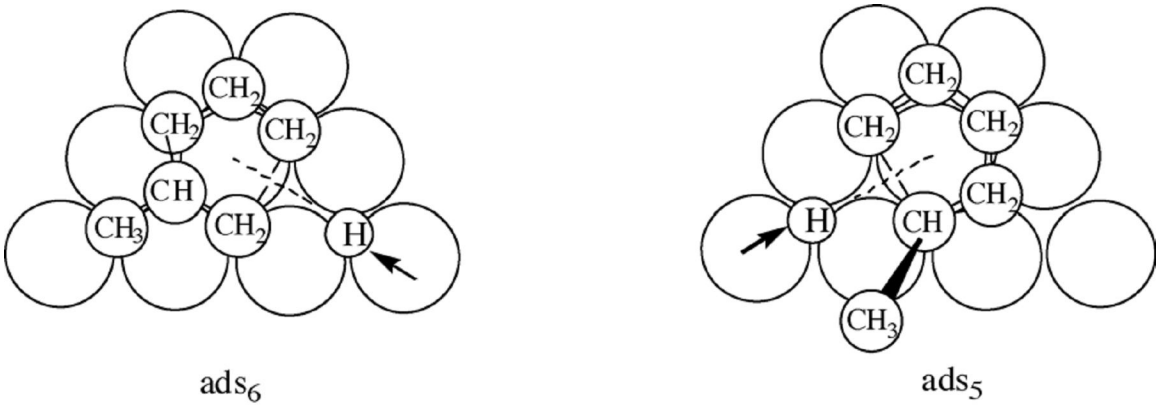

Figure 2.2.4: Hydrogenolysis of methylcyclopentane via the multiplet mechanism (Gault et al., 1981)

The tertiary–secondary C–C bonds in alkylcyclopentane could be ruptured via the five-atom adsorbed mode. For cyclobutanes, all four C–C bonds are stretched, resulting in higher reactivity but lower selectivity. In contrast, there is no stretching when cyclohexanes and paraffin adsorb on the metal surface, as all the carbon atoms can fit the interstices of the Pt(111) plane. As a result, cyclohexanes and paraffin are usually not hydrogenolysized, but preferably dehydrogenated or isomerized. Alternatively, the dicarbene mechanism involves the chemisorption of the cyclic hydrocarbon molecules on the metal surface after the rupture of several C–H bonds, forming carbon–metal bonds or p-adsorbed olefins (Figure 2.2.4). The nonselective ring opening of MCP on metal catalysts can be accounted for by thep-adsorbed olefin mechanism. Similar to that in the sextet-doublet mechanism, MCP is adsorbed parallel to the metal surface, but in a quasi-planar manner involving only one metal atom. The selective ring opening of MCP, on the other hand, involves 1,2-dicarbene complexes that bond to several metal atoms and stand perpendicular to the metal surface. Owing to steric hindrance, the hydrogenolysis of the tertiary–secondary C–C bonds is retarded. On some occasions, however, an exocyclic alkyl substituent participates in the formation of a metallocyclobutane intermediate, resulting in the selective breaking of tertiary– tertiary and tertiary–secondary C–C bonds.

Kubicka et al. (2004b) studied the decalin ring opening on the bifunctional platinum modified zeolites and extended the mechanism that the decalin transformation into isomers, ring opening and cracking products proceeds via a bifunctional mechanism in addition to the mechanism observed on the proton form zeolites. The presence of platinum dehydrogenates decalin to form olefin which forms carbenium ion when protonated by a Brønsted acid site which in turn undergo isomerization or ring opening

products. They observed that isomerization is an essential step for the ring opening of decalin. The importance of the Brønsted acid sites is observed by conducting decalin conversion over Pt-promoted VPI-5 (no Brønsted acid sites) which gives no isomerization or ring opening reactions. In a mechanism proposed by Arribas et al. (2002) for the ring opening of methyltetralin on bifunctional Pt/USY catalysts, protonation of methyltetralin took place on acid sites followed by the isomerization and the corresponding carbenium ion converts to olefin. The formed olefin will be hydrogenated on metal sites or undergo β-scission to produce ring opening products.

2.3 Methods for catalyst development

Conducting experiments with a laboratory-scale reactor is a prerequisite in the development of catalysts for a new process or the improvement of existing processes (Kapteijn, 1996a,b; Forni, 1997). Discovering, developing, and optimizing new catalytic materials using current approaches is predominantly a process of trial and error, sequentially generating data from one experiment to another. Trial and error experiments are time scaling and expensive. Before a new or modified process, the catalyst development work requires many stages such as (i) catalyst preparation, (ii) catalyst screening, (iii) establishing reaction networks, (iv) kinetic studies, (v) stability tests, and (vi) scale-up on pilot plant level. The objectives of the different development stages are different. In the *combinatorial stage*, many catalyst formulations need to be prepared, investigated, and roughly compared on activity, selectivity, and stability. During the development, there will be a continuous feedback from one activity to another to optimize the catalyst and/or the catalytic process. More recently, theoretical chemistry as a tool and high throughput experimentations are the main approaches for the development

of catalysts formulations which are mainly adopted in pharmaceutical industry. High-throughput synthesis and screening of the catalysts in a qualitative sense allow a rapid identification of potential “lead” catalysts. In the secondary stage, the potentially interesting catalysts from the preliminary stage on a more quantitative basis are performed. Determination of the reaction kinetics and obtaining a first insight into the catalytic stability will be tested in this stage. Time consuming kinetic studies are important for the development of the design, operation, and process control of a large-scale catalytic reactor. They require an exhaustive description of the catalytic rate as a function of the process variables, such as temperature, pressure, space–time, and composition of the reaction mixture. The basis for the kinetic modeling studies is obtained by investigating the catalytic reaction mechanism and establishing the reaction networks. Stability studies, in which the catalyst is tested during a longer time on stream, should be carried out to evaluate the practical application of the new catalyst before the scale-up is initiated.

2.3.1 Theoretical chemistry as a tool

Theoretical chemistry is a useful alternative tool for developing new catalysts to the present existing experimental methods. With out conducting the experiments the catalyst models can be developed and the bevaviour of various reactions can be modeled on the catalysts surface using modern computational methods like quantum chemical simulations. These methods are inexpensive compared to the costs involved with experiments and materials. When multiple species present, the identification of the real surface species and details of adsorption is paramount importance for the understanding of the mechanism of reactant adsorption on metal surface. Obviously, some reliable

theoretical predictions will be necessary in this case. Quantum chemical calculations and molecular dynamical simulations provide a useful method in modeling the surface chemistry of hydrocarbons at a molecular level. However, the detail study of energy-assistant catalysis at molecular-level is challenging due to involvement of large number of atoms and computational times. The modeling of real catalyst surfaces is a challenging job and normal procedures follow some assumptions to reduce the computational times.

2.3.2 High throughput development of catalysts

High throughput experimentation methods, invented in the pharmaceutical industry for fast discovery of new drugs have attracted a lot of attention in the catalysis research field (Hendershot, 2005). This technology was adopted by many research institutes and companies when searching for new catalysts or for improving existing catalyst performance. High throughput experimentation method allows for testing of tens and even hundreds of materials at one time, greatly speeding up the catalyst development process. Such techniques will provide new opportunities in searching for bi- or multi-metallic metal catalyst with high-performance and sulfur resistance for selective ring-opening catalysis, and/or improving hydrocracking catalysts with well-balanced acid and metal functions. With the guidance of today's advanced computational methods, the search will be even more markedly shortened by zeroing in a limited number of promising candidates.

2.4 Catalysts used for ring opening reactions

Six-membered naphthenic compound ring opening reaction is less studied due to its less activity (de Jong, 1991). Moreover C_6 ring compounds require acidic function of the catalyst to isomerise into C_5 compounds and ring-opening takes place (Kresge, 1992).

Even fused-ring naphthenic compounds like decalin are more sensitive to the acidity of the catalyst supports like zeolites (Kubicka, 2004).

2.4.1 Unsupported catalysts

Pt black is used as a catalyst for ring opening of cyclopentane, methyl-, ethyl-, 1,1-, 1,2- and 1,3-dimethylcyclopentanes at 603K (Zimmer, 1989). Ring-opening product yield is increased monotonically with increase in pressure. Where as, at low pressures olefins are the predominant products. Kubica et al. (2004) studied the ring opening of decalin over proton form zeolites (H-beta 25, H-beta-75, H-Y-12, H-Mordenite-20 and H-MCM-41) in a stainless steel (SS) fixed bed reactor at 260 to 327 ^{0}C and 2000 KPa. The skeletal isomerizations, stereoisomerization, ring-opening and cracking were the prevailing reactions and direct ring-opening was not observed. Decalin first isomerised to alkyl substituted bicyclononanes or bicyclooctanes, then the ring-opening took place.

2.4.2 Acidic supported catalysts

Selective ring-opening of the naphthenic rings can be accomplished by hydrogenolysis on certain noble metal catalysts like Pd, Pt, Ir, Ru and Rh supported on alumina or silica and was shown efficiently in the ring-opening of methylcyclopentane to alkanes (Gopal, 2002; Teschner, 2000; vaarkamp, 1995; Paal, 1997; Gault, 1981; Fenoglio, 1990; Bai, 1991; vaarkamp, 1996; Alvarez, 1996; Hayek, 1997). Six-membered naphthenic compound ring-opening reaction is less studied due to its less activity (De Jong, 1991). Moreover C_6 ring compounds require acidic function of the catalyst to isomerise into C_5 compounds and for ring opening (Kresge, 1992). Even fused ring

naphthenic compounds like decalin is more sensitive to the acidity of the catalyst supports like zeolites.

Five membered ring naphthenes can be easily converted to alkanes without loss of molecular weight especially on Ir catalysts. But it is very difficult to open the six membered ring naphthenes directly by using metal hydrogenolysis reaction. Low acidic supports like Al_2O_3, SiO_2–Al_2O_3, SAPO-11 favors the low ring-contraction yields but high acidity supports like USY, LZY-82, beta zeolite favors the cracking products. Supports with controlled acidity such as ECR-32 and USY, the non-branched isomeric products yield is maximum and moderate acidity favored the maximum ring-opening yields. Therefore, the potential route is the use of metal and acid balanced bifunctional catalysts to isomerise six membered ring naphthenes to five membered ring naphthenes prior to ring opening. Non branching isomerization is required to achieve the good selective ring opening yields.

McVicker et al. (2002) studied the selective ring-opening of five-membered and six-membered naphthenic compounds on noble metals supported on alumina and silica in a down flow reactor at 250 to 550 ^{0}C and 5500 to 8000 KPa. Ir on alumina yields maximum of 52 % conversion with 99 % ring opening selectivity for unsubstituted five-membered ring naphthenes. For substituted five-membered naphthenes Pt on alumina gave maximum activity with 91% conversion and 61.9% of ring opening yield. For six-membered naphthenes, the overall conversion is less for Ir/Al_2O_3 (35%) compared to the 1.5% Ru/SiO_2. But the ring opening selectivity for Ir is 87% compared to 4% for 1.5% Ru/SiO_2 which is very good. So, Ir on alumina catalyst yielded higher ring opening yields for C_5 and C_6 naphthenes.

Kubica et al. (2004) studied the ring opening of bicyclic naphthenic molecule decalin over Pt modified zeolites (H-beta 25, H-beta-75, H-Y-12, H-Mordenite-20 and H-MCM-41) in a stainless steel fixed bed reactor at a temperature of 260 to 327^0C and a pressure of 2000 KPa. Ring opening yields for platinum modified catalysts are 3 to 4 times more than the proton form zeolites which indicated the importance of the metal hydrogenolysis reaction. Pt/H-Beta catalyst which is moderately acidic gave good ring opening yield at moderate temperatures which indicates the importance of moderate acidity. 270 °C temperature favored the cracking products than ring opening products for all the catalysts. As the temperature increases from 220 to 250 °C, shift is observed from isomers to RO products which indicated the importance of isomerization step prior to ring opening. The ring opening of decalin and tetralin on HY and Pt/HY catalysts at 260 to 327 °C temperature and 2000 KPa pressure was studied and the catalyst HY zeolites are effective for ring-contraction and ring-opening of decalin (Santikunaporn, 2004). The activity of the catalysts increased with acidity of the catalyst where low acidity gave low conversions. By adjusting the acid site density, higher conversions were observed and this acid density should be maintained at optimum level as too much density may lead to fast deactivation of the catalyst. RC and RO products initially increase with conversion, but at some point the RC products levels off and start decreasing with conversion which clearly showed that the ring-opening products are obtained as secondary products through ring-contraction followed by cracking. The products from the decalin ring opening contained low cis to trans ratio of decalin due to high selectivity of cis products to convert into RO products. When Pt metal is added to the HY zeolite, for any conversion the RC/RO ratio is higher than of the any of proton form zeolite (Santikunaporn, 2004). It

was also observed that the presence of Pt is effective in obtaining higher concentration of RO and RC products from decalin.

McVicker et al. (2002) studied the importance of acidity and the effect of Pt and Ir on alumina and USY supports at a pressure of 5500 to 8000 KPa and a temperature of 250 to 550 °C. Conversion of decalin increases by 3 to 4 times on Pt modified zeolites than on proton form zeolites. The acidity of the Pt modified zeolites is much smaller than the Proton form zeolites but the conversion is very high which shows the importance of metal hydrogenolysis reaction. As Brønsted acid sites are crucial in the ring-opening activity, it is expected that the Pt modified zeolites should give less ROP due to its less acidity compared to the proton form. But Kubicka et al. (2004) observed that the Pt modified zeolites give comparable conversions with the proton form zeolites. The reason for this was hydrogenolysis of some of the isomers on the Pt sites.

The acidity plays an important role in the selective ring opening of bicyclic naphthenes as shown by Kubicka et al. (2004). The activity of the catalyst increased with increasing temperature and acidity. No isomerization and ring opening reactions are observed by using Pt modified VPI-5, a material having no Brønsted acid sites (Kubicka, 2004). This confirms the importance of Brønsted acid sites in the formation of isomers from the decalin followed by the ring opening and cracking via bifunctional mechanism on the proton formed zeolites. The initial activity of the catalysts increased with the acidity of the catalyst. H-MCM-41 and H-Beta-75 have almost the same Lewis acid sites but the difference in the Brønsted acid sites is large which leads to the conclusion of importance of Brønsted acid sites in the selective ring opening reaction. The activity of proton form zeolites followed the trend of increasing catalyst acidity.

Studies were conducted by Eliche-Quesada et al. (2003) and Rodr´iguez-Castellón et al. (2003, 2004) on the ring opening of the tetralin and naphthalene on noble metal supported on zirconium doped mesoporous silica (Si/Zr ratio of 5) catalysts. They used the operating conditions 250 to 400^0C and at a pressure of 6000 KPa. Hydrogenation and ring opening of the tetralin on Ni-W (Eliche-Quesada, 2003), Pt, Pd, Rd and Pd-Pt (Rodr´iguez-Castellón, 2004), Ni (Rodr´iguez-Castellón, 2003) doped on Zr-mesoporous materials have been studied. The introduction of hetero atoms like Al, Zr and Ti into the siliceous framework increases the acidity of the mesoporous support. The activity of the tetralin is performed in a high pressure fixed bed continuous flow SS reactor operated in the downward flow. They achieved a conversion of higher than 85% at temperatures of 250 to 350 C. At higher temperatures the conversion is low due to thermodynamic restrictions as the hydrogenation reaction is exothermic.

2.4.3 Basic supported catalysts

The basic supports like L-zeolite, hydrotalcite, theta and gamma aluminas, SiO_2 modified with potassium (Galperin, 2003) are used for Pt catalysts for the ring opening studies of methyl cyclopentane. On these catalysts the RO selectivity is very high upto 98%. The acid based cracking and isomerization reactions are completely suppressed. They got 25 to 35% conversion and above 90% ring opening selectivity on these basic supports. Increase of K loading from 0 to 2.5% on Pt/ gamma alumina increase the RO selectivity from 70 to 98% where as the conversion is decreased due to the deactivation of metal sites by potassium. The same conversion can be achieved by using the high platinum loading. A decrease in chlorine loading from 1 to 0.14 wt% on Pt/gamma alumina increases the RO selectivity without much change in the conversion.

2.4.4 Bimetal supported catalysts

To achieve the good ring opening yields bifunctional catalysts are tried by McVicker et al. (2002) in the ring opening of PCP and BCH. For six membered ring naphthenes the large ring opening yields and the selectivities by admixtures of acid – metal catalysts like 0.9% Ir/Al_2O_3 + 0.9% Pt/USY clearly indicates the importance of metal-acid site balance in the ring opening yields.

Iridium and platinum based bimetallic catalysts are studied by Nylen et al. (2006). They used 2 wt% Pt and Ir on different acidic supports like g-Al_2O_3 , SiO_2-Al_2O_3, H-SA , ZrO_2, MgO, SiO_2, and CeO_2 and also studied the effect of iridium loading on the amount of carbonaceous deposits. At 325^0C and atmospheric pressure they found maximum activity (about 60%) with CeO_2 support. Increased amounts of iridium up to 95% (total 2 wt% bimetallic) leads to inhibit the carbonaceous precursors which is observed from TG-MS analysis thus an increase in the catalytic activity. Nylen et al. (2004) also studied the effect of 2 wt% Pt and Ir on boehmite support at 325^0C and atmospheric pressure. Cracking activity of the Ir altered by the addition of platinum and Pt alone is not selective towards ring opening products at atmospheric pressure. They also observed large Ir-Pt clusters (20-100nm) from the TEM analysis, otherwise they are well dispersed.

Arribas et al. (2004) observed that the activity of bimetallic Pt-Pd/USY catalyst on tetralin decreased to 55% of its initial activity before becoming stable which is not the case with monometallic catalysts. They described it as the higher electon density induced by iridium on the platinum sites which leads to decrease in the effective site density and

decrease in the ring opening yields. This is quite controversial with the conclusions given by the Nylen et al. (2006)

Rodriguez-Castellón et al. (2004) studied the ring opening of the tetralin and naphthalene on Pd-Pt supported on zirconium doped mesoporous silica (Si/Zr ratio of 5) catalysts. They used the operating conditions of 250 to 400 ^{0}C temperatures and a pressure of 6000 KPa. The activity of the tetralin is performed in a high pressure fixed bed continuous flow SS reactor operated in the downward flow. The main reaction product in all cases is trans decalin (60-80% at 315 C). The bimetallic SiZr-2PdPt catalyst yielded low cracking products but with high decalin yield which is in good agreement with the high hydrogenation yield of bimetallic catalyst. The stability of the bimetallic catalyst is very good as they recover their initial activity very fast.

2.4.5 Importance of pore structure

Corma et al. (2001) studied the ring opening reactions by taking the probe molecules of decalin and tetralin at 450 ^{0}C. They used the catalysts of 10, 12 and 14 ring zeolites and observed that 10-ring zeolites (MCM-22, ZSM-5) will produce short chain olefins and favor the gaseous products. Large pore zeolites (12, 14-ring zeolites) favor the ring-opening of naphthenes. Therefore, the smaller the pore size the greater the possibility of cracking and gaseous products. Arribas et al. (2002) studied the conversion of 1-methylnaphthalene in a fixed bed reactor with catalyst Pt on acidic zeolite supports like USY-1, USY-2, Al-MCM-41 and H-beta at reaction conditions of 40 bar total pressure, 275 to 350 ^{0}C, WHSV of 2h^{-1} and H_2/1-MN molar ratio of 30. The most active catalysts are Pt/MCM-41 and Pt/H-Beta at especially low temperatures whose Pt dispersion is also high compared to other catalysts. In the studied range of temperatures

Pt/MCM-41 gives good yields of selective ring opening products compared to other catalysts due to its uniform and mesoporous structure which favors the good dispersion of the metal on the surface, thus providing high hydrogenation rates. Mild acidic nature of MCM-41 greatly reduced the unwanted cracking products.

2.4.6 Thioresistance

It has been observed that the noble metals give good ring opening yields but they have less sulphur resistance. In presence of 10 ppm of sulfur, most of the single noble metal catalysts on mesoporous supports show the same conversion as of sulphur free feed (Albertazzi, 2003). But at high concentration of DBT in the feed resulted in heavy loss in conversion of naphthalene. It is believed that the sulfur tolerance of a noble metal catalyst is related to the electron density of metal clusters. The sulfur poisoning is mainly due to the fact that adsorption of H_2S decreases the metal-support interaction, which promotes platinum migration and leads to a growth of platinum particle size (Lin, 1995). Therefore, the sulfur tolerance can be increased by decreasing Pt electron density and/or enhancing metal-support interactions. Poisoning of noble metal catalysts by sulphur compounds involves a strong chemisorption on the metal sites followed by hydrogenolysis which gives H_2S, which probably gives rise to the formation of a stable and inactive M-S species (Albertazzi, 2004).

$M + H_2S \leftrightarrow M\text{-}S + H_2$ …….... 2.4.1

In the above equilibrium, the strength of the M-S bond weakens when H_2 pressure is increased which leads to the formation of electron deficient metal sites. By using the bimetallic catalysts or changing the acid properties of the support the metal ions can be modified by interaction of the reduced metal with the Brønsted acid sites (Rousset, 2001;

Yasuda, 1991; Fujikawa, 2000). The influence of the Brønsted acid sites on the thioresistance was studied on acid supports (Simon, 2002; Yasuda, 1998; Matsubayashi, 1998), and observed that Pt and Pd are highly thioresistant when metallic or bimetallics are supported on highly acidic zeolites (Yasuda, 1999; Yasuda, 1998; Matsubayashi, 1998; Yasuda, 1997). Hydrogenation and ring opening of tetralin as a model reaction, Hernandez-Huesca et.al. (2004) investigated the thio-tolerence of Ni-Mo supported on alumina pillared α-zirconium phosphate catalyst. With 1000 ppm of DBT, the catalyst maintains very high conversion (65%), after 7 hr of reaction time. The better thioresistance of bifunctional catalyst is justified by the presence of Ni^0 and Ni^{2+} ions on their surface observed from the XPS studies. The presence of Ni^0 does not react with sulphur but participates actively in the hydrogenation reaction (Sepulveda, 1995; Duprez, 1987). Therefore, it is possible to improve the sulphur resistance by using the bimetallic catalysts. By choosing tetralin hydrogenation as a model reaction for aromatics reduction, Chiou et al. (1995) investigated the effect of sulfur on the deactivation of Pt/γ-Al_2O_3 catalysts. They found that the reversible reaction scheme is unable to explain the decreased reactivation rate with the severity of sulfur poisoning. TPR, fast FTIR, and electron probe microanalysis (EPMA) suggested that the interactions between CO and Pt, and H_2 and Pt were weakened due to the increase in sulfur poisoning. A sintering of platinum particles occurred, promoted by the H_2S adsorption at the Pt-alumina interface, which may have decreased the Pt-alumina interaction. Generally the feed stocks contain sulphur in the range of thousands of ppm which deactivates the noble metal catalyst very fast. Therefore, in order to use these catalysts, there is a need to pretreat the feed to reduce the sulphur level to acceptable limits. Therefore, there is an urgent need to

develop the selective ring opening catalyst which should have good thioresistance to eliminate the pre-treatment costs.

2.5 Thermodynamic limitations

The endocyclic cracking of a carbon-carbon bond on naphthenic rings proceeds at a much slower rate than that of breaking a *C-C* bond in acyclic hydrocarbons (Weitkamp and Ernst, 1984). There are two mechanistic routes suggested in the literature for the ring opening of naphthenes on solid acid catalysts. One route follows the classical model of Mills et al. (1953), where a naphthene is dehydrogenated on the metal sites to form a cyclic olefin, which is then protonated on a Brønsted acid site to produce a cyclic carbenium ion. Subsequently, the cyclic carbenium ion undergoes β-scission to form an alkenyl cation. The other mechanism is suggested by Brandenberger et al. (1976) in which a *C-C* bond of a naphthene is directly attacked by a proton causing bond cleavage to produce an alkyl cation. The cations produced via both the mechanisms undergo deprotonation to regenerate the catalytic site. Egan et al. (1962) suggested that the alkenyl cation formed by β-scission of a cycloalkyl cation has a strong tendency to recyclize, thus favoring the reverse reaction (ring closure) but not the ring opening. Weitkamp et al. (1984) mentioned that this argument stems from a thermodynamic point of view. From a kinetics perspective, Brouwer and Hogeeven (1970) explained that the slower rate of ring opening by β-scission is due to the unfavorable orientation of the vacant *p*-orbital on the carbon carrying the positive charge with respect to the *C-C* bond on the β-position.

Certain noble metals such as Pt, Pd, Ir, Ru, and Rh have been found to be selectively active for the ring opening of cyclic hydrocarbons, and the activity and selectivity of a metal catalyst depends on the nature of the metal, particle size, and crystal morphology,

etc (Du et al., 2005). The mechanistic details of ring opening reactions of naphthenic molecules on metal sites, derived from steady state kinetic studies and surface science experiments, are presented in several excellent reviews (Anderson, 1973; Clarke and Rooney, 1976; Gault, 1981; Hayek et al., 1997).

Several research groups have studied the ring opening reaction of decalin (Corma et al., 2001; McVicker et al., 2002; Santikunaporn, 2004; Kubicka et al., 2004b; Mouli et al., 2007, 2009) on metal loaded acidic catalysts. The rate of ring opening of two six-member ring molecules such as decalin is much slower than that of the five-member ring compounds (McVicker et al., 2002). Brønsted acid sites are responsible for the cleavage of *C-C* bonds in decalin by the formation of carbenium ions (Corma et al., 2001). Ring contraction is an essential step for the ring opening of decalin (Kubicka et al., 2004a, b; Santikunaporn, 2004). Controlling the inter-conversion of six- and five-member rings via an acid-catalyzed ring-contraction step is of special importance because selective conversion of six-member naphthenic rings to five-member rings considerably influences the ring opening rates and selectivity (Santikunaporn, 2004).

The selection of reaction conditions is an intriguing issue and needs to be justified by theoretical calculations to minimize the experimental complexity. It is therefore important to see the thermodynamic limitations on the product yields and selectivity of ring opening reactions. The objectives of this work are to (i) analyze, using thermodynamic functions, the endocyclic cracking of naphthenes as compared to that of the acyclic and exocyclic cracking, (ii) calculate thermodynamic equilibrium composition of the multicomponent mixture obtained from hydrocracking of decalin, and (iii) investigate, using the

thermodynamic predictions, the effect of temperature on the yield and selectivity of ring opening products of decalin.

Ring opening of naphthenic molecules is an area of immense interest to us as well as to other catalysis researchers due to the processing difficulties of heavy oil and bitumen fractions having high concentration of aromatics and naphthenes. Catalyst researchers are facing a problem in achieving higher selectivities of ring opening products. There are two ways in which this problem can be researched upon: (i) continue developing new/improved catalyst formulations, (ii) analyze from a thermodynamic and kinetic perspective on root cause of the problem for not able to achieve higher yields and selectivities. We have taken the second approach in our present work in order to obtain useful and fundamental information about process variables from thermodynamic analysis of ring opening reactions.

2.6 Quantum chemical simulations

Achieving higher ring opening yields from naphthenic molecules is a challenge to the researchers as these are hampered by exocyclic cracking reactions such as side chain cracking and dealkylation (Mcvicker, 2002). Thermodynamic studies show that side chain cracking and dealkylation reactions are more favored than the ring opening reactions. Cycloparaffins ring opening can be catalyzed on the Brønsted acid sites via carbenium intermediates through protolytic cracking (Galperin, 2003). The high cetane number ring opening products are resulted from the endocyclic C-C bond breakage of the cyclic compounds. The endocyclic C-C bond cracking in cycloparaffins is much slower than in aliphatics (Weitkamp, 1984). This is due to the recyclizing tendency of the alkenyl cation formed by the β-scission of a cycloalkyl cation or because of a lower

bscission rate in cylcoalkylcarbon ions caused by an unfavorable orientation of the p-orbital at the positively charged carbon atom and the bond to be broken. As a result, the overall ring opening rates are predominated by isomerization and subsequent dealkylation of side chains of cyclic hydrocarbons, particularly of those having substituents with more than five carbon atoms, leading to significant dealkylation of pendant substituents on the ring. Consequently the ring opening yields are low due to the undesired dealkylation reactions which are confirmed in the literature (Kubicka, 2004a; kubicka, 2004b; Arribas, 2002; Arribas, 2004; Nylen, 2004). Kinetic information on elementary steps and associated energetics of dealkylation and ring opening reactions of naphthenes on the surface of solid acid catalysts is not available in the open literature. Ring protonated propylcyclopentene yields a stable secondary carbenium ion upon dealkylation in the gas phase and is an important intermediate in ring opening reactions. The present study aims to understand the detailed kinetic mechanism of the dealkylation and ring opening reaction of propenylcyclopentane in gas phase and on a Brønsted acid site using Hartree-Fock and Density Functional Theory (DFT) methods.

From the above literature review it is evident that a suitable catalyst is yet to be derived for the selective ring opening of the naphthene molecules. The chemistry of the ring opening reactions shows that the potential pathway for the ring opening is through the exocyclic or endocyclic C-C bond breaking. To achieve the objective of this work i.e the selective ring opening of the naphthenic molecules, a careful literature survey was conducted to select the suitable catalyst. The mechanism of SRO reactions suggests that the Brønsted acid sites are required to the formation of both the isomerization and the ring opening products (Kubica, 2004a&b). From the ring opening mechanism, it is

evident that skeletal isomerization is needed prior to ring opening. The zeolite supported metal catalysts with their acidity enhance the isomerization rate from six to five membered rings and leads to ring opening (Mc.Vicker, 2002). Mc.Vicker at al showed that ring opening rate of alkyl substituted $C_6 - C_{10}$ mono-naphthenes on Ir catalyst was decreased with extent of alkyl substitution and directly proportional to number of secondary-secondary C-C bonds. The same authors observed that Pt is more active in breaking the substituted C-C bonds but were sensitive to the cis to trans ratio of methyl substituted cyclopentanes and decreased with increasing trans isomer concentration.

Ring opening of more complex molecules containing two fused rings is investigated less. It was reported that Pt/MCM-41 was suitable for simultaneous hydrogenation and ring opening of di-aromatics because Pt/MCM-41 is mildly acidic and having uniform mesopore size distribution and high surface area. From the literature review it was found that metal and acid site promoted hydrocracking and dealkylation reactions must be avoided to minimize the losses in the middle distillate yield. Selective ring opening of both the five and six membered rings is an essential reaction. Secondary isomerization of product alkanes must be avoided, as increased branching greatly reduces the cetane values. It has been identified in the literature, that selective ring opening catalyst should meet the following properties: (1) should be mildly acidic, so that the unwanted cracking reactions can be avoided, (2) should have high surface area, (3) The pore size should be in the mesopore range, so that the multi ring aromatic compounds can penetrate easily into the pores, (4) Should have high thioresistance, and (5) It should have low selectivity towards (i) hydro cracking and dealkylation reactions, and (ii) secondary isomerization of product alkanes which will increase branching and reduces the cetane

values. Ir-Pt and Ni-Mo carbide are the best candidates available in the literature having all the above mentioned properties to achieve the better ring opening yields and selectivities. A different set of acidic supports such as Zr-MCM-41, Al-SBA-15, HY, H-beta, Si-Al are selected as supports due to their mild acidic nature.

2.7 Knowledge gaps

From the the literature review the following knowledge gaps were outlined.

1. Model compounds are mostly used as feed to study ring opening reactions. Reports on real feed is rare in literature.

2. The catalysts which can selectively open both five and six carbon ring naphthenes simultaneously are not reported.

3. No report is available on selective ring opening of naphthene using bifunctional catalysts containing both Pt and Ir supported on Zr-MCM- 41.

4. No report is available on selective ring opening of naphthenes using Ni-Mo carbides supported on HY and H-beta catalysts.

5. Thorough kinetics of the SRO is not available in the literature.

6. No attempt is made in the literature to examine the energitics of elementary steps in competitive ring opening and dealkylation reactions.

7. No report in the open literature is available about the thermodynamic feasibility of ring opening of decalin.

2.8 Hypothesis

1. The use of ring opening catalyst comprising Ir in combination with Pt will be effective for opening both five and six membered naphthene ring-containing compounds and also substituted naphthenic compounds.

2. The less acidic mesoporous supports such as Zr-MCM- 41 and Al-SBA -15 allow largest naphthenic feed molecules (decalin) to access the active sites which would lead to selective ring opening of naphthene molecules and prevent undesirable cracking activity.

3. Thermodynamic equilibrium calculations give better insight into the thermodynamic limitations on ring opening reactions.

4. Ni-Mo carbides have better sulfur resistance with similar range of hydrogenation activity as noble metals and in combination with acidic supports such as HY and H-beta give better ring opening yields.

5. Molecular level simulations on energetics of dealkylation and ring opening reactions give better insight about the feasibility of these competitive reactions

2.9 Objectives

The overall objective of this work is to develop new catalyst system for ring opening of naphthene molecules present in heavy gas oil obtained from Athabasca bitumen.

The sub objectives of this work are as follows

1. Study the selective ring opening reaction of model compound decalin reaction on catalysts Pt-Ir catalysts supported on mesoporous Zr-MCM-41.
2. Thermodynamic equilibrium analysis of decalin ring opening reaction.

3. Compare the selective ring opening reaction of model compound decalin reaction on Pt-Ir catalysts supported on HY and H-beta zeolites and Ni-Mo/carbide catalysts supported on HY, H-beta, γ-alumina, Al-SBA-15 and silica-alumina.
4. Study the Athabasca bitumen derived hydrotreated light gas oil (HLGO) on the best catalysts in the studied range for fuel quality improvement and study the kinetics on the best catalyst at optimum conditions.
5. Study the energetics of the competitive ring opening and dealkylation reactions using quantum chemical simulations.

2.10 Research methodology

The detailed research methodology was discussed in five phases.

Phases I: Study the selective ring opening reaction of model compound decalin on catalysts Ir-Pt supported on mesoporous Zr-MCM-41

Zirconium doped MCM-41 synthesis will be optimized by varying the synthesizing parameters such as time of reaction and temperature. The Si/Zr ratio will be varied for getting the optimum acid strength. The sodium form of Zr-MCM-41 will be transformed to NH_4-form by the ion exchange method using ammonium chloride solutions. The supports will be completely characterized by small angle XRD, TPD and BET surface area.

Different wt.% of Ir and Pt will be loaded on Zr-MCM-41 using wet co-impregnation technique. The different catalysts will be prepared with 0-1.75 wt. % Ir in combination with 0 to 1.75 wt. % Pt using statistical design software for minimization of experiments. Important physical and chemical properties of the catalysts are crystallinity, surface area, pore volume, elemental composition, surface morphology, reducibility of

metals, acid site strength, oxidation states of metals impregnated and thermal stability. These properties will be estimated by using using various characterization techniques such as BET surface area, pore volume and pore size distribution, CO chemisorption, TPR, TPD, ICP, TGA and FTIR. The catalysts which would meet the targeted range of physiochemical properties will be tested for selective ring opening of model compound decalin. Bitumen derived heavy gas oil contains complex naphthenic compounds with more than one fused rings. Therefore, decalin is chosen as a model compound as it represents fused saturated naphthenic compound. Catalyst performance will be tested using decalin as a feed in a trickle bed reactor at the temperature, pressure and liquid hourly velocity (LHSV) of 200-350 °C, 3-6 MPa and 1 h^{-1}, respectively. H_2 to feed ratio will be maintained at 600. The 10% solution of decalin in dodecane will be used as a feed. Dodecane will be used as an internal standard as it would not participate in the reaction and can be used an internal standard for calibration of GC and GC-MS. Process conditions will also be optimized for maximum selective ring opening products. The product analysis will be carried out by using GC and GC-MS.

The probable outcome from this study will be the development of best ring opening catalyst for model compound decalin. As mesoporous materials have large pore diameter, the heaviour molecules in the heavy gas oil can have access to the active sites inside the pores and higher activities can be achived. Mild acidity of Zr-MCM-41 supports will minimize the unwanted secondary cracking reactions. The main disadvantage of these catalysts is their low thermal stability and deactivates fast in the presence of sulfur.

Phases II: Thermodynamic equilibrium analysis of decalin ring opening reaction

Thermodynamic equilibrium calculations will be performed on ring opening of decalin with an assumption that the reaction mixture behaves as an ideal gas. The list of products that should be considered in the equilibrium calculations will be obtained from the experiments in phase 1. The quantum chemical method, G3MP2, will be used to calculate the standard free energy change of formation for compounds for which the thermochemical data are not available in the open literature. Thermochemical properties of individual endocyclic, acyclic and exocyclic cracking of naphthenes will also be studied. The ratios of equilibrium constants for individual endocyclic cracking reactions over exocyclic and acyclic cracking reactions with increasing temperatures will be studied. The equilibrium calculations will reveal the effect of temperature and pressure on selectivity of ring opening products of decalin. Equilibrium calculations will also give information about the thermodynamic limitations on ring opening reactions.

Phases III: Study the selective ring opening reaction of model compound decalin on catalysts Ir-Pt and Ni-Mo carbide supported on HY, H-beta, γ-alumina, silica-alumina and Al-SBA-15.

In this phase of study effect of Ir-Pt on other supports such as HY, H-beta will be studied on model compound decalin. Pt and Ir catalysts are costly and prone to sulfur poison. In order to develop cheap catalyst system, Ni-Mo carbide catalysts supported on HY, H-beta, Al-SBA-15 and silica-alumina will also be tested with model compound decalin for ring opening yields. The optimum percentage of Ir and Pt loadings on the supports will be used based on the experiment conducted in phase 1. The preparation and characterization of catalysts and the ring opening reaction over decalin feed follow same

methodology described in phase 1. A comparison will be made between the Ir-Pt and Ni-Mo carbide catalysts. The best catalysts from the phase 1 and phase 3 studies will be selected and used for studies with real feed.

Phases IV: Study the Athabasca bitumen derived hydrotreated light gas oil (HLGO) on the best catalysts in the studied range for fuel quality improvement.

Hydrotreated light gas oil will be supplied by the NCUT, Devon. It is well known fact that Ir and Pt are less sulfur resistant and the real feed needs pretreatment for sulfur and nitrogen removel to compare the ring opening activity of different catalysts. Therefore, hydrotreated light gas oil will be used as feed. The preparation and characterization of the catalysts follow the same methodology discussed in phase 1 and 3. The three best catalysts selected will be tested on HLGO in a downflow trickle bed reactor. The boiling point distribution of the product samples will be calculated by running simulated distillation unit. The quality improvement of the fuel LGO will be tested by calculating cetane index using ASTM D6352 method. The best catalyst under the studied conditions will be further tested by varying the LHSV and temperature in the range of 0.5-2 h^{-1} and 200-375 °C, respectively. Percentage of aromatics, naphthenes and paraffins present in the feed and products will be calculated from the proton NMR study based on the method described in the literature (Kapur, 2000). The kinetic parameters will be calculated based on the best performance catalyst activity by changing the operating variables temperature and LHSV.

Phases V: Study the energetics of the competitive ring opening and dealkylation reactions using quantum chemical simulations.

In this phase molecular level simulations will be carried out on the propenylcyclopentane molecule to see the energetics of the ring opening and deaakylation reactions. The calculations will be performed in gas phase as well as on Brønsted acid sites. The dealkylation and ring opening reaction of propenylcyclopentyl ion will be examined in the gas phase by using HF and DFT-PBEPBE level theories using standard 6-31G (d) basis set. The "ab initio" quantum calculations will be performed by using GAUSSIAN 03 program (Frisch, 2003). Studies on the mechanisms of catalytic reactions were modeled using Brønsted acid sites on zeolites in the form of cluster models successfully (Sauer, 1994; Kramer, 1995; Blaszkowski, 1997). Different levels of theories will be used to compare the results. In this study a simple 1T and 5T clusters were used to represent the immediate vicinity of the acid site present in zeolites, where 1T and 5T contains one and five hetero atoms. Due to the relatively large size of hydrocarbon fragments small size cluster 1T (H(OH)AI(OH)) and medium size cluster 5T ($OH_3Si(OH_3Si)A1(OH_3Si)OHSiH_3$) will be used to model the Brønsted acid sites of the zeolites. The structures of the reactants, products and transition states will be determined using ab initio electronic molecular techniques. Thermochemical properties (ΔH_f^0, ΔS_f^0, and C_p^0) for all the reactions are calculated from energy and frequency calculations (Foresman, 1996). The rate constant is calculated from transition state theory. The out come of this study will be useful to the academic as well as industry people to realize the energetic of the lementary steps involved in the ring opening and dealkylations reactions.

3 EXPERIMENTAL

This chapter contains a discussion on catalysts preparation and characterization in detail. A detailed description about the statistical design of experiments, the experimental plan and procedure including operation of the fixed bed reactor and apparatus used to obtain data in this work. A discussion of the feed and product analysis is also included in this chapter.

3.1 Catalyst preparation

This section gives a detailed description about the preparation of the catalysts used in this work. Catalyst preparation methods are very diverse and each catalyst may be produced via different routes. Several successive steps are involved in the preparation of catalysts. All supported metal and oxide catalysts are prepared by the succession of impregnation, drying, calcinations and activation. Zeolite catalysts are prepared by precipitation of gel, crystallization, washing, ion exchange and drying. There are three fundamental stages of catalyst preparation namely preparation of first precursory solid associating all the useful components (e.g., impregnation or co-precipitation, or, in the case of zeolites, crystallization), processing of that primary solid to obtain the catalyst precursor, activation of the precursor to give the active catalyst and reduction to metal.

3.1.1 Zr-MCM-41 support preparation

A wide range of synthesis conditions, including initial gel composition, pH, time of synthesis and temperature were used to prepare Zr-MCM-41 materials, as shown in Figure 3.1.1. The materials used in the synthesis were sodium silicate solution ($Na_2Si_3O_7$, Aldrich) as silica source and zirconium nitrate ($Zr(NO_3)_4$, Aldrich) as zirconium source.

The template used for the preparation of Zr-MCM-41 was hexadecyltrimethylammonium bromide (CTMABr, Aldrich). The aqueous solution of sodium silicate was added to the zirconium nitrate under vigorous stirring and then the aqueous solution of template was added and the required pH was adjusted by adding 1M hydrochloric acid. The final composition of the gel mixture was $xZrO(NO_3)_2$:$1SiO_2$:$0.67Na_2O$:0.2CTMABr:$102H_2O$. After stirring for 3 h at room temperature, the resulting gel was introduced into the teflon lined stainless steel autoclave.

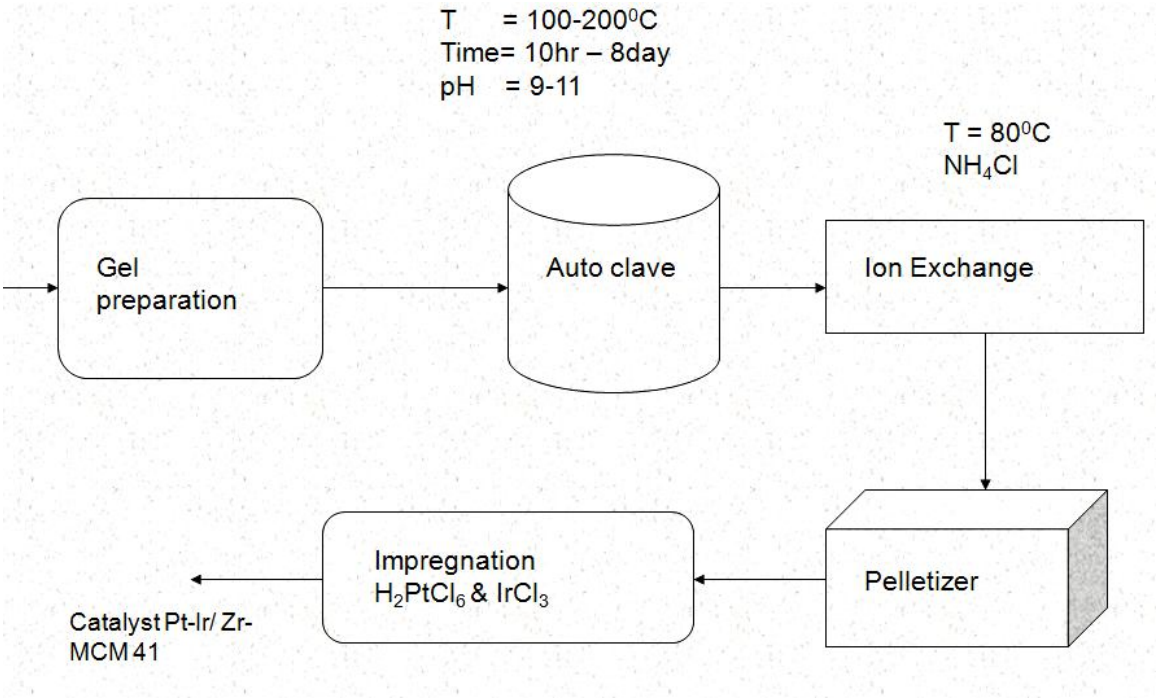

Figure 3.1.1: Schematic representation of preparation of Ir-Pt/Zr-MCM-41

The synthesis conditions were optimized by varying the temperature from 100 to 200 °C, pH from 9 to 11 and time from 1 to 8 days. The resulting crystalline product was washed with water many times to remove the template molecules and dried at 120 °C. The as-synthesized material was calcined at 550 °C at heating rate of 3 °C per minute. As

synthesized Na-form of Zr-MCM-41 was ion exchanged by 1M NH_4Cl solution at 80 °C and calcined at 550 °C for 5 hours to convert into proton form.

3.1.2 Impregnation of Ir-Pt on Zr-MCM-41

Response Surface Method (RSM) of statistical experimental design was used for the catalysts syntheses with the aim of optimizing the parameters for high catalyst activity. The Central Composite Circumscribed (CCC) of RSM was chosen to provide high quality predictions over the entire design space with minimum number of experiments.

The proton form of Zr-MCM-41 was used as a support to prepare Ir (0-1.5%) and Pt (0-1.5%) bimetallic catalysts. The precursors for iridium and platinum were $IrCl_3$ (Aldrich) and H_2PtCl_6 (Aldrich). The aqueous solution of iridium and platinum precursors was prepared and impregnated on the support by incipient wetness impregnation method. The impregnated catalysts were calcined for 3 h at 500 °C in the presence of air.

3.1.3 Ir-Pt catalysts supported on HY and H-Beta catalysts

The NH_4 form of HY and H-Beta (Zeolyst International) were calcined at 500 °C to be converted to the proton form. The 1.5%Pt-0.75%Ir supported on HY and H-Beta were prepared by using precursors $IrCl_3$ (Aldrich) and H_2PtCl_6 (Aldrich). The aqueous solution of iridium and platinum precursors was prepared and the supports were impregnated with the solution by the incipient wetness method. The impregnated catalysts were calcined for 3 h at 500 °C in the presence of air.

3.1.4 Ni-Mo carbide catalysts supported on HY, H-Beta, γ-Alumina, Al- SBA-15 and silica-alumina catalysts

The Ni-Mo carbide (2.5 wt% Ni and 12 wt% Mo) catalysts supported on commercial HY, H-Beta, silica-alumina, γ-alumina and also Al-SBA-15 synthesized in our laboratory were prepared in two stages. The Al-SBA-15 synthesis and characterization are reported in our previous work (Sundaramurthy, 2008). In the first stage, the oxide form of the catalysts was prepared by the wet impregnation method from the precursors. The precursors for Ni and Mo are nickel nitrate (99% BDH) and ammonium heptamolybdate (99.9% Aldrich). The impregnated catalysts were dried at 120 °C for 5 h and calcined at 500 °C for 5 h. 20% CH_4/H_2 (v/v) was used to convert the oxide form catalysts into the carbide form. In the setup used to synthesize the carbide form of catalysts, the oxide form catalyst was placed at the center of an inconel reactor which is surrounded by a temperature-programmed furnace. The temperature program used for carbidation process is shown in Figure 3.1.2. The sample was heated from room temperature to 400 °C in the presence of He at a ramping rate of 3 °C/min. Then, the gas is switched to 20% CH_4/H_2 (v/v) and the sample was heated up to 700 °C at a ramping rate of 1°C/min. Outlet gases from the reactor were analyzed for CO and CO_2 by using a gas chromatograph (HP 5890). The reaction was carried out until there was no formation of CO and CO_2. Then the gas was shifted to He from CH_4/H_2 and the system was cooled down to room temperature. The carbide catalysts were passivated by using 1%O_2 in He (v/v) for 4h to avoid strong bulk oxidation. The synthesis and characterization of Ni-Mo/γ-alumina carbide catalysts are reported in our earlier paper (Sundaramurthy, 2007).

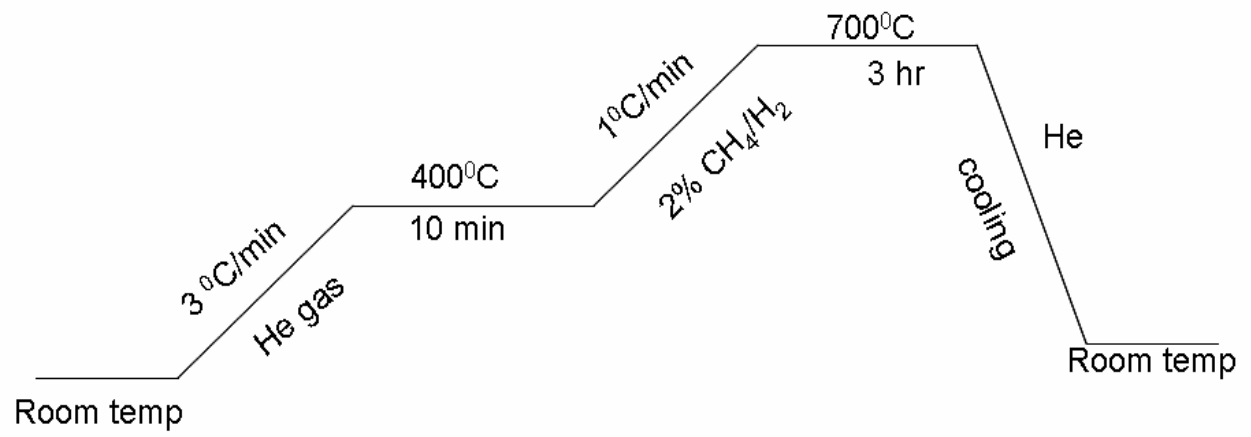

Figure 3.1.2: Schematic representation of carbidation of Ni-Mo catalysts

3.2 Catalyst characterization

The complete and accurate knowledge of the properties of a catalyst is fundamental for evaluating its performance. Detailed information on the texture (specific surface area, pore volume distribution), crystal phases, active element dispersion, specific activity and selectivity, is not always available or has varied to a great extent since the start-up of the reactor. A full characterization of the catalyst is needed if an optimization of the process conditions is desired, or if a change of the catalyst, of its texture or the dispersion of the active elements is needed. In order to achieve the above said characteristics, a detailed description of the various catalyst characterization techniques is presented in this section.

3.2.1 Powder X-ray diffraction

Powder X-ray diffraction (XRD) studies were performed at low angle of 2θ to characterize mesoporous support. XRD analysis was performed using Rigaku diffractometer (Rigaku, Tokyo, Japan) using Cu Kα radiation filtered by a graphic

monochromator at a setting of 40 kV and 130 mA. The powdered catalyst samples were smeared on glass slide with methanol and dried at room temperature. The X-ray diffraction analysis was carried out in the (2θ) range of 1.5–10° at a scanning speed of 0.2°/min.

3.2.2 BET surface area, pore volume and pore size measurements

The BET surface area, pore volume and pore size measurements of the Zr-MCM-41 and Ir-Pt/Zr-MCM-41 catalysts were performed using a Micromeritics adsorption equipment (Model ASAP 2000, Micromeritics Instruments Inc., Norcross, GA, USA) at 78 K using liquid N_2. Before analysis, sample (0.1 g) was evacuated at 200 °C for 4 h in a vacuum of 5×10^{-4} atm to remove all adsorbed moisture from the catalyst surface and pores.

3.2.3 Temperature programmed desorption

The temperature programmed desorption (TPD) of ammonia was performed using Quantachrome equipment (Model ChemBET 3000, Quantachrome Corporation, FL, USA) for the measurement of the acidic properties of catalysts. 0.1 g sample was placed in an adsorption vessel (U-shaped) and heated to 450 °C in He flow for 1h (heating rate 10 °C/min). Then it was cooled to 100 °C in He flow. At this temperature 0.1% NH_3 in N_2 was passed through the sample for 1 h. Then, NH_3 gas was shifted to He and cooled to room temperature. TPD was run from room temperature to 500 °C at heating rate of 10 °C /min with He flow at 35 ml/min. The calibration of TPD instrument for the amount of ammonia adsorbed is shown in Appendix A.

3.2.4 Thermo gravimetric Analysis

A PerkinElmer TG/DTA thermogravimetric differential thermal analyzer was used to analyze the thermal stability of the impregnated supports. The temperature heating rate was fixed at 10 °C/min and argon flow rate of 100 ml/min was used.

3.2.5 Transmission electron microscopy

The morphology of samples was studied by transmission electron microscopy (TEM). Sample specimens for TEM studies were prepared by ultrasonic dispersion of the catalysts in ethanol, and the suspensions were dropped onto a copper grid. TEM investigations were carried out using a Hitachi H-7500 (120 kV). Several TEM micrographs were recorded for each sample and analyzed to determine the particle size distribution.

3.2.6 Temperature programmed reduction

Temperature programmed reduction (TPR) analysis was performed using Quantachrome equipment (Model ChemBET 3000, Manufactured by Quantachrome Corporation, FL, USA). The sample U tube containing 0.1 g of catalyst was placed in an electric furnace and heated from 30 to 600 °C at 10 °C/min and one atmosphere pressure in a reducing gas of 3 mol% H_2 in N_2 (obtained from Praxair, Mississauga, Ont., Canada) with a flow rate of 30 mL/min. H_2 consumption during the TPR experiments was measured with a thermal conductivity detector (TCD). The TPR plots were logged using an on-line data acquisition system.

3.2.7 Diffuse Reflectance Infrared Fourier transform spectroscopy (DRIFTS) of CO adsorption analysis

Diffuse Reflectance Infrared Fourier transform spectroscopy (DRIFTS) of CO adsorption analysis was performed using a Perkin Elmer FTIR spectrometer with insitu DRIFT cell (thermo spectra cell). Powdered sample (5 mg) was reduced with hydrogen at 400 °C for 1 h in in-situ DRIFT cell, cooled to 30 °C in the presence of He gas. After taking the background with helium, CO adsorption was carried out for 20 min and then purged with He for 15 minutes before recording the final spectrum. All spectra were recorded after 64 scans at a resolution of 4 cm^{-1} in order to achieve desired signal to noise ratio.

3.2.8 Diffuse Reflectance Infrared Fourier transform spectroscopy (DRIFTS) of NH_3 analysis

Diffuse Reflectance Infrared Fourier transform spectroscopy (DRIFTS) of NH_3 analysis was performed using a Perkin Elmer FTIR spectrometer with in-situ DRIFT cell (thermo spectra cell) following the above procedure of CO adsorption with NH_3 gas instead of CO.

3.3 Experimental plan

Decalin (10% by volume) in n-heptane was used as the feed. 13 catalysts (4 repeats) will be synthesized by using CCC statistical design by varying the Ir and Pt composition. 5 ml of catalyst diluted with SiC will be loaded in the isothermal region of the reactor. The reactor calibration for temperature and calibration of mass flow controller is shown in the Appendix A. The catalyst is reduced in-situ using H_2 at 400 °C for 3 hours. Temperature, pressure, LHSV and H_2/feed will be varied and the products will be collected and analyzed. Temperature and pressure will be varied from 300 - 400

°C and 2000 - 6000 KPa respectively. LHSV is kept at 1 h^{-1}. The reaction will be carried out for 7 days before being deactivated

Same feed was used for studies on Ir-Pt/HY, Ir-Pt/H-Beta and Ni-Mo carbide catalysts. Temperature was varied from 200 to 300 °C. The reaction was carried out for 7 days on each catalyst to see the product distribution at different temperatures. At the end of the runs with all the catalysts, the best catalysts with each category were tested for thio- tolerance.

The best catalysts from the above screening studies were selected for real feed studies. Hydrotreated LGO was used to test the effect of catalysts on the improvement of cetane index. The best catalyst from the screening studies was selected to study the kinetics using the real feed. For kinetics study, different runs were conducted by varying the parameters such as temperature and LHSV.

3.4 Experimental setup

3.4.1 Reactor description

The Catalytic experiments were performed in trickle bed reactor under typical industrial conditions which is shown in Figure 3.4.1. The high pressure reaction set up used in this study simulates the process that takes place in industrial hydrotreater. As shown in Figure 3.4.1, the system consisted of liquid and gas feeding sections, a high-pressure reactor, and a furnace with temperature controller for precisely controlling the temperature of the catalyst bed and a high pressure gas–liquid separator. The length and internal diameter of the reactor were 240 and 14 mm, respectively.

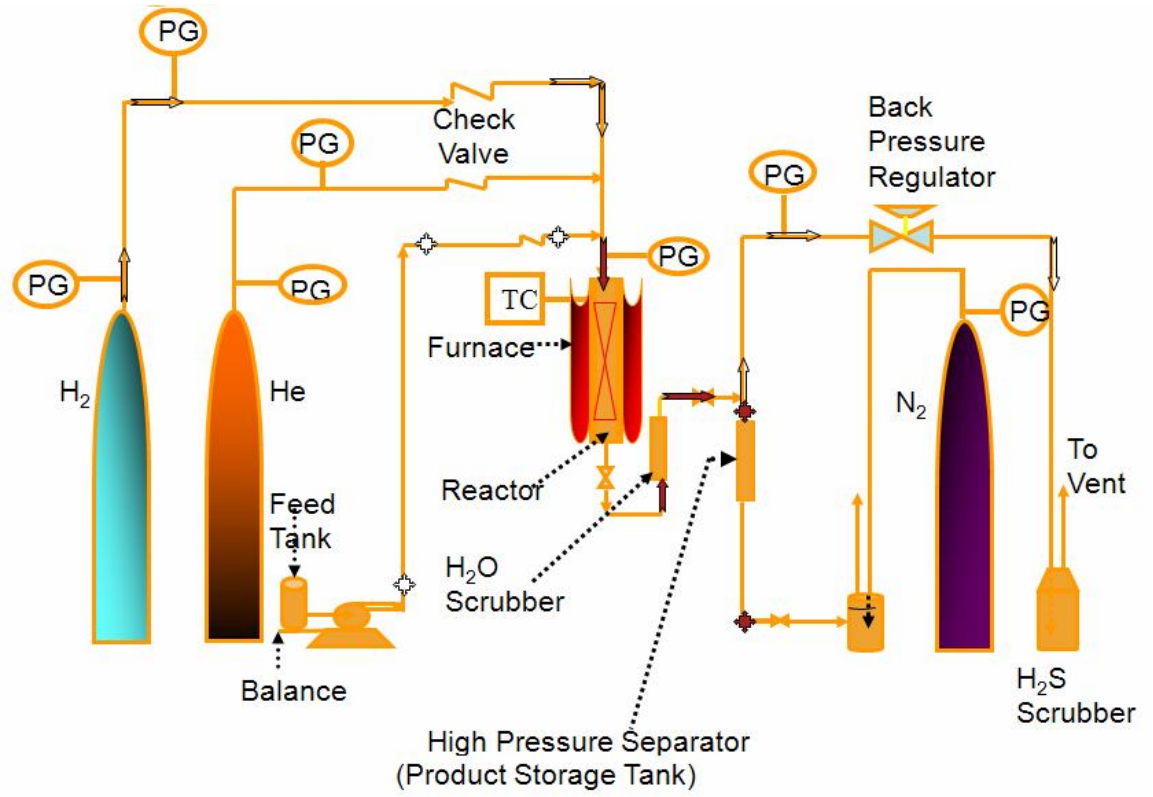

Figure 3.4.1: Experimental setup

A back pressure regulator is provided to control the pressure in the reactor and a mass flow controller is used to control the flow rate of hydrogen into the system. A water scrubber is provided immediately after the reactor to remove the hydrogen sulfide. A variable feed pump is used to control the feed flow rate.

3.4.2 Catalyst loading

For loading the catalyst, the reactor was packed from bottom to top in nine parts as shown in Figure 3.4.2.

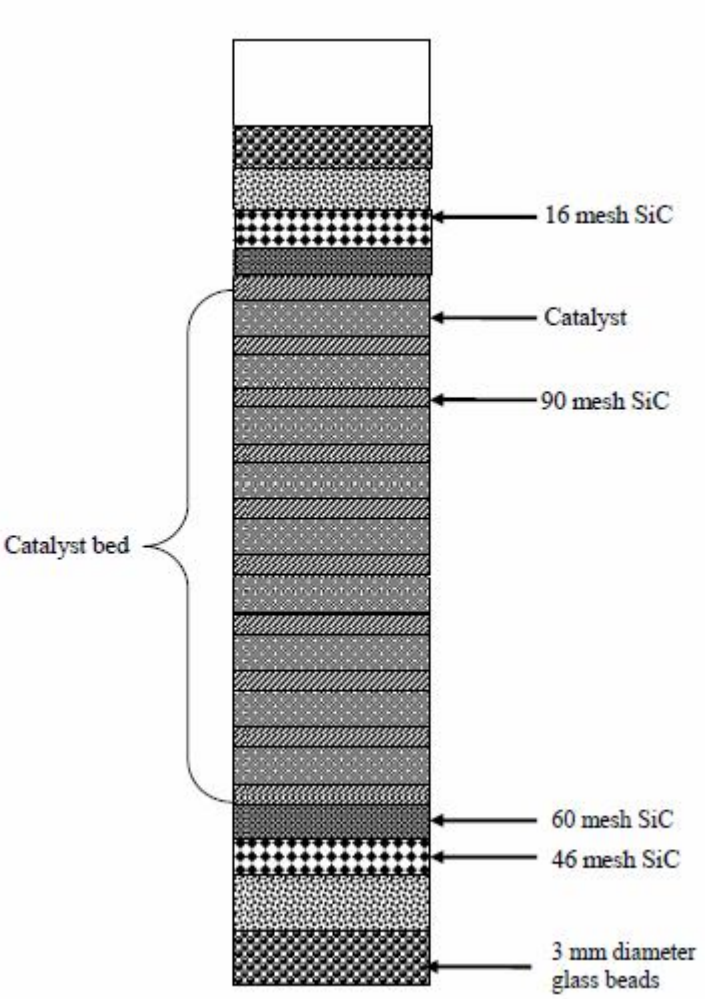

Figure 3.4.2: Schematic diagram of catalyst loading in the reactor

The bottom 7 cm was first loaded with 3 mm size glass beads, 16 mesh, 46 mesh and 80 mesh silicon carbide. Then the catalyst bed approximately 10 cm long, was packed with 5 cc of catalyst (2 g) and 12 cc of 90 mesh silicon carbide.The top part of the catalyst bed was loaded with 80 mesh (0.8 cm), 46 mesh (0.8 cm), 16 mesh (0.8 cm) silicon carbide and finally with 3.5 mm glass beads (2.0 cm). Then the reactor was placed in the unit. Before each catalytic run, the Ir-Pt/Zr-MCM-41 catalysts were reduced in

flowing H_2 at 400 °C for 4 h. The reactor was then brought to the reaction temperature and pressurized to 5 MPa

3.4.3 Typical reaction run

A typical reaction run is shown in table 3.4.1.

Table 3.4.1: Typical reaction run data sheet

Operator: Mouli **Date:**

Catalyst: **Feed:**

Date	Time	TOS	Hydrogen system pressure (psig)				Temperature Deg C		Pump Set point	Oil wt(g)	Oil Flow rate (g/h)	H_2 MFM Reading %	LHSV (h^{-1})	Remark
D:M:Y	(h)	(h)	Cylinder	PG1	PG3	PG4	Furnace	Reactor						

The samples are collected periodically and the information is saved in the data sheet shown below. LHSV of the feed is being changed gy varying the feed pump set point.

3.5 Analysis of product samples

3.5.1 Gas Chromatography– Mass Spectroscopy (GC-MS)

The liquid products were collected and were identified by using GC-MS. The GC was equipped with a Varian CP-Sil 8 CB low bleed / MS capillary column (30m-0.25mm-0.25µm) which is coated with a 5% phenyl 95% dimethylpolysiloxane low bleed phase. The following temperature program was used for GC-MS: initial temperature 50

°C, initial temperature hold time of 5min, heating rate of 10 °C/min, final temperature of 200 °C, final temperature hold time of 10 min and the detector temperature of 230 °C.

3.5.2 Quantification of hydrocarbons by GC

The same capillary column and temperature program are used for the Varian 3400 GC for the quantification purpose.

3.5.3 Simulated distillation

The products from the hydrotreated LGO conversion on the catalysts were analyzed by simulated distillation and proton NMR. Simulated distillation was performed using ASTM D6352 method in order to study the boiling range distribution of different product samples at different temperatures using a Varian model CP3800 gas chromatograph coupled to a Varian CP 8400 auto sampler. A capillary column (10 m x 0.53 mm diameter x 0.88 mm nominal film thickness) was used to separate hydrocarbons present in different product samples based on the order of their boiling range. To identify different boiling fractions, a calibration curve was used which was obtained by chromatographic analysis of a mixture of known boiling point compounds. A flame ionization detector (FID) was used to detect different boiling ranges using helium as a carrier gas at a flow rate of 30 mL/min. The hydrogen and air flow were maintained at 35 and 400 mL/min, respectively. The detector temperature and oven final temperature were maintained at 375 and 380 C, respectively.

3.5.4 Cetane Number

Cetane number (CN) is commonly used to describe the ignition properties of diesel fuels. Cetane number is the performance rating of a diesel fuel, corresponding to the percentage of cetane ($C_{16}H_{34}$) in a cetane-methylnaphthalene mixture with the same ignition performance. A higher cetane number indicates greater fuel efficiency. The cetane number (CN) is measured using a standard diesel test engine according to ASTM D613 test method and is a function of both the chemical and physical characteristics of the fuel. Molecular structures of its constituent hydrocarbons influence the chemical properties. For example, CN generally improves with the presence of a high proportion of normal unbranched paraffins (C_nH_{2n+2}) in the fuel, especially those with long molecular chains. However, presence of cycloparaffins and aromatics reduces the CN. Since measurement of CN by standard engine testing requires special equipment as well as being time consuming and costly, they are estimated using mathematical correlations. The number derived is called the cetane index and is a function of the physical properties of the fuel such as the boiling point, aniline point, gravity and density of the sample. A product of high aniline point will be low in aromatics and naphthenes and, therefore, high in paraffins. There are number of correlations available for estimating cetane index. ASTM D976 and ASTM–D-4737 are the commonly used correlations for estimating cetane index. Use of these correlations have a number of limitations; it can only be applied to fuels containing no additives for boosting CN, they are also applicable to pure hydrocarbons and synthetic fuels although substantial inaccuracies may occur when used for estimating CI of crude oils, residuals or products having a low volatility. ASTM D 4737 is a newer method and this method calculates CI using a four variable equation

based on diesel's low, mid and high boiling points as well as density. Calculated Cetane Index is shown in eq. 3.5.1:

$$CI_{4737} = 45.2 + 0.0892T_{10N} + [0.131 + 0.901B]T_{50N} + [0.0523 + 0.420B]T_{90N} + 0.00049[T^2_{10N} - T^2_{90N}] + 107B + 60B^2 \quad \text{..... 3.5.1}$$

Where:

D = density at 15°C [g/mL] determined by Test Method ASTM D 1298,

$B = [e^{(-3.5)(D - 0.85)}] - 1$,

$T_{10N} = T_{10} - 215$, $T_{50N} = T_{50} - 260$, and $T_{90N} = T_{90} - 310$.

T_{10} = 10% distillation temperature [°C] determined by Test Method ASTM D 86 and corrected to standard barometric pressure,

T_{50} = 50% distillation temperature [°C] determined by Test Method ASTM D 86 and corrected to standard barometric pressure,

T_{90} = 90% distillation temperature [°C] determined by Test Method ASTM D 86 and corrected to standard barometric pressure,

3.5.5 Product analysis by ^{1}H NMR

Feed and product analysis was carried out directly from the proton nuclear magnetic resonance (^{1}H –NMR) spectroscopy. The spectra were obtained in the Fourier Transform (FT) mode operating at a frequency of 500 MHz. The instrumental conditions were: pulse delay of 4 s, sweep width of 27.7 kHz and inverse gated proton decoupling. Overall time for each sample was 12 minutes for 128 scans. Deuterated chloroform, $CDCl_3$ was used to dilute the samples.

4 METHODS FOR THEORITICAL CALCULATIONS

In **t**his chapter, section 4.1 gives the details about the internal and external mass transfer limitations and procedure for eliminating these resistances. Section 4.2 describes the theoretical background and equations involved in the thermodynamic equilibrium calculations by using Lagrangian multiplier method. This section also mentions about the calculation of thermo chemical properties of some compounds that are not available in the open literature. Section 4.3 describes in detail about the quantum chemical simulations and energetics of elementary reactions.

4.1 Development of kinetic model

Internal and external mass transfer diffusions contribute significantly on the reaction rate of heterogeneous catalytic reactions. As shown in Figure 4.1.1, external diffusion is important when the reactants have to diffuse from the bulk of the fluid to the surface of the catalyst pellet. Subsequently, internal diffusion is important when the reactants move from the surface to the internal parts of the pellet. These two resistances play a major role in the transfer rate of reactants to heterogeneous catalysts, and therefore, in the study of intrinsic rates of reaction. Therefore the effects of internal and external mass diffusion have to be eliminated to get the meaningful kinetic data. Otherwise, incorporation of the mass transfer parameters should take place in the reaction rate equation.

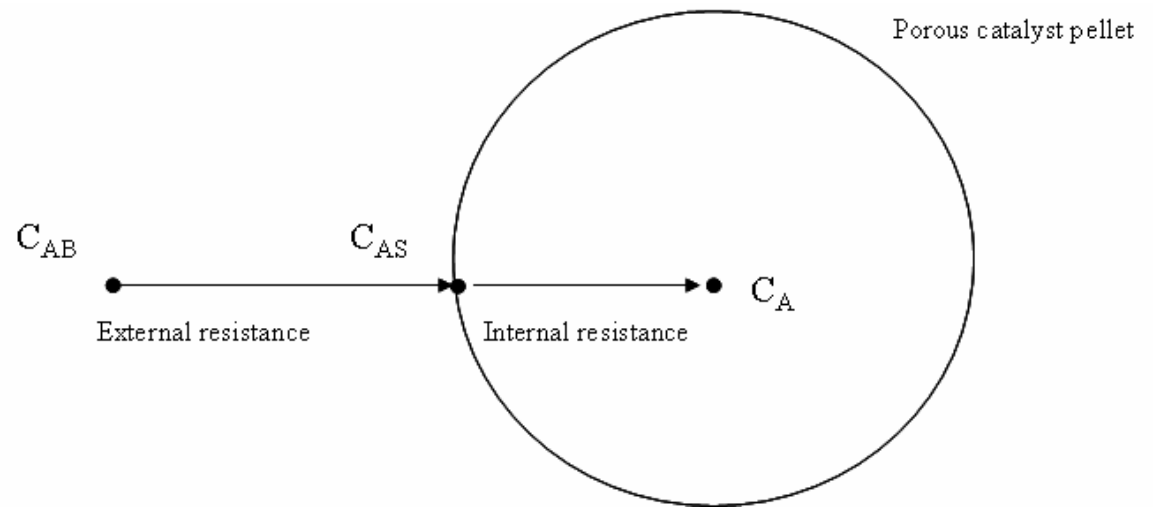

Figure 4.1.1: Mass transfer and reaction steps for a catalysts pellet.

4.1.1 External mass transfer limitations

In many industrial reactors, rate of mass transfer of bulk reactants and products between the bulk fluid and the catalyst surface is small and limits the overall rate of the reaction. Generally laboratory reactors should be operated at high fluid velocities or with small catalysts particle size to eliminate the external mass transfer resistances. To study the effect of external mass transfer limitation, Mears proposed criteria as follows.

$$C_m = \frac{-r'_A \rho_b Rn}{k_c C_{Ab}} \pi\ 0.15 \quad \text{.....4.1.1}$$

Where, C_m is the ratio of reaction rate to the external diffusion rate. r_A, ρ_b, R, n, k_c, and C_{Ab} are reaction rate per unit mass of catalyst (kmol/kg-s), bulk density of the catalyst bed (kg/m^3), catalyst particle radius (m), reaction order, mass transfer coefficient (m/s), and bulk concentration (kmol/m^3) respectively.

$$\rho_b = (1 - \varepsilon)\ \rho_c \quad \text{.....4.1.2}$$

ε = catalyst bed porosity,

ρ_c = catalyst density,

If C_m value is less than 0.15, the external diffusion resistance is negligible.

4.1.2 Internal mass transfer limitations

Catalytic sites present in the inner pore channels of the catalysts. The concentration of a particular reactant at the outer surface of the catalysts is different than the concentration at the inner channels as shown in Figure 4.1.2. If the diffusion through the channels is slow and the with low diffusion mass transfer coefficients, the overall rate of the reaction will be controlled by the internal mass transfer limitations. Effectiveness factor (η) is a parameter that describes the effect of internal diffusion resistance on the overall rate of the reaction.

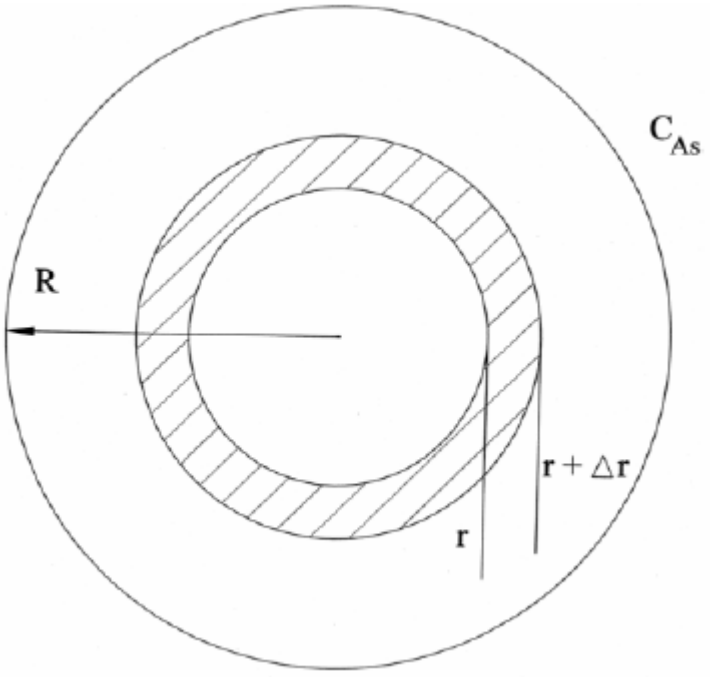

Figure 4.1.2: Internal mass transfer shell balance

η = actual overall rate of reaction/rate of reaction that would result if entire interior surface were exposed to the external pellet surface conditions C_{As}, T_s.

$$\eta = \frac{3}{\phi_1^2}\left(\phi_1 \coth \phi_1 - 1\right) \quad \text{……..4.1.3}$$

Where, ϕ_n is the Thiele modulus for nth order reaction.

$$\phi_n^2 = \frac{k_n \rho_c S_a C_{As}^{n-1} R^2}{D_e} \text{ = “a” surface reaction rate/”a” diffusion rate …… 4.1.4}$$

When the Thiele modulus is large, internal diffusion limits the rate of the reaction. If the Thiele modulus is small, surface reaction is rate limiting.

k_1 = rate constant for 1st order reaction, $(mol/m^3)^{n-1}(m/s)$

C_{As} = concentration of *A* at the catalyst surface (mol/m^3),

ρ_c = catalyst density (kg/m^3),

S_a = catalyst surface area (m^2/kg catalyst),

R = radius of catalyst particle (m),

and D_e = effective diffusivity (m^2/s).

$$D_e = \frac{D_{AB}\phi_p \sigma}{\xi} \quad \text{……4.1.5}$$

Where

D_{AB} = the bulk or Knudsen diffusivity of *A* in *B*, _

Φ_p = pellet porosity = (Volumeof void space/total volume (voids and solids)),

σ = construction factor,

and ξ = tortuosity (actual distance a molecule travels between two points/shortest distance between those two points).

The Weisz-Prater criterian uses the measured values of observed rate of reaction to determine whether the internal diffusion is significant or not.

Weisz-Prater parameter $C_{WP} = \eta \phi_n^2$ = actual reaction rate / "a" diffusion rate

$$C_{WP} = \frac{-r_{A(observed)} \rho_c R^2}{D_e C_{As}} \qquad \text{.....4.1.6}$$

If , $C_{WP} << 1$, no internal diffusion resistance

If , $C_{WP} >> 1$, internal diffusion limits the reaction.

4.1.3 Kinetic parameters estimation

The products detected from HLGO reaction have been grouped into naphthenes, paraffins and aromatics. Using lumps in kinetic modeling is a common practice (Sanchez, 2005). This lumping method is useful and less complex in predicting the effect of operating variables on the products that are of interest (Ancheyta, 2005). Moreover, the number of kinetic constants is limited and, hence, they can be accurately calculated. It is assumed that, under the conditions studied, no olefins are present in the product stream, due to severe hydrotreating conditions.

The kinetic constants, the activation energies and the reaction orders have been calculated by fitting the experimental concentrations *xi* to the values calculated by numerical integration of differential rate equations using Matlab R14 routines. The numerical integration of these equations has been carried out by using ode45 codes, while the minimization of errors by the *fminsearch* function, which finds the minimum of a scalar function of several variables, starting at an initial estimate. This is an unconstrained nonlinear optimization which uses the function sum of squares (SS).

$$SS = \sum_{i=1}^{N} (F_{Calc}(k, x_i) - F_{Exp})^2 \quad \text{.....4.1.7}$$

Where, N represents number of data points, F_{calc} and F_{exp} are model predicted and experimental values.

4.2 Thermodynamic equilibrium calculation of hydrocracking of decalin

The hydrocracking of a mixture of *cis*- and *trans*-decalin on catalyst Ir-Pt/HY yields more than 50 compounds, which are identified and quantified using an online GC-MS and a GC respectively.(Mouli et al., 2009). For thermodynamic equilibrium calculation, a total of 46 compounds are considered. The classical thermodynamic equilibrium problem calculates the mole numbers of the chemical species in a reaction mixture by minimizing the total Gibbs energy G^t with respect to the material balance constraints. Let n_i be the mole number of the chemical species i, a_{ik} be the number of atoms in the k th element of species i, and A_k be the total number of atoms of element k as determined by the initial composition of the system. The material balance constrains can be added to the total Gibbs energy by using Lagrangian multipliers λ_k for each element k and the resulting objective function is given by the following equation (Smith et al., 2005),

$$F = G^t + \sum_k \lambda_k \left(\sum_i n_i a_{ik} - A_k \right); \quad i = 1, 2, ..., N_S, \; k = 1, 2, ..., N_E \qquad \text{..... 4.2.1}$$

Where, N_S and N_E are the total number of chemical species and total number of elements respectively. By taking the first derivates of the function F in eq. 4.2.1 with

respect to variables n_i and λ_k and setting them to zero, a set of N_S nonlinear and N_E linear algebraic equations is obtained as given in equations 4.2.2 and 4.2.3 respectively.

$$\Delta G^0{}_{f_i} + RT \ln\left(\frac{n_i}{\sum n_i}\right) + \sum_k \lambda_k a_{ik} = 0 \qquad \ldots\ldots\ldots\ldots\ldots\ldots\ldots\ldots\ldots\ldots\ldots\ldots\ldots\ldots\ldots\ldots 4.2.2$$

$$\sum_i n_i a_{ik} - A_k = 0 \qquad \ldots\ldots\ldots\ldots\ldots\ldots\ldots\ldots\ldots\ldots\ldots\ldots\ldots\ldots\ldots\ldots\ldots\ldots 4.2.3$$

Equation 4.2.1 is valid for a mixture of ideal gases with a standard state pressure of P^0. Finding the solution of eqs 4.2.2 and 4.2.3 is straight forward provided standard Gibbs free energy change of formation $\Delta G^0{}_{f_i}$ and a set of suitable initial guesses for all the variables at required temperatures are available.

4.2.1 Calculations of thermo chemical properties

If the experimental values are not available for $\Delta G^0{}_f$ in the open literature for a particular compound, quantum chemical simulations can be effectively used to calculate the same. In this work the compound method *G3MP2*, (Curtiss et al., 1999) as implemented in the commercial software *Gaussian-03*, (Frisch et al., 2003) was used to calculate $\Delta G^0{}_f$ values. In general, errors in quantum mechanical calculations arise from limited correlation treatments and the use of finite basis sets. The *G3MP2* method attempts to minimize these errors by estimating the energy of a system at the fully correlated, complete basis set limit. This is done by approximating the basis set limit energy using a low-level correlation method (*MP2*) with large basis sets and full correlation using higher-level correlation (*QCISD(T)*) using small basis sets. The

combination of these methods gives an approach that can be applied efficiently to 20-30 atoms and gives results in agreement with experimental enthalpy of formation data with about 1-3% error (Curtiss et al., 1999).

Out of 46 compounds considered for equilibrium calculation in the present work, thermochemical properties are not available in the open literature for 12 compounds. For these 12 compounds, ΔH_f^0, ΔS_f^0, and ΔG_f^0 values calculated using G3MP2 values at temperatures 298 K, 400-1000 K. The thermochemical properties required at higher temperatures other than 298 K are calculated using the utility program "*freqchk*" in *Gaussian 03* with the zero point correction obtained from scaled (0.8929) *HF/6-31G(d)* frequencies (Curtiss et al., 1999).

4.2.2 Generation of initial estimates for the equilibrium problem

If the number of nonlinear and linear algebraic equations involved in equilibrium calculations is greater than 4 or 5, choosing initial estimates arbitrarily by trial and error for the mole numbers and Lagrangian multipliers can be time consuming. A systematic way has been suggested by Smith et al. (1968). In this procedure, a linear programming problem (*LP*) is first solved to get initial estimates for N_E (or $< N_E$) mole numbers which are then used to calculate the chemical potential for all N_S species. The methodology requires the generation of a set of independent reactions for the reaction mixture. From the set of independent reactions, equilibrium extents are calculated using total number of moles in the system, ΔG_f^0 and chemical potential for individual species, and stoichiometric coefficients of individual reactions. The *LP* solution and the equilibrium extents are finally used to calculate the initial estimates for N_S mole

numbers. This procedure has been used to obtain initial estimates for all 46 species involved in hydrocracking of decalin. A total of 44 independent reactions have been identified using row and column operations (Smith and Missen, 1979). Different sets of initial estimates have been calculated for different temperatures (at which the equilibrium problem is solved) because initial estimates calculated for one temperature did not work well with other temperatures. The *LP* problem and the set of nonlinear equations are solved using the commercial IMSL® Fortran Numerical Library routines *dlprs* and *neqnf* in double precision form.

4.3 Quantum chemical calculations

Molecular mechanics and electronic structure theory are two broad areas devoted to the structure of molecules and their reactivity. These two methods are capable of performing calculations like energy of a particular molecular structure, properties related to the structure, performing geometry optimizations which depend on the gradient of the energy and computing the vibrational frequencies of the molecules resulting from the interatomic motions within the molecules.

Molecular mechanics use the laws of classical physics whereas electronic structure methods use the laws of quantum mechanics. Molecular mechanics neglect the electrons means in the calculations. Therefore, they cannot treat chemical problems where electronic effects predominate. On the other hand electronic structure methods uses *ab initio methods*, uses no experimental parameters in their calculations and uses the first principles of laws of quantum mechanics and a small number of physical constants. *Ab initio methods* compute solutions to the Schrödinger equation using a series of mathematical approximations. Gaussian offers the entire range of electronic structure

methods to perform simulations on large molecule systems. Information about the structure of the intermediates, elementary steps and corresponding activation barriers obtained from this study are expected to help in rational design of suitable catalyst systems for selective ring opening of naphthenic molecules.

4.3.1 Theoretical background

Quantum mechanics explains how entities like electrons have both particle and wavelike characteristics. The Schrödinger equation describes the wave function of a particle as

$$i\frac{\partial}{\partial t}\Psi(x,\,t) = -\frac{1}{2m}\nabla^2\Psi(x,\,t) + V(x)\Psi(x,\,t). \quad \text{.....4.3.1}$$

V is the potential field in which the particle is moving. Ψ is the wave function and $|\Psi|^2$ is the probability distribution of the particle. By using appropriate boundary conditions, energy and many other properties of the particle can be calculated by solving the Schrödinger equation. An exact solution to the Schrödinger equation is not possible, however a number of simplifying assumptions and approximations lead to a possible solution for a system with large number of molecules. All of the modern a*b initio* molecular orbital computational methods make use of the Hartree-Fock (HF) approach to approximating the molecular wave function. Hartree-Fock theory uses the assumption that the many-electron wave function for a free atom or an ion with only closed shells can be represented by a single determinantal wave function composed of single-electron spin-orbitals. Density functional theory (DFT) includes some component of electron correlation for much the same computational cost as HF methods. This means that it is a highly efficient way of performing a more advanced calculation on the system and will

treat more accurately systems that are too large for post-HF methods (MP2, CCSD(T), CISD). Applications of HF and DFT methods include calculation and stability of structures, equilibrium, transition state and reaction intermediates.

4.3.2 Model chemistries

Model chemistry is a theoretical model to predict the properties of the chemical system. A model chemistry generally consists of the combination of a theoretical method with a basis set. A different pair of model chemistry and basis set represents a different approximation to the Schrödinger equation. A basis set is the mathematical description of the orbitals within a system used to perform the theoretical calculation (Foresman et al., 1996). Fewer restrictions on the locations of electrons in the space will be imposed by larger basis sets. Therefore, larger basis sets approximates accurate results about the properties of molecules. Gaussian offers wide range of predefined basis sets as shown in Table 4.3.1. The columns represent theoretical methods and the rows correspond to different basis sets. Therefore, each cell represents one model chemistry. When we move right across any row, the level of correlation increases as well as the computational cost. The bottom right corner represents complete solution of the Schrödinger equation and each method try to approximate that.

Table 4.3.1: various model chemistries definable via ab initio methods and standard basis sets (Foresman et al., 1996)

Electron Correlation →

basis set	HF	MP2	MP3	MP4	QCISD(T)	….	Full CI
Minimal STO-3G							
Split valence 3-21G							
Polarized 6-31G(d)							
6-31G(d,p)							
Diffuse 6-311+G(d,p)							
High ang. Momentum 6-311+G(2d,p)							
6-311++G(3df,3pd)							
…							
∞	HF Limit						Schrödinger equation

Selecting an appropriate method is necessary to predict the energetics of the reaction with minimum computational cost. HF theory is a good base level theory which is useful in providing first level predictions in many systems. However it neglects the electron correlations make it unsuitable for some systems. Møller-Plesset (MPn) methods are next generation methods which use electronic correlations and give more accurate results than HF methods. In the last few years DFT methods gain popularity and with only light expensive costs one can achieve accurate results with DFT methods. Less expensive electron correlation methods are incorporated in the DFT theory to achieve accurate results with less cost. Structural changes within the molecule produce changes in properties and energy of the system. Potential energy surface represents the change in the

energy of the system with the change in the structure of the system as shown in Figure 4.3.1.

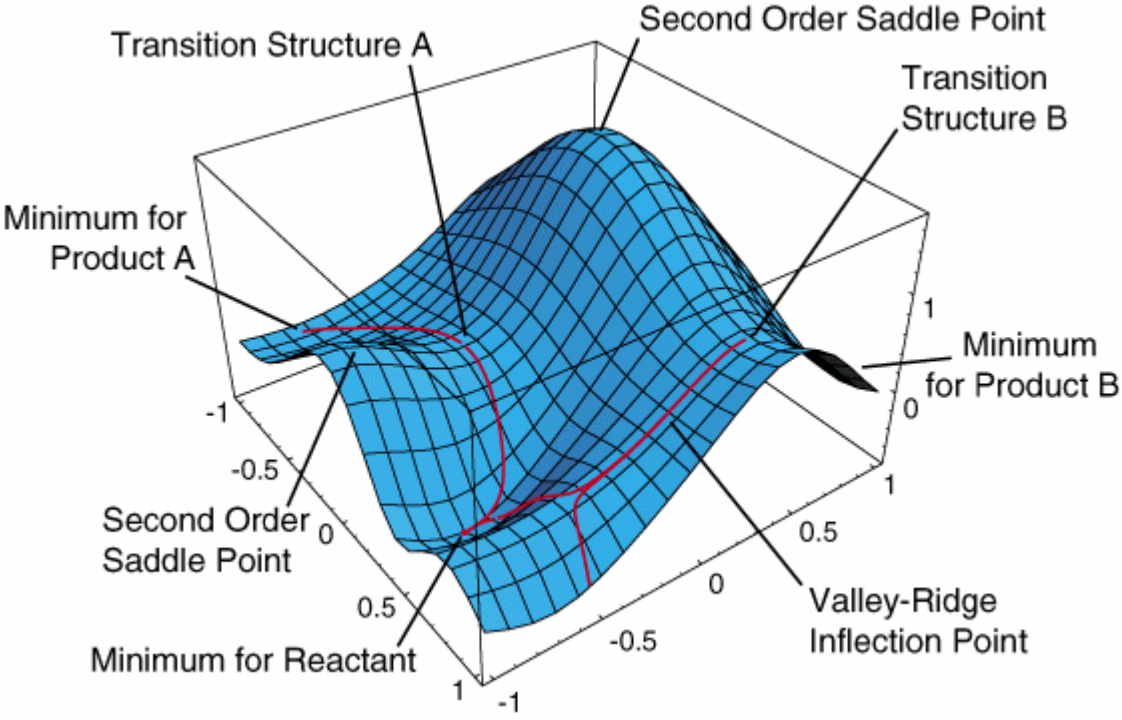

Figure 4.3.1: Potential energy surface scan for a reaction

Minima on a potential energy surface are the bottom of the valley. Local minimum is the minimum in a particular region whereas the global minimum is the minimum on the whole potential energy surface. Minimum occurs at different confirmations or structural isomers for the case of molecules and reactants or products for the case of reactions. Saddle point is a point on potential energy surface where it is minimum in one direction and maximum in the other direction. On a potential energy surface a saddle point represents the transition state connecting the two equilibrium structures.

4.3.3 Gas phase calculations

The dealkylation and ring opening reaction of propenylcyclopentyl ion will be examined in the gas phase by using HF and DFT-PBEPBE level theories using standard 6-31G (d) basis set. The "ab initio" quantum calculations were performed by using GAUSSIAN 03 program (Frisch, 2003). The geometries of the interested structures are fully optimized at HF and DFT-PBEPBE level theories using standard 6-31G (d) basis set. Elementary steps are postulated and transition state structures are identified as saddle points, having not more than one negative frequency. The gradient technique was applied for these optimizations. Analytical frequency calculations were performed in order to verify the nature of the obtained stationary points. In addition, intrinsic reaction coordinate method (IRC) was applied for passing from each transition state to the initial and the final products. Corrections for zero-point energy (ZPE) obtained from frequency calculations and were included in final activation energies.

4.3.4 Cluster simulations

Studies on the mechanisms of catalytic reactions were modeled using Brønsted acid sites on zeolites in the form of cluster models successfully (Sauer, 1994; Kramer, 1995; Blaszkowski, 1997; Becke, 1993; Haase, 1995; Beck, 1995; Broclawik, 1995; Himei, 1995; Capitan, 1995; Ugliengo, 1996; Krossner, 1996; Blaszkowski, 1996; Arbuznikov, 1996; Evleth, 1996; Mota, 1996; Ochterski, 2000). In the present study a simple 1T and 5T clusters were used to represent the immediate vicinity of the acid site present in zeolites, where 1T and 5T contains one and five hetero atoms. These clusters are modeled by using a skeleton of Si-Al-OH-O-Si. Due to the relatively large size of hydrocarbon fragments small size cluster 1T (H(OH)AI(OH)) and medium size cluster 5T

($OH_3Si(OH_3Si)A1(OH_3Si)OHSiH_3$) were used to model the Brønsted acid sites of the zeolites. The structures of the reactants, products and transition states are determined using ab initio electronic molecular techniques. Transition state was found by analyzing the vibrational normal mode and conducting intrinsic reaction coordinate (IRC) search to find out the local minimums in the reaction path to confirm the reactants and products.

4.3.5 Estimation of kinetic parameters

Thermochemical properties (ΔH_f^0, ΔS_f^0, and C_p^0) for all the reactions are calculated from energy and frequency calculations (Foresman, 1996). The rate constant is calculated from transition state theory. The equation is described below

$$k(T) = \frac{k_B T}{hc^0} e^{-\Delta G^0 / RT} \quad \text{.....4.3.2}$$

Where, k(T) is rate constant at temperature T

k_B is Boltzmann constant (J/K), h is Planck's constant (Js)

c^0 = Concentration (taken to be 1), ΔG^0 Gibbs free energy of activation

R = Gas constant = 8.31441 J/(mol K)

5 RESULTS AND DISCUSSION

This chapter describes the results obtained at the different phases of the research. Section 5.1 deals with the study of the selective ring opening of the model compound decalin on the catalysts Ir-Pt/Zr-MCM-41 with Ir and Pt loading are 0-1.75 wt.% range. Optimization of the metal loading and reaction conditions are discussed in this section. A study of the comparison between catalysts Ir-Pt/zeolites and Ni-Mo carbides/Zeolites on ring opening of decalin was studied in detail in section 5.2 . This section also gives details on the characterization and activity of various catalysts on decalin ring opening reaction.

Section 5.3 describes the catalytic activity of the best catalysts from sections 5.1 and 5.2 on the fuel quality improvement of hydrotreated light gas oil. Section 5.3 also gives details about the kinetic study and kinetic parameter estimation using lumped parameter model. Section 5.4 describes the thermodynamic equilibrium calculations carried out on decalin cracking using Lagrangian multipliers method. This section also gives details about the thermodynamic feasibility of individual exocyclic and endocyclic reactions.

Finally, Section 5.5 describes the energetics of dealkylation and ring opening of alkylcyclopentane on a Brønsted acid site using molecular modelling techniques. This section also gives details about the HF and DFT theories and activation barrier calculations using GAUSSION.

Some of the selected catalysts were tested for the reproducibility of the runs and the results are tabulated in Table 5.1. Maximum deviations observed for conversion and ring opening yield are ±1.4 and ±1.6 respectively.

Table 5.4.3.1: Reproducibility data on various catalysts for selected runs

			Conversion (wt%)			RO Yield wt%)		
Catalyst	**Feed**	**Temperature, °C**	**Run**	**repeat**	**SD**	**Run**	**repeat**	**SD**
Ni-Mo carbide/H-Beta	Decalin	240	37.7	37.0	±0.5	12.9	13.2	±0.2
Ni-Mo carbide/H-Beta	Decalin	260	51.1	51.9	±0.6	19.5	19.2	±0.2
Ni-Mo carbide/HY	Decalin	260	99.9	99.8	±0.0	16.3	18.3	±1.4
Ni-Mo carbide/HY	Decalin	240	97.5	97.0	±0.4	33.7	35.9	±1.5
1.5% Pt-0.75% Ir/HY	Decalin	260	99.9	99.9	±0.0	0.3	0.1	±0.1
1.5% Pt-0.75% Ir/HY	Decalin	240	92.4	90.4	±1.4	11.7	9.5	±1.6
1.5% Pt-0.75% Ir/H-Beta	Decalin	240	70.1	69.2	±0.6	8.3	7.5	±0.6
1.5% Pt-0.75% Ir/H-Beta	Decalin	260	81.6	79.8	±1.3	15.2	14.1	±0.8
1.5%Ir-0.75%Pt/Zr-MCM-41	Decalin	350	19.3	18.5	±0.6	6.1	5.8	±0.2
1.28%Ir-1.28%Pt/Zr-MCM-41	Decalin	350	18.0	17.4	±0.4	5.6	5.4	±0.1

5.1 Ring opening of decalin on Ir-Pt/Zr-MCM-41

This chapter gives a detailed description about the preparation and characterization of Ir-Pt/Zr-MCM-41 catalysts. The activity of the catalysts on the ring opening of decalin will be studied in detail at different temperatures. CCC statistical design is used to design the catalysts to get the better results in the response surfaces.

5.1.1 Introduction

Mesoporous materials like MCM-41 and SBA-15 have pore size in the range of 20 to 500 Å. Heavy molecules present in HGO can easily transport through this pores and can convert to products. If sufficient acidic sites are incorporated in these mesoporous materials, great ring opening yields can be achieved by using these materials as supports. Incorporation of hetero atoms like Al and Zr in the lattice structure increases the acidity of these materials. In the present study the combination of Iridium and platinum supported on Zr modified MCM-41 catalysts were prepared and the ring opening of decalin was studied at 5 MPa in a down flow trickle bed reactor.

5.1.2 Characterization of support

The synthesis conditions of the support Zr-MCM-41 are optimized by choosing the parameters such as temperature (100-200 °C), time of synthesis (10 h - 8 days), pH (9 - 11) and Si to Zr ratio 2 to 40. Their optimum values are temperature of 150 °C, synthesis time of 1 day, pH of 10.5 and Si/Zr ratio of 5.

Figure 5.1.1 shows the XRD patterns of the Zr-MCM-41 support with Si/Zr ratio of 5 prepared at above mentioned optimized conditions. The XRD pattern shows characteristic peak at 2θ value of 2 which well matches with the reported 2θ value of MCM-41 materials (Wang et al., 2001). The XRD peak intensity does not change much

with the calcinations and ion exchange, which indicates that the hexagonal structure of the support did not collapse during the above said processes.

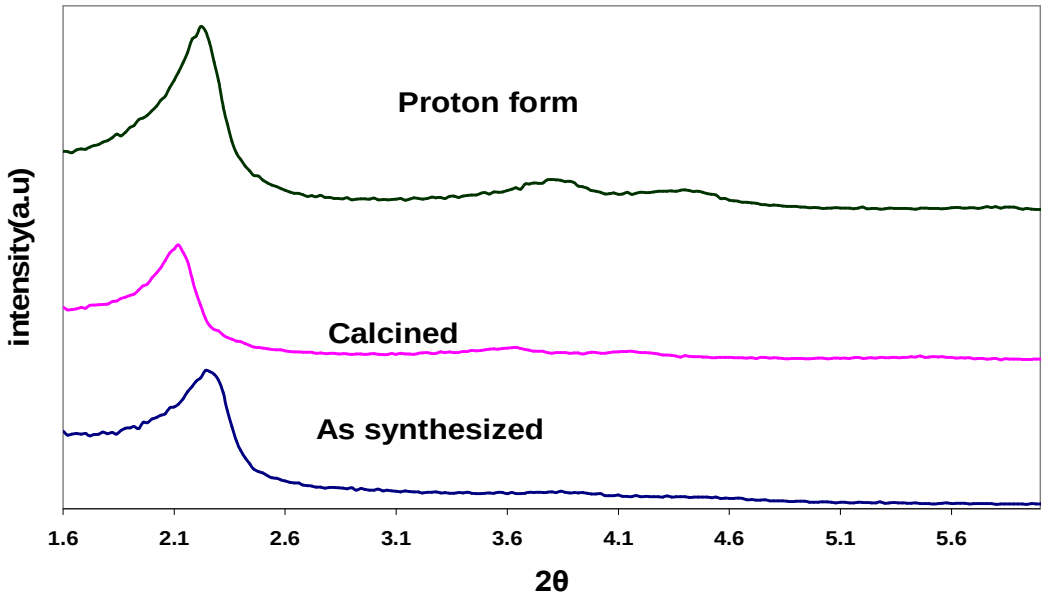

Figure 5.1.1: XRD patterns of (a) as synthesized (b) calcined and (c) proton form of Zr-MCM-41with Si/Zr = 5.

BET analysis shows that the Zr-MCM-41 with Si/Zr=5 having a surface area of 642 m^2/g with average pore diameter of 65 Á. Further it exhibit type IV isotherm, which confirms the mesoporosity of the support. The acidity of the Zr-MCM-41 with Si/Zr=5 was tested by temperature programmed desorption using ammonia as an adsorption medium and shown in Figure 5.1.2. A peak at 150 °C shows that the support has only mild acidity.

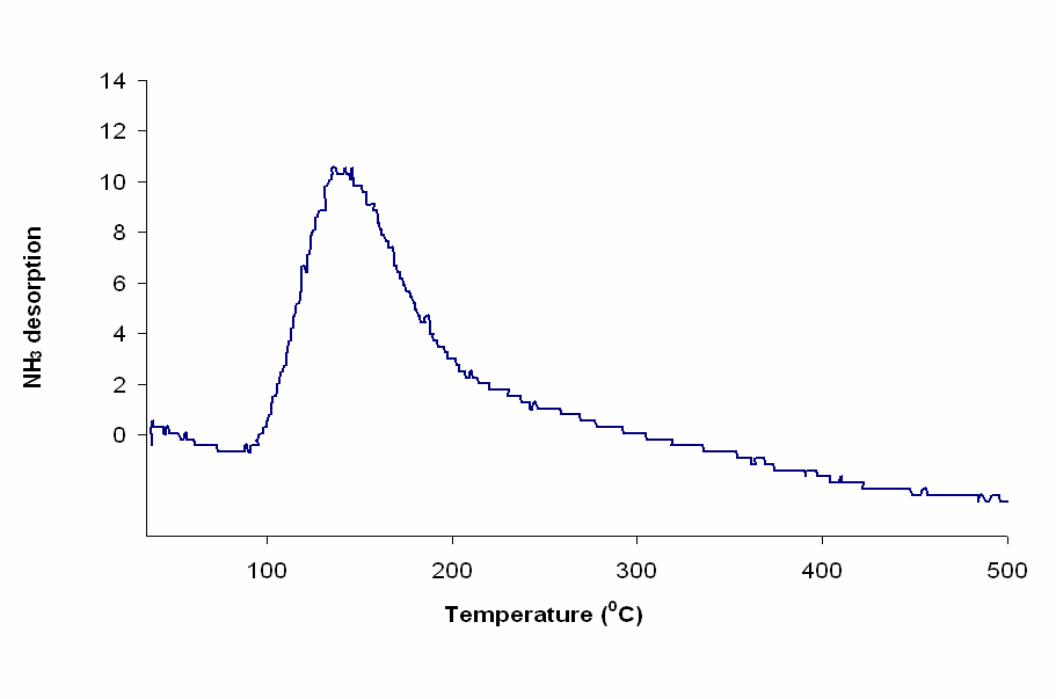

Figure 5.1.2: TPD of NH_3 of proton form of Zr-MCM-41 with Si/Zr = 5.

The DRIFT spectra of ammonia adsorption on Zr-MCM-41 support are shown in Figure 5.1.3. The spectrum was collected on the in situ reduced (H_2, 400 °C) sample at 100 °C. The peaks correspond to 1468 cm^{-1} and 1730 cm^{-1} are Brønsted acid sites and peaks at 1290cm^{-1} and 1625cm^{-1} correspond to Lewis acid sites (Bars, 1992; Nylen, 2006). The presence of both Lewis (1290 and 1625 cm^{-1}) and Brønsted acid sites (1468 and 1730 cm^{-1}) in Zr-MCM-41 support is evidenced by DRIFT of NH_3 adsorption.

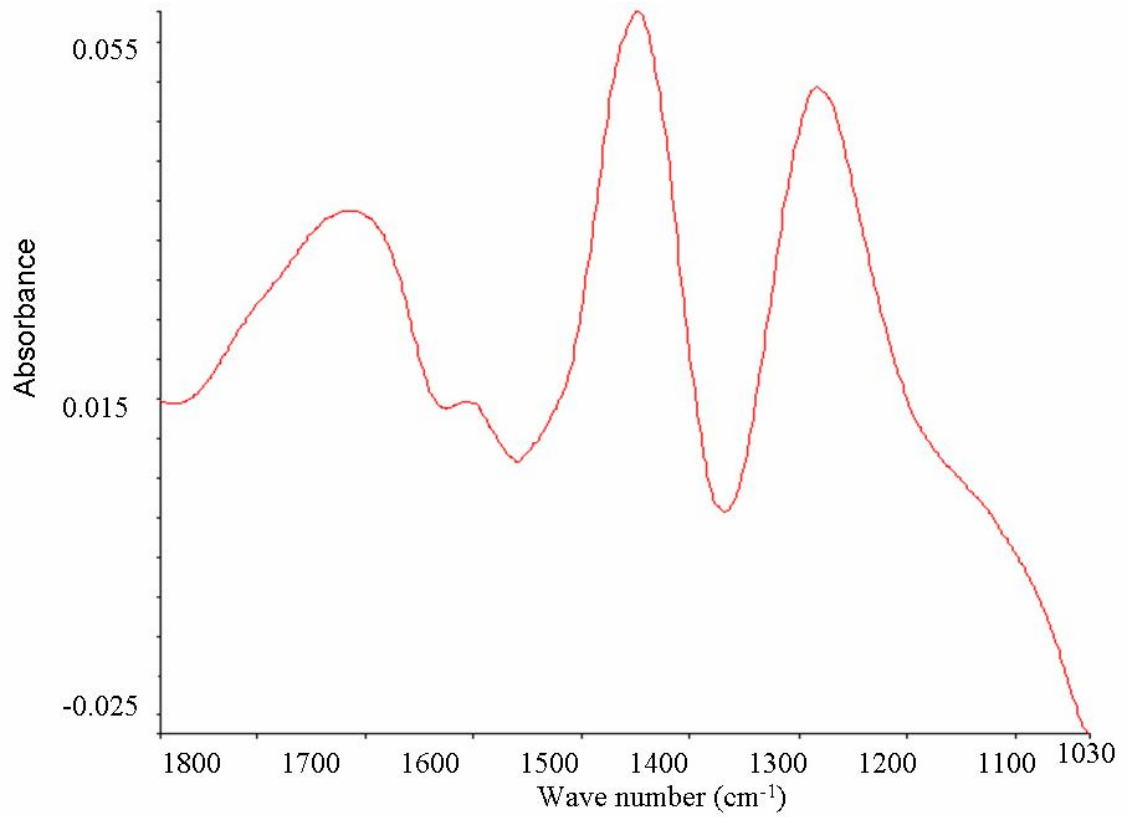

Figure 5.1.3: DRIFT spectra of NH_3 adsorbed on proton form of Zr-MCM-41 with Si/Zr = 5.

5.1.3 Characterization of Ir-Pt/Zr-MCM-41 Catalysts

Response Surface Method (RSM) of statistical experimental design was used for the catalysts syntheses with the aim of optimizing the parameters for high catalyst activity. The Central Composite Circumscribed (CCC) of RSM was chosen to provide high quality predictions over the entire design space with minimum number of experiments. The total number of experimental runs (N') recommended by the design is given by the formula

$$N' = (\text{Factorial Points}) + (\text{Star Points}) + (\text{Center Points})$$

i.e. $$N' = 2^F + 2F + n_C \quad \text{.....5.1.1}$$

where F is the number of factors (parameters) and n_C the number of center points (i.e. one center point with $n_C - 1$ replicates). Center points are repeated 4 times to get a good estimate of pure error (experimental error) and inherent variability. With two factors (Ir and Pt) under study, the total number of catalysts required according to Equation 1 was 13. The different catalyst loadings as recommended by the CCC design are shown in Table 5.1.1.

Table 5.1.1: Bimetallic Ir-Pt/Zr-MCM-41 catalysts prepared by CCC design.

Cat. no.	Ir (wt%)	Pt (wt%)
1	0	0.75
2	0.75	0
3	0.22	0.22
4	1.28	0.22
5	0.75	0.75
6	0.75	1.50
7	0.22	1.28
8	1.28	1.28
9	1.50	0.75

The thermo gravimetric (TG) analysis for the Ir-Pt impregnated sample prior to the calcination is shown in Figure 5.1.4. It was indicated clearly that the weight loss is significant up to 400 °C. Therefore calcination is required above this temperature to

completely decompose the precursor of Ir and Pt. Hence, these catalysts are calcined at 500 °C.

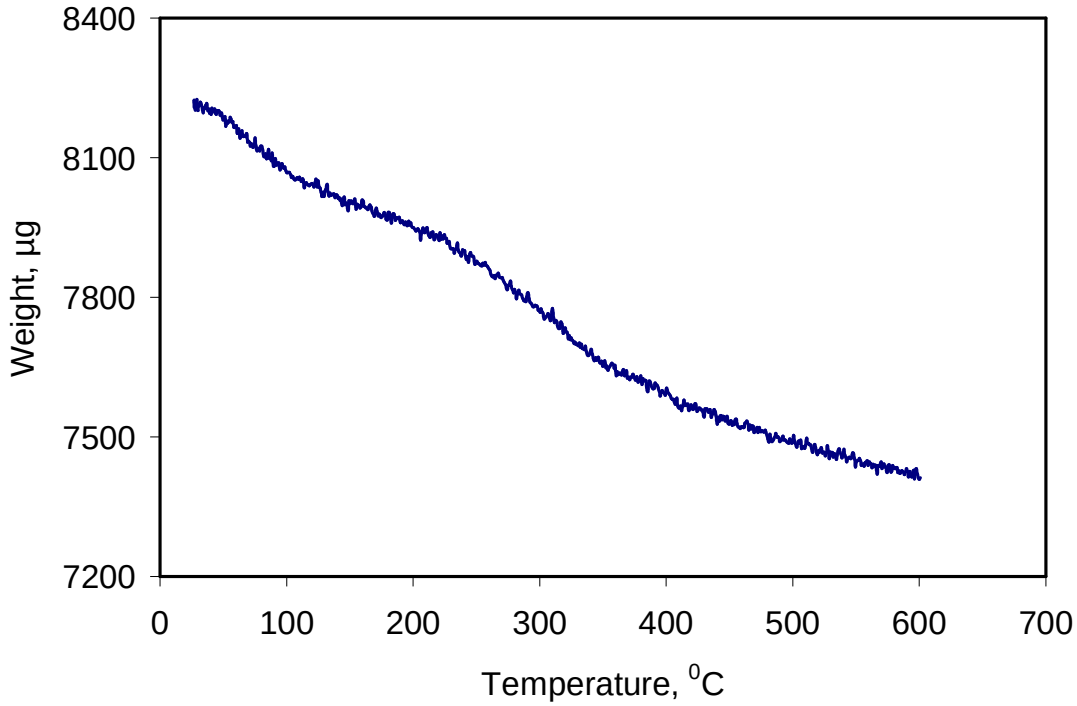

Figure 5.1.4: TG profile of typical Ir-Pt/Zr-MCM-41 before calcination.

The TEM images of selected catalysts such as cat 7 and cat 9 are shown in Figure 5.1.5. The TEM indicates the dispersion of the metals are good and the particle size is in the range of 7-12 nm. Further TEM evidences that some of the metal particle size is greater than the pore size of the support and stays on out side of the pores.

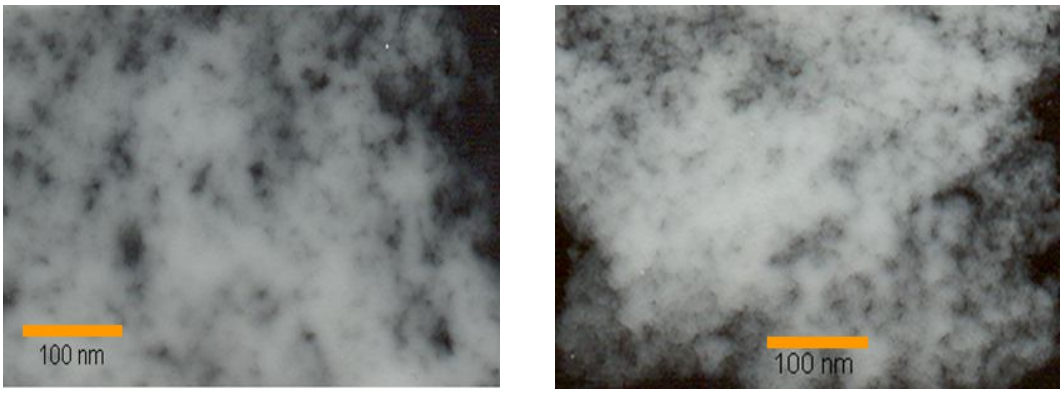

(a) (b)

Figure 5.1.5: TEM of Ir-Pt/Zr-MCM-41 (a) Cat 7 (b) Cat 9.

The BET surface area results of the various catalysts are shown in Table 5.1.2. All the catalysts show less surface area than the support. The decrease in pore volume of the support on Ir-Pt metal additions showed that some of the metal particles occupied the pores of the support.

Table 5.1.2: BET surface area, pore volume and average pore diameter of Ir-Pt/Zr-MCM-41 catalysts.

Ir (wt.%)	Pt (wt.%)	Surface area (m^2/g)	Pore volume (cc/gm)	Pore diameter (A)
0	0.75	592	1.19	80
0.75	0	585	1.13	73
0.22	0.22	598	1.09	73
1.28	0.22	585	1.07	74
0.75	0.75	509	0.90	71
0.75	1.50	465	0.92	80
0.22	1.28	514	1.03	80
1.28	1.28	537	0.70	52
1.50	0.75	454	0.84	74

Two and three fold peaks is an indication of poor dispersion. There are three distinguished peaks observed in the catalysts studied. First one at 2010 to 2015 cm^{-1} which are displayed by almost all the catalysts except cat 1 and the second one is a shoulder at 2020 to 2027 cm^{-1}. The third one at 2075 to 2080 cm^{-1}, which is dominant with cat 1 and cat 6 which contains high loadings of Pt. with high loading of Iridium (1.5%) this band is shifted to 2110 cm^{-1} as shown in the Figure 5.1.6. The interpretation of these bands in the literature is inappropriate and controversial. Some authors (Solymosi, 1980a; Solymosi, 1980b; Erdohelyi, 1996) suggest that bands at 2015 cm^{-1} correspond to the well dispersed, small Ir particles with more support interaction.

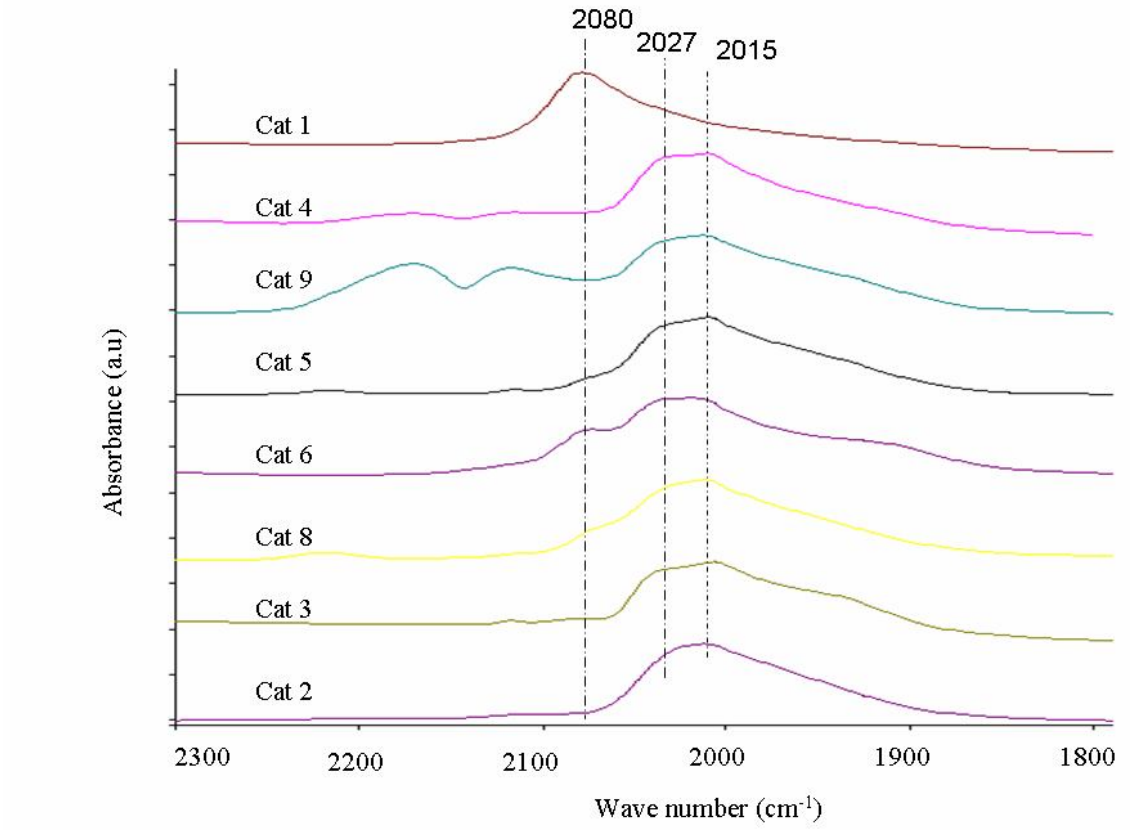

Figure 5.1.6: DRIFT spectra of adsorbed CO on Ir-Pt/Zr-MCM-41 catalysts.

At high loading, the shift of the peaks clearly indicates the alloying effect. Platinum is in Pt^0 and Pt^1 states (Mihut, 2002; Otten, 1994) after the reduction which was confirmed by the peak observed at 2078 cm^{-1}. This is the only peak observed on cat 1 and the intensity of this peak is increased with Pt loading and decreased with Ir loading. Schmal et. al. (2005) suggest that the band at 2130 cm^{-1} associated with CO adsorption on Pt – zirconia interface. band at 2180 cm^{-1} of Cat 9 correspond to the CO adsorption on cationic sites (ZR^{+3} and Zr^{+4}) (Schmal, 2005).

The DRIFT of ammonia adsorption spectra for Ir-Pt/Zr-MCM-41 catalysts is shown in Figure 5.1.7. The spectrum is collected on the in situ reduced (H_2, 400 °C) sample. The DRIFT peaks at 1468cm^{-1} and 1730cm^{-1} are associated with the Brønsted acid sites and at 1290cm^{-1} and 1625cm^{-1} are Lewis acid sites (Bars, 1992; Nylen 2006).

5.1.4 Ring Opening of decalin

The catalytic activity was studied at different temperatures using decalin. The total pressure, liquid hourly space velocity and H_2 flow rate were maintained at 5 MPa, 1.5 h^{-1} and 50 ml/min respectively. The Decalin was diluted with n-heptane and dodecane was used as an internal standard. The feed composition is 80-10-10 vol.% heptane, dodecane and decalin.

Products were identified by using GC-MS and quantified using Varian 3400 GC. The GC was equipped with the Varian CP-Sil 8 CB low bleed / MS capillary column (30m-0.25mm-0.25µm # CP 5860) which is 5% phenyl 95% dimethylpolysiloxane low bleed phase. Same capillary column and program are used for the Varian 3400 GC for the quantification purpose. The following program used for GC-MS: initial temperature 50

°C, initial temperature hold time of 5min, heating rate of 10 °C/min, final temperature of 200 °C, final temperature hold time of 10 min and the detector temperature of 230 °C.

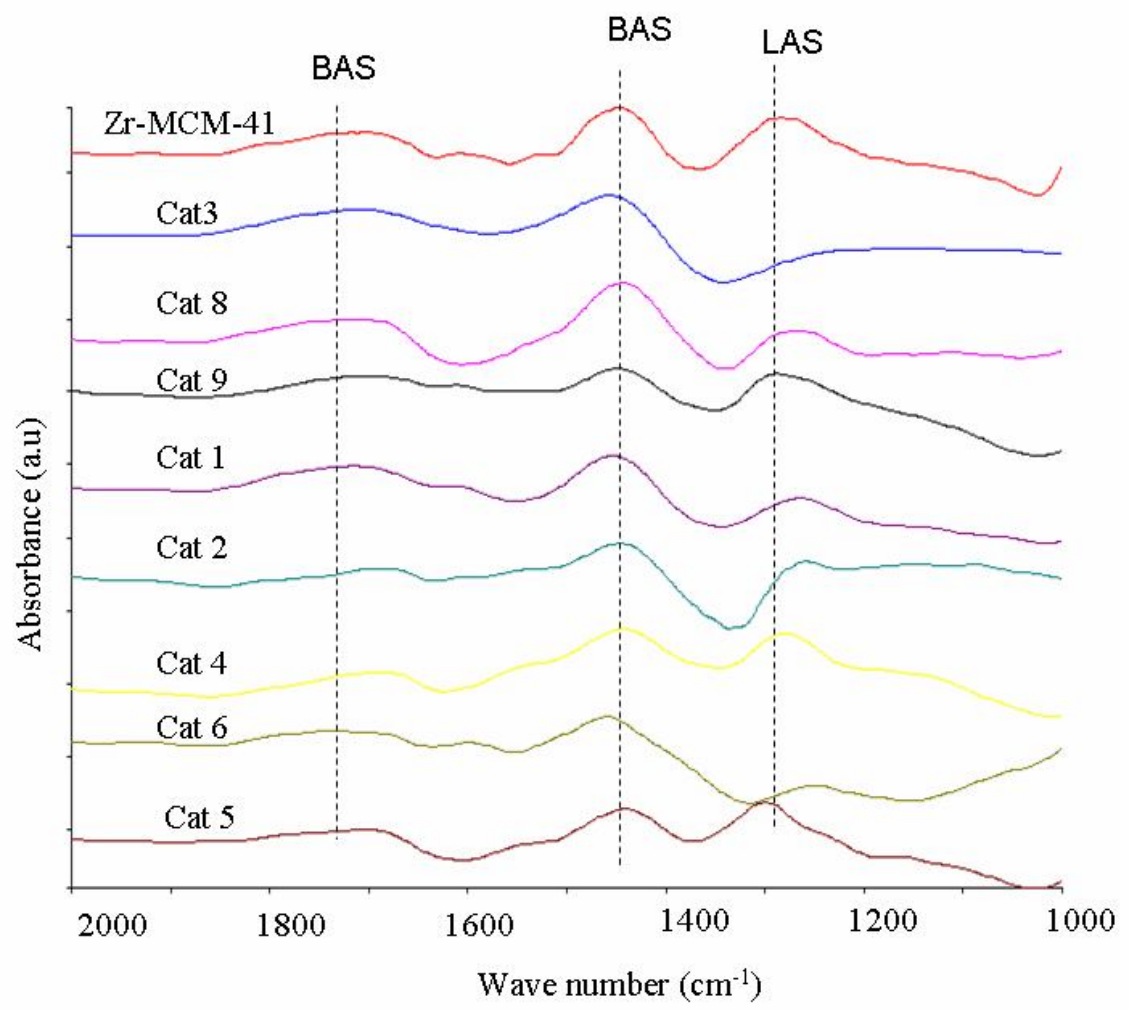

Figure 5.1.7: DRIFT spectra of NH_3 adsorption Ir-Pt/Zr-MCM-41 catalysts.

The conversion, yield and selectivity are represented on mass basis and calculated based on the following terminology. Conversion is the amount of decalin reacted to the total amount of decalin fed to the reactor. The yield is defined as the amount of product (A) formed to the total amount of decalin fed to the reactor. The selectivity of A is the amount of product (A) formed to the total amount of decalin reacted.

The ring opening of decalin at temperature, pressure and LHSV of 350 °C, 5MPa and 1.5hr-1 respectively on cat 7 was studied. A typical decalin conversion with time is given in Figure 5.1.8 for the cat 7 with loading of 0.22 wt% Ir and 1.28 wt%. Initially conversion increased and then stabilized after 24 hours as shown in the Figure 5.1.8. Therefore, the samples collected after 24 h were used for analysis to compare the activity of various catalysts.

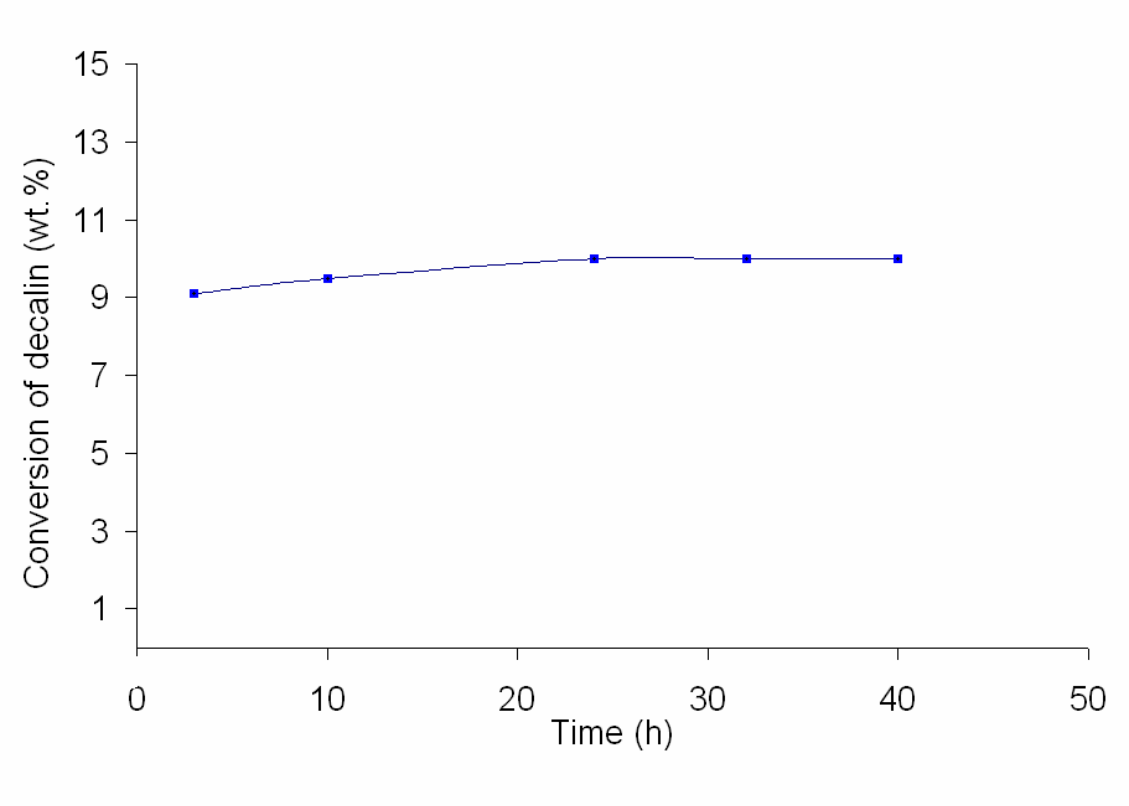

Figure 5.1.8: The conversion of as a function of time on catalyst 7. (Temperature 300 °C; Pressure = 5 MPa; and LHSV = 1.5 h^{-1}).

The decalin conversion at different temperatures with cat 1-9 is shown in Figure 5.1.9. All the catalysts show very low activity (<10 wt.%) at 300 °C and the decalin conversion is not much improved with increase of either Ir or Pt loading.

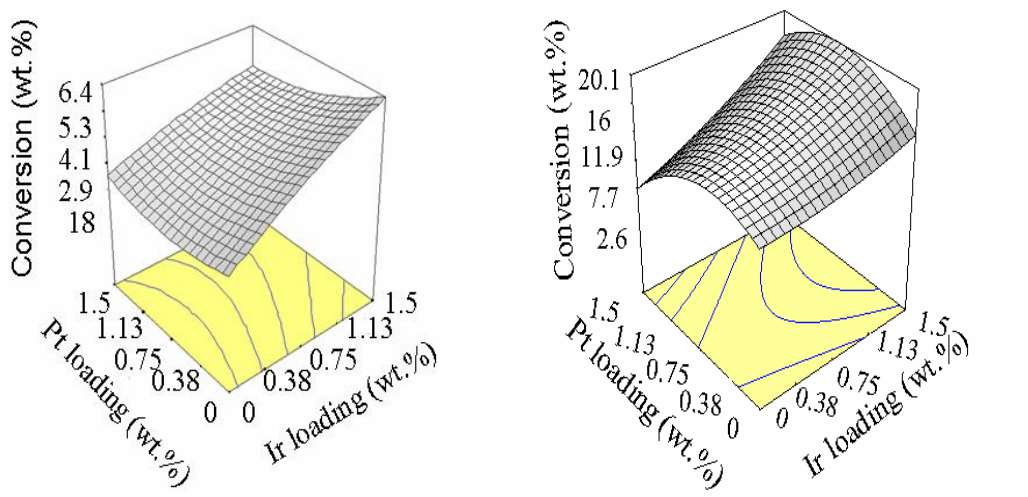

(a) **(b)**

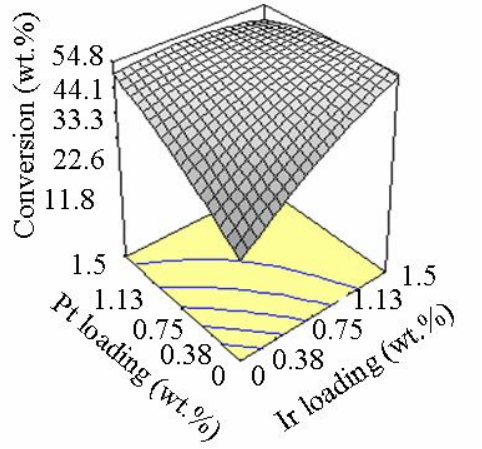

(c)

Figure 5.1.9: The Conversion of decalin with different Ir and Pt loadings at (a) 300 °C (b) 350 °C (c) 400 °C. (Pressure = 5 MPa; and LHSV = 1.5 h^{-1}).

The decalin conversion is increased with increase of temperature from 300 to 400 °C. At 350 °C, maximum conversion of 20 wt.% was observed for 1.5 wt% Ir and 0.75 wt% of pt loading. This same trend of decalin conversion is also observed at 400 °C with

a maximum conversion of 56 wt.% for the above loading. It has been observed that the conversion is increased with the increase of Ir loading at 350 °C and 400 °C.

The products formed from decalin ring opening over Ir-Pt/Zr-MCM-41 catalysts were identified by GC-MS and were classified into following three groups

i) Ring opening products : alkyl/alkenyl cyclohexane, or cyclohexenes or benzenes [1-butyl cyclohexane, cyclohexane, 1-methyl-4(1-methyl ethynyl), 1-ethyl 4-ethynyl benzene, bycyclopentane-7 butyl, cyclohexane 5-methyl-2-(1-methyl ethyl)], 3,5-dimethyl octane, bicyclo (4,1,0) heptane 7-butyl, 1-methyl indan, 9-methyl bicyclononane, nonadecane, 4,4,dimethyl cyclooctane, 2,2,3,3 tetramethyl pentane, 6-ethyl-2-methyl decane.

ii) Cracking products (less than 10 carbon containing compounds): alkyl cyclopentanes, and C_6-C_{10} hydrocarbons.

iii) Heavy and dehydrogenated products: tetralin and naphthalene, and cyclopenta-cycloheptane

The ring opening yield over all the catalysts at 350 and 400 °C are shown in Figure 5.1.10. The product distribution indicated that the percentage of cracking products is surprisingly low (<2 wt.%) even at 400 °C contrast with many workers (Corma, 2001; Santikunaporn, 2004; Kubicka, 2004b).

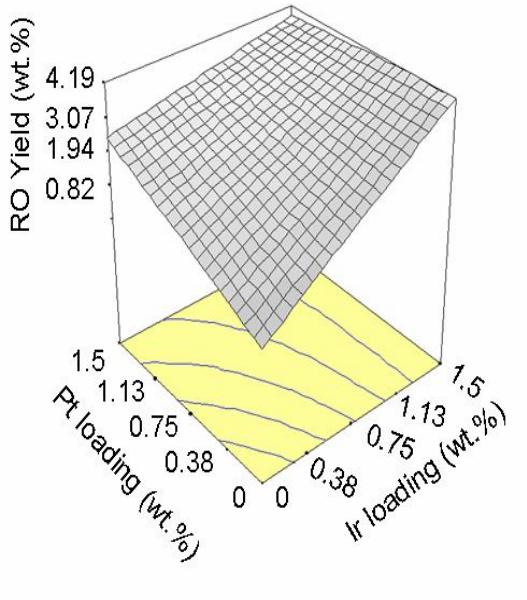

(a)

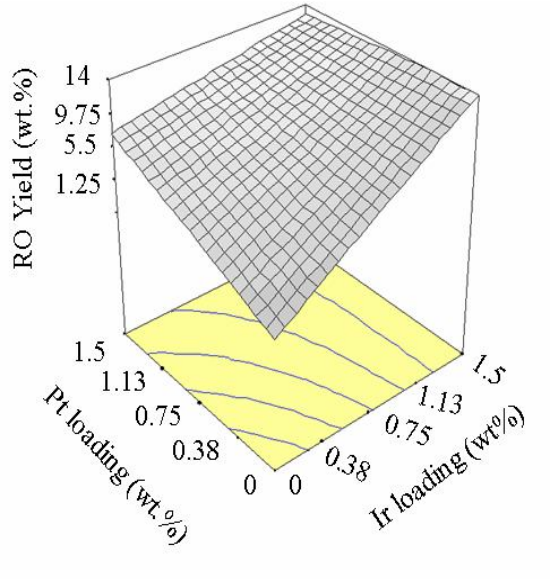

(b)

Figure 5.1.10: Decalin ring opening yield with different Ir and Pt loadings (a) 350 °C and (b) 400 °C. (Pressure = 5 M Pa; and LHSV = 1.5 h^{-1}).

Surprisingly methane formation is negligible as indicated by the GC analysis. The reason for this is due to moderate acid strength of the Zr-MCM-41support as shown by

the DRIFT of adsorbed NH_3. Strong acidity of the support leads to increase in the yield of undesired cracking products (Paal, 1997; Corma, 2001). The acidity plays an important role in the selective ring opening of bicyclic naphthenes as shown by Kubicka et al. (2004a, 2004b).

Product distribution from decalin conversion indicates the importance of protolytic cracking, skeletal isomerization and ring opening reactions from the mechanisms proposed by Kubicka et al (2004). The presence of products like bicyclo (4,1,0) heptane, 9-methyl bicyclononane, 4,4,dimethyl cyclooctane clearly indicates the strong action of metal on ring contraction reaction.

The ring opening selectivity over all the catalysts at 300, 350 and 400 °C are shown in Figure 5.1.11. Figure 5.1.10 shows that at 350 °C the optimum ring opening yield is observed with cat 9. Five membered ring naphthenes can be easily converted to alkanes without loss of molecular weight especially on Ir catalyst, but it is very difficult to open the six membered ring naphthenes directly by using metal hydrogenolysis reaction (McVicker, 2002). The ring opening yield and selectivity are increased with the increase of iridium loading from 0 to 1.5 wt.%, while the optimum ring opening selectivity was observed with a combination of 0.75% of platinum loading. Ir is a suitable catalyst for the ring opening reactions and in a controlled combination with platinum leads to open the selective rings among the studied temperature range. 300 °C is always favored for ring opening products selectivity as shown in the Figure 5.1.11, but the overall conversion is less at this temperatures.

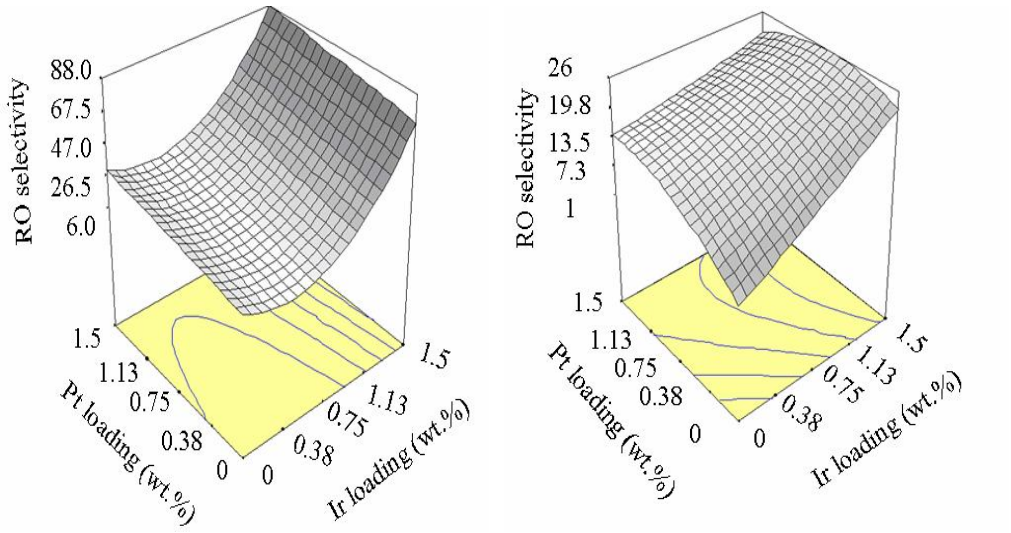

(a) (b)

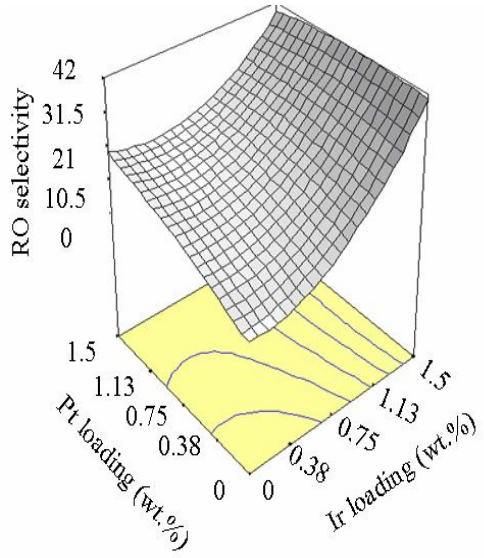

(c)

Figure 5.1.11: Decalin ring opening selectivity at (a) 300 °C (b) 350 °C (c) 400 °C. (Pressure = 5 MPa; and LHSV = 1.5 h^{-1}).

As the temperature increase from 300 to 400 °C the formation of products like tetralin, naphthalene are prominent as shown in Table 5.1.3.

Cetane improvement is an important factor in the ring opening reaction. Some of the products from the ring opening of decalin have low cetane number than the feed decalin. Less branched products formed from decalin have higher cetane numbers than the decalin. Products like butyl cyclohexane, butyl cyclohexene, n-pentyl cyclopentane, isopropyl cyclohexane, n-decane, 4,4 dimethyl cyclooctane, methyl nonane, ethyl octane are considered as less branched ring opening products and having high cetane values. The ratio of less branched products to highly branched products is designated as L/H. This is given in Table 5.1.3. The high cetane value products favored at 400 °C than 350 °C. This may be due to the high cracking activity required for opening the second ring. This clearly indicates high temperature favors the high cetane value products.

Table 5.1.3: Decalin products yield on different catalysts at different temperatures.

Catalyst	L/H		Heavy yield			Trans-decalin/cis-decalin		
	350^0 C	400^0 C	3000 C	3500 C	4000 C	3000 C	3500 C	4000 C
cat 1	0	0.27	1.47	9.71	30.90	7.12	6.78	6.13
cat 2	0	0.16	3.56	9.64	40.72	5.25	7.38	8.50
cat 3	0	0.34	1.62	1.71	10.90	6.70	7.30	8.40
cat 4	0.25	0.38	2.69	14.06	33.40	7.27	8.26	6.24
cat 5	0	0.28	1.97	12.82	43.87	5.95	6.65	7.46
cat 6	0.15	0.32	0.55	3.20	35.90	8.56	7.36	6.24
cat 7	0	0.25	1.23	5.28	20.50	8.45	7.78	7.26
cat 8	0.20	0.31	0.25	12.48	28.10	8.21	8.02	7.70
cat 9	0.25	0.39	0.85	10.10	22.06	5.40	8.40	8.38

Higher temperatures (>350 °C) are not thermodynamically favorable for ring opening reactions and leads to dehydrogenation. Dehydrogenation is favored by the Ir and Pt combination at and above 350 °C. The product analysis indicated the increase of trans- to cis- ratio of decalin with the increase in Ir loading and decrease of Pt loading. This indicates clearly that the reactivity of trans-decalin increases with the presence of platinum than the presence of iridium. Form this, it is observed that the stereo isomerization as an important intermediate step for ring opening of decalin. High ratios of trans- to cis- ratio of decalin at low temperatures indicate the high reactivity of cis-decalin and low reactivity of trans-decalin. At high temperatures the trans-decalin also get converted to products.

5.1.5 Thioresistance

It is well known that noble metals are sensitive to sulfur and show less thioresistance. Metals like Pt incorporated on MCM-41 type materials show fast deactivation with 1000 ppm of dibenzothiophene (DBT) (Carri´on, 2006). But bimetallic catalysts show better thiotolarence (Carri´on, 2005). The thiotolarence study was conducted with the best catalyst (cat 9) from the prepared catalysts. 1000 ppm DBT was added to the feed and the reaction was carried out for 3 days at temperature, pressure and LHSV of 350 °C, 5MPa and 1.5 h^{-1}. Figure 5.1.12 shows the conversion of decalin as a function of time with and without DBT. Typical catalyst, cat 9 showed good thioresistance, and drop of only 2 to 3 wt.% in conversion is observed.

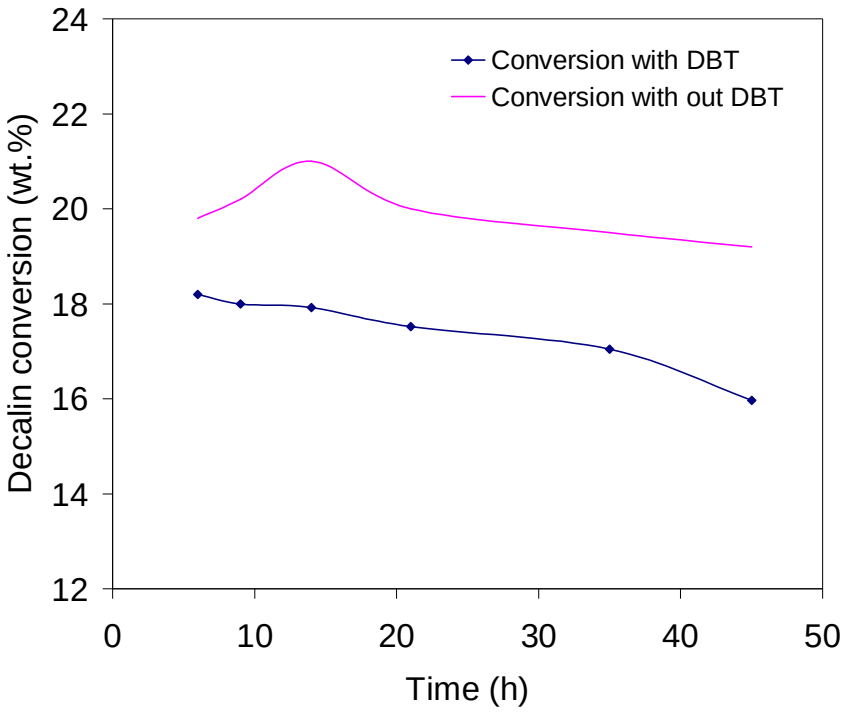

Figure 5.1.12: Decalin conversion versus the time on stream for the catalyst 9 in the presence of 1000 ppm dibenzothiophene.

5.1.6 Summary

Mesoporous Zr-MCM-41support with hexagonal nature and moderate acidity was prepared. Pt and Ir were loaded on the above support. DRIFTS of CO adsorption on Ir-Pt/Zr-MCM-41 catalysts indicated different type of metallic phases on the support. Pt was in Pt^0 and Pt^1 states and there was interaction between Pt and Zr. DRIFTS of ammonia indicated that all the catalysts contain both Brønsted and Lewis acid sites. Selective ring opening of decalin was studied at different temperatures over the above catalysts. Catalyst stabilization study showed that the catalysts activity is stabilized after 24 hours. The optimum temperature for the ring opening yield and selectivity in the studied conditions is 350 °C. Optimum loading was observed as 1.5% Ir and 0.75% Pt for getting

maximum ring opening yield of 16 wt.% and selectivity of 26 wt.% from decalin at 350 °C. Dehydrogenation was a dominant reaction at and above 350 °C. High temperatures are favored for the high cetane number products. Pt presence caused an increase in the trans-decalin reactivity. The Ir-Pt/Zr-MCM-41 showed good thioresistance in the studied temperature and time range.

5.2 Thermodynamic equilibrium calculations for ring opening of decalin

5.2.1 Introduction

This chapter gives detailed information about the thermodynamic limitations on ring opening reactions by taking decalin cracking as a model reaction. 46 compounds are considered in obtaining the thermodynamic equilibrium composition of the cracking of decalin in the temperature range from 300 to 1000 K. Individual reactions are also considered to study the equilibrium constants for acyclic, exocyclic and endocyclic reactions.

5.2.2 Acyclic, Exocyclic, and Endocyclic Cracking of Paraffins and Naphthenes

The standard enthalpy change, entropy change, and Gibbs free energy change of cracking reactions in presence of hydrogen are tabulated for selected paraffins and naphthenes in Table 5.2.1 (Stull et al., 1969). The reactions are grouped under three categories: (i) acyclic cracking – a paraffin molecule is cracked into two smaller species, (ii) exocyclic cracking – a side chain is removed from a naphthene and (iii) endocyclic cracking – cleavage of *C-C* bond occurs on the ring. It can be observed from Table 5.2.1 that the standard enthalpy change of reaction remains negative for all three types of cracking reactions, whereas the standard entropy change is a positive quantity for acyclic and exocyclic cracking reactions but a negative quantity for endocyclic ring opening reactions.

Table 5.2.1: Thermochemistry of selected hydrocracking reactions[†]

Reactions	ΔH_R^0 *kcal/gmol*	ΔS_R^0 *kcal/gmol*	ΔG_R^0 *cal/gmol K*
Acyclic cracking			
1. *n*-Hexane + H_2 ⇔ Propane + Propane	-9.68	4.98	-11.16
2. *n*-Octane + H_2 ⇔ Propane + *n*-Pentane	-10.00	5.15	-11.53
3. *n*-Octane + H_2 ⇔ *i*-Butane + *n*-Butane	-10.48	5.48	-12.11
4. *n*-Undecane + H_2 ⇔ Propane + *n*-Octane	-10.04	5.37	-11.63
Exocyclic cracking			
5. Propylcyclopentane + H_2 ⇔ cyclopentane + Propane	-7.89	3.57	-8.95
6. Butylcyclopentane + H_2 ⇔ cyclopentane + Butane	-8.39	3.87	-9.54
7. Propylcyclohexane + H_2 ⇔ cyclohexane + Propane	-8.05	4.31	-9.33
8. Pentylcyclohexane + H_2 ⇔ cyclohexane + *n*-Pentane	-8.55	4.58	-9.91
Endocyclic cracking			
9. Cyclopropane + H_2 ⇔ Propane	-37.56	-23.45	-30.56
10. Cyclobutane + H_2 ⇔ *n*-Butane	-36.52	-20.52	-30.40
11. Cyclopentane + H_2 ⇔ *n*-Pentane	-16.54	-17.81	-11.23
12. Methylcyclopentane + H_2 ⇔ *n*-Hexane	-14.46	-19.62	-8.61
13. Cyclohexane + H_2 ⇔ *n*-Hexane	-10.53	-9.67	-7.65
14. Methylcyclohexane + H_2 ⇔ *n*-Heptane	-7.89	-11.00	-4.61
15. Ethylcyclohexane + H_2 ⇔ *n*-Octane	-8.77	-11.10	-5.46
16. Pentylcyclohexane + H_2 ⇔ *n*-Undecane	-8.72	-10.62	-5.56

The cracking reaction in a hydrocracking environment is a combination of both *C-C* bond scission and hydrogenation. The entropy change for the *C-C* bond scission in all three types of cracking reactions remain positive but it becomes negative for the hydrogenation step. In case of endocyclic cracking, the entropy change in bond scission is lower as compared to that of other two types of scissions and becomes negative when added with the entropy change for the hydrogenation step. For example, in case of reaction 4 (acyclic cracking) in Table 5.2.1, the entropy changes (Stull et al., 1969) for bond scission and hydrogenation are 35.58, -30.21 kcal/gmol K at 298 K respectively, which make the combined entropy change for the reaction as a positive quantity. In case of reaction 16 (endocyclic cracking), the entropy changes for the bond scission and hydrogenation are 19.59, -30.21 kcal/gmol K at 298 K respectively, which make the combined entropy a negative quantity.

If the hydrogenation step is not considered then the entropy change for all three types cracking reactions (only C-C bond scission) are positive. However the entropy change for C-C bond scission in endocyclic cracking is small enough to make entropy change negative for the combination of C-C bond cracking and hydrogenation. The negative entropy change for endocyclic cracking (bond scission + hydrogenation) should not be confused with the total entropy change or the entropy change of the universe, $\Delta S_{Tot}^{\ 0}$ $(=\Delta S_R^{\ 0} - \Delta H_R^{\ 0}/T)$ which is positive for this type and also for other two types of the cracking reactions. The adverse entropy effect observed in endocyclic reactions supports the thermodynamic argument made by Egan et al. (1962).

The negative change in entropy, which distinguishes endocyclic cracking from acyclic and exocyclic cracking reactions in a hydrocracking environment, has an effect in the position of the equilibrium. The equilibrium constants as a function of temperature are shown for an acyclic, exocyclic, and endocyclic cracking reaction (reactions 4, 8, and 16 in Table 5.2.1) in Figure 5.2.1. At all temperatures, acyclic and exocyclic cracking are thermodynamically more favored than the endocyclic cracking reaction and the corresponding equilibrium constants continuously decrease with increase in temperature. The negative entropy change for endocyclic cracking causes the equilibrium constant to become less than unity beyond 773 K as seen in Figure 5.2.1.

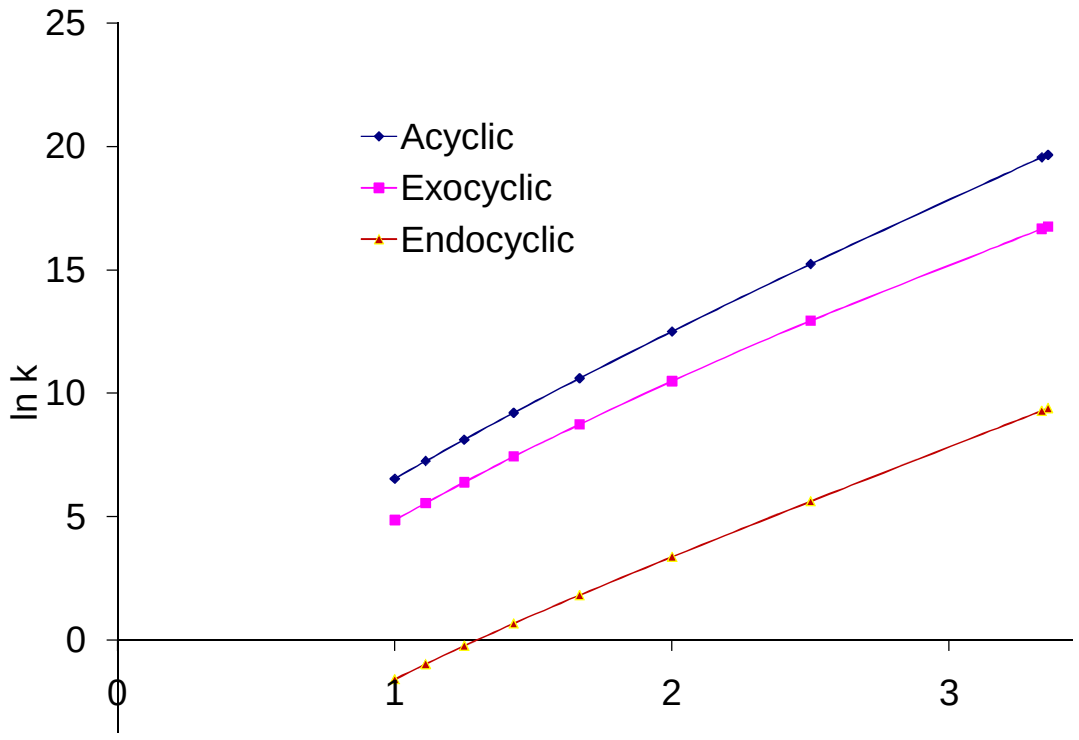

Figure 5.2.1: Effect of temperature on equilibrium constants for reactions 4 (acyclic), 8 (exocyclic), and 16 (endocyclic) in Table 5.2.1.

If the cracking reactions alone are considered without hydrogenation then the equilibrium constants for all three types of reactions continuously increase with increase in temperature due the fact that C-C bond scissions (without hydrogenation) are endothermic. In this case too, endocyclic scission is the least favored among the three types of cracking reactions. This observation is important because the scission of C-C bonds in naphthenes is not a problem and can be accomplished by any existing hydrocracking or catcracking catalyst but the real problem is to avoid secondary cracking of ring opened products due to exocyclic and acyclic cracking reactions that are thermodynamically more favored than the ring opening reactions.

The above analysis is informative but it does not provide any information regarding whether the temperature can be manipulated to increase the favorability of endocyclic cracking over other two cracking reactions. An answer to this problem can be found by observing the effect of temperature on the ratio of equilibrium constants (endocyclic/acyclic and endocyclic/exocyclic) as shown in Figure 5.2.2.

Both the ratios increase with increase in temperature suggesting that although the endocyclic cracking reaction is the least favored among the three type of cracking reactions, its favorability over the other two cracking reactions improves with respect to increase in temperature. The same trend is observed irrespective of the presence or absence of hydrogen. The hydrogenation step that follows the ring opening reaction in hydrocracking environment is thermodynamically controlled and its equilibrium constant reduces with respect to increase in temperature due to the negative change in entropy. This limitation is eliminated in catalytic cracking where there is no external source of hydrogen and reactor temperatures are kept at much higher levels compared to that of

hydrocracking. However, the presence of hydrogen is very important to suppress the coke forming reactions.

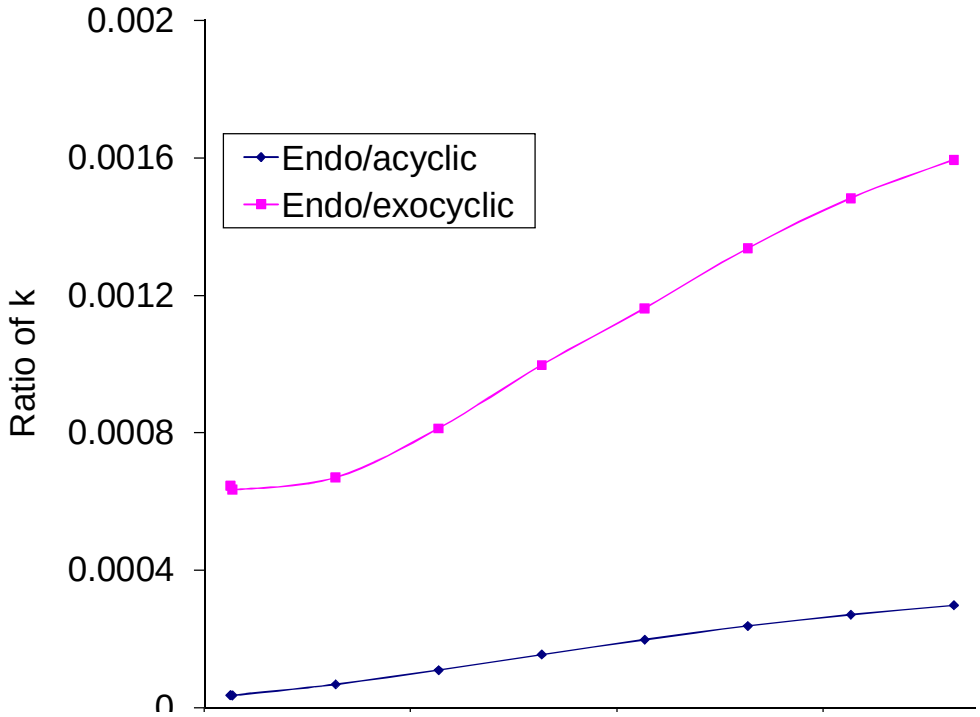

Figure 5.2.2: Effect of temperature on ratio of equilibrium constants for reaction 16 (endocyclic) to reaction 4 (acyclic) and reaction 16 to reaction 8(exocyclic). Refer Table 5.2.1.

The observations from the thermochemical analysis of single reactions carried out in this section are summarized as follows: (i) Favorability of ring opening reaction over acyclic and exocyclic cracking reactions increases at increasing temperatures. (ii) If unsaturated ring opening compounds are allowed to form in a weak hydrogenating environment which is favored at high temperatures then the yield and selectivity of ring opening products will be increased.

One must be cautious in extending these observations to actual hydrocracking or catalytic cracking processes because what we are looking at are single reactions but in reality multiple sequential and simultaneous reactions occur in these processes and they produce numerous products. To verify the concepts proposed in this section we carried out thermodynamic equilibrium calculations for a reaction mixture obtained from the hydrocracking of decalin, which are explained in the following section.

5.2.3 Thermodynamic equilibrium calculations for ring opening of decalin

The products from hydrocracking of decalin on Ir-Pt/HY are classified as follows (Mouli et al., 2009):

(i) Cracking products (CP): Methane, ethane, propane, isobutane, isopentane, methylcyclopentane, methylcyclohexane, *n*-hexane, *n*-octane, 1-octene, *n*-nonane, 1-nonene, 1, 4-dimethylcyclohexane, propylcyclohexane, 1, 3, 5-trimethylcyclohexane, ethylbenzene, and ethylcyclohexane.

(ii) Ring contraction products (RC): methylbicyclo[4.3.0]nonane, 3,7,7-trimethylbicylco[4.1.0]heptane, 3,7-dimethylbicyclo[3.3.0]octane, 1-methylbicyclo[3.3.1]nonane, 1,1-bicyclopentyl, spiro[4.5]decane.

(iii) Unsaturated ring opening products (USRO): butylbenzene, pentenylcyclopentane, butenylcyclohexane, 4-methyl-1-(1-methylethyl)cyclohexene, 1-methyl-4-(1-methylethylidene) cyclohexane, and 1-decene.

(iv) Saturated ring opening products: pentylcyclopentane, butylcyclohexane, *n*-decane, 3,4,5-trimethylheptane, 3,5-dimethyloctane, 4-methylnonane, 3-ethyl-2-methyl heptane, and 4-ethyl-3-methyl heptane.

(v) Dehydrogenation products (DH): Benzene, toluene, m-xylene, naphthalene, 1-methylindan, and tetralin.

The reaction mixture is treated as an ideal gas mixture and its equilibrium composition is calculated at 298 to 1000 K and 1 bar. It is possible that non-ideal phase behavior and multiple phases can exist in the reaction mixture with the actual reaction conditions. However, considering the large number of parameters such as critical properties and interaction coefficients, which are not available in the open literature for many of the compounds present in the reaction mixture, solving a complete chemical and phase equilibrium problem (CPE), is not attempted in this work.

In the initial unreacted state, the reactor feed is a mixture of *cis*-, and *trans*-decalin and hydrogen. The *cis*- and *trans*-decalin are in the molar ratio of 40:60. A hydrogen-to-hydrocarbon molar ratio of 2.433 is used in the calculation.

Out of 46 compounds considered for equilibrium calculation in the present work, thermochemical properties are not available in the open literature for 12 compounds. For these 12 compounds, ΔH_f^0, ΔS_f^0, and ΔG_f^0 values calculated using G3MP2 values at temperatures 298 K, 400-1000 K are listed in Table 5.2.2. The thermochemical properties required at higher temperatures other than 298 K are calculated using the utility program "*freqchk*" in *Gaussian 03* with the zero point correction obtained from scaled (0.8929) *HF/6-31G(d)* frequencies (Curtiss et al., 1999).

Table 5.2.2: Standard Gibbs free energy of formation (ΔG_f^0) in kcal/gmol calculated by G3MP2 methodology.

Compound name	Temperature							
	298 K	400 K	500 K	600 K	700 K	800 K	900 K	1000 K
1-methyl indane	38.38	50.10	62.13	74.47	87.0	99.65	112.37	125.12
methyl bicyclo [4.3.0] nonane	27.87	48.67	69.93	91.69	113.76	136.01	158.35	180.74
3,7 dimethyl bicyclo [3.3.0] octane	40.84	61.32	82.17	103.52	125.14	146.93	168.79	190.69
3,7 dimethyl bicyclo[3.3.0]octane	29.68	50.26	71.28	92.79	114.60	136.58	158.65	180.75
1-methyl bicyclo [3.3.1] nonane	19.67	41.00	62.77	85.05	107.64	130.41	153.28	176.18
1,1 bicyclopentyl	24.95	44.70	64.92	85.65	106.68	127.89	149.21	170.55
spiro[4.5] decane	26.86	47.78	69.16	91.04	113.24	135.61	158.07	180.57
butenyl cyclohexane	38.85	58.18	77.93	98.16	118.67	139.35	160.11	180.90
4-methyl-1-(1-methyl ethyl) cyclohexene	41.94	61.96	82.38	103.28	124.47	145.84	167.29	188.77
1-methyl-4-(1-methyl ethyl) cyclohexane	28.48	48.60	69.09	90.06	111.30	132.71	154.21	175.73
methylethylidene) cyclohexane	28.88	48.67	68.84	89.47	110.38	131.90	152.62	173.80
tetralin	39.75	51.51	63.59	76.00	88.61	101.35	114.15	126.99

While analyzing the equilibrium compositions of different compounds and how they change with respect to temperature a few interesting details have been observed. Out of 46 compounds, methane and naphthalene have the highest and lowest *H/C* ratios (exclude hydrogen) of 4 and 0.8 respectively and these two compounds make up the most of the mixture at all temperatures (99.96 wt% at 298 K and 89.96 wt% at 1000 K). Methane and naphthalene correspond to the lowest and highest Gibbs free-energy change of formations in the mixture. Further, the *LP* solution for the initial estimates, as discussed earlier, identifies these two components as the ones having non-zero weight fractions.

The guidance for selecting *a set of components* (Smith and Missen, 1979) based on lowest and highest Gibbs free energy of formation or lowest and highest *H/C* ratios or the components having non-zero weight fractions in *LP* solution can be quite useful in deriving a set of independent reactions for the reaction mixture. The *LP* solution of the mole fraction of the compounds remains the same at all temperatures though the value of the objective function changes. This means that the *LP* problem needs to be solved only at one temperature and using the same *LP* solution the initial estimates for mole fractions of all compounds can be obtained at all other temperatures.

The effect of temperature on the yields of cracking (CP), dehydrogenation (DH), and ring contraction (RC) products are shown in Figure 5.2.3. The total yield of cracking products decrease and the yield of dehydrogenation products increase with increase in temperatures respectively. The weight fraction of methane in the equilibrium mixture starts to reduce significantly after 700 K as the formation of aromatics from methane is highly favorable at higher temperatures (Qiu et al., 1997), which suggest further

fragmentation and subsequent formation of aromatics from cracking products are favorable at higher temperatures. Endothermic dehydrogenation reactions are favored at high temperatures as the yield of DH products increase with temperature as shown in Figure 5.2.3. Ring contraction is believed to be an intermediate step in ring opening reaction.

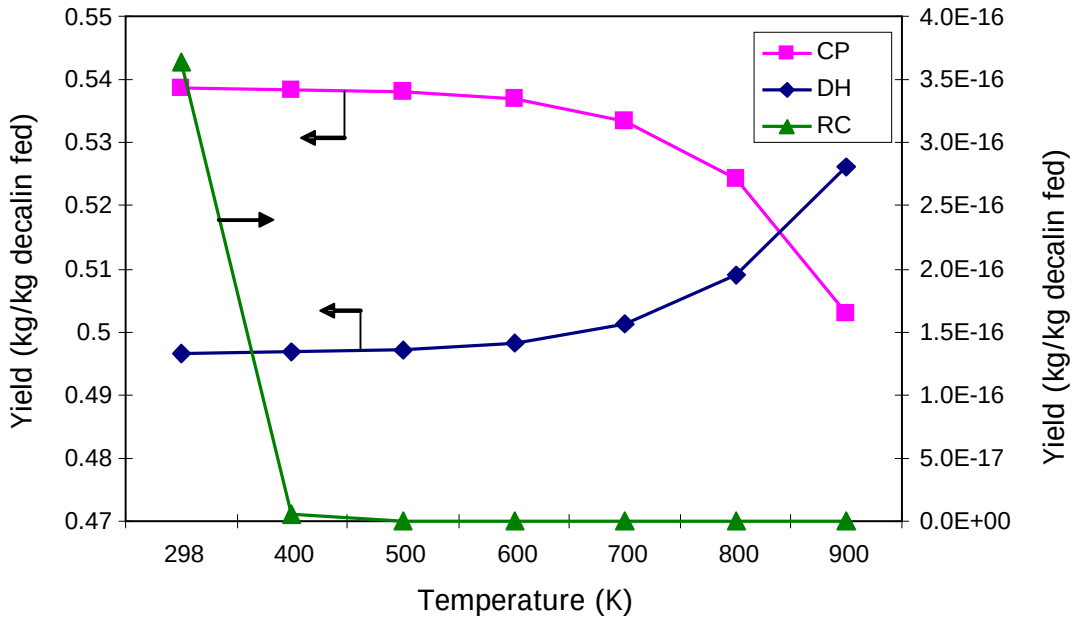

Figure 5.2.3: Yields of cracking (CP), ring contraction (RC), and dehydrogenation (DH) products, as a function of temperature, obtained from the thermodynamic equilibrium calculations.

The thermodynamic calculations show that the yield of RC products decreases drastically with increase in temperature and becomes almost zero at temperatures beyond 500 K. There are two possible reasons: (i) RC products considered in the equilibrium calculations are all saturated and their formation becomes unfavorable with respect to

increase in temperature and (ii) RC products undergo ring opening and subsequent cracking reactions.

The valuable information regarding the ring opening of decalin comes from analyzing the yield and selectivity of ring opening products. The yield of total ring opening products, as shown in Figure 5.2.4, increases with increase in temperature.

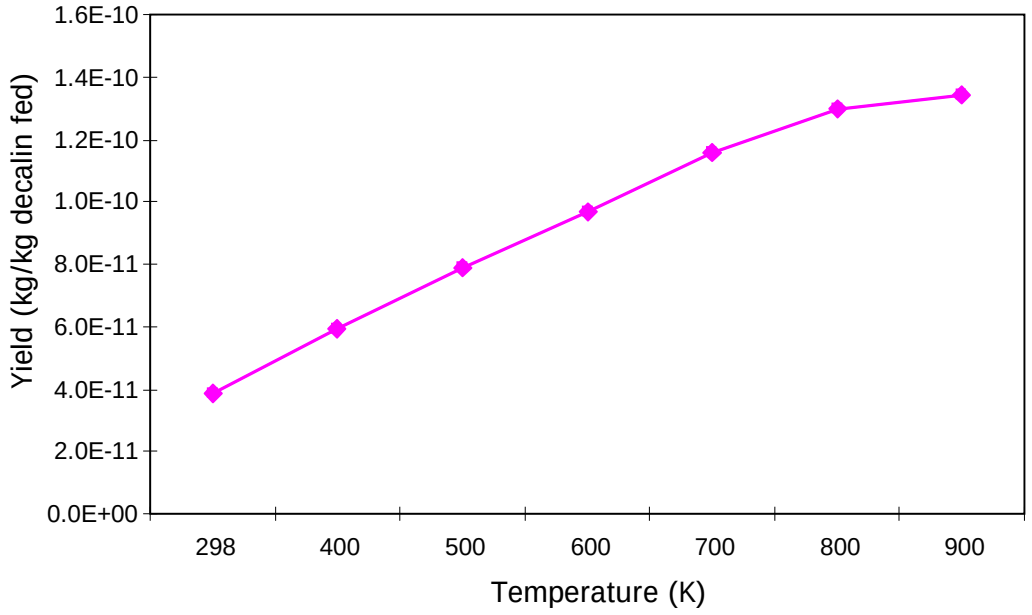

Figure 5.2.4: Yield of total ring opening (RO) products, as a function of temperature, obtained from thermodynamic equilibrium calculations.

We have mentioned earlier that ring opening reactions in hydrocracking environment are thermodynamically favored at low temperatures, however what is seen in Figure 5.2.4 is that increase in temperature favors both yield and selectivity. The reason behind this

can be understood by analyzing the yields of the two different groups of components which make up the total ring opening products.

The yields of SRO and USRO are shown in Figure 5.2.5. The yield of SRO products reduces and the yield of USRO products increases with increase in temperatures. As discussed in the earlier section, the saturated products form by hydrogenation after the ring opening reaction. The hydrogenation reactions are exothermic, which become unfavorable with increase in temperature. However, the unsaturated products, whether formed directly from ring opening or through dehydrogenation of saturated products, are very much favorable at higher temperatures as the equilibrium shifts towards cracking (without saturation) as well as towards dehydrogenation when the temperature increases. The yield profile for saturated ring opening products is similar to that of ring contraction products (cf. Figure 5.2.3).

An important observation made from this analysis is that in order to increase the yield and selectivity of ring opening products, the reactor temperature needs to be increased. Although the lower operating temperatures are suitable for producing saturated products via cracking followed by hydrogenation, higher selectivities and higher yields can only be achieved by maximizing the unsaturated ring opening products. However, increase in temperatures and the subsequent production of unsaturated species can be a problem with respect to excessive cracking and formation of coke precursors. In these situations, operating conditions and catalyst acidity are optimized by means of kinetic experiments in order to maximize yield and selectivity.

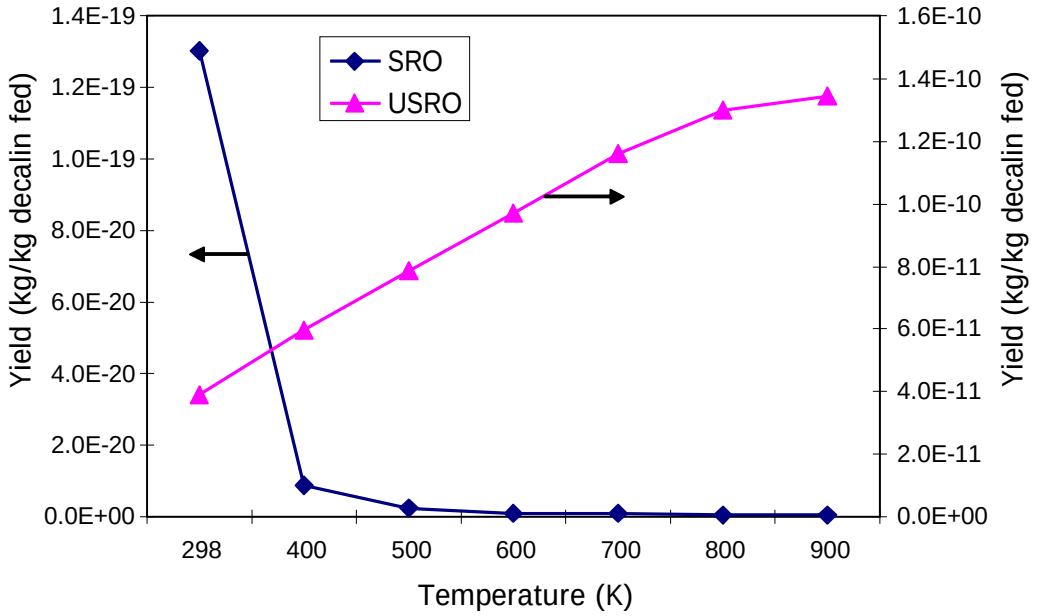

Figure 5.2.5: Yields of saturated (SRO) and unsaturated (USRO) ring opening products, as a function of temperature, obtained from the thermodynamic equilibrium calculations.

Cetane number improvement is an important factor in the ring opening reaction. Two-ring opening products formed from decalin have higher cetane numbers than that of decalin. The effect of temperature on yield of the two-ring opening products is shown in Figure 5.2.6. The two-ring opening products are *n*-decane, 1-decene, 3, 4, 5-trimethylheptane, 3, 5-dimethyloctane, 4-methylnonane, 3-ethyl 2-methylheptane, and 4-ethyl 3-methylheptane. Figure 5.2.6 presents the effect of temperature on the interplay between ring opening with and without hydrogenation at equilibrium. The yield of all saturated ring opening products reduces with increase in temperature (cf. Figure 5.2.5) however the production of unsaturated species 1-decene becomes dominant at higher

temperatures and increases the yield of two-ring opening products beyond 700 K. The ratio of yields of two-ring opening products to total ring opening products follows the same trend as that of Figure 5.2.6.

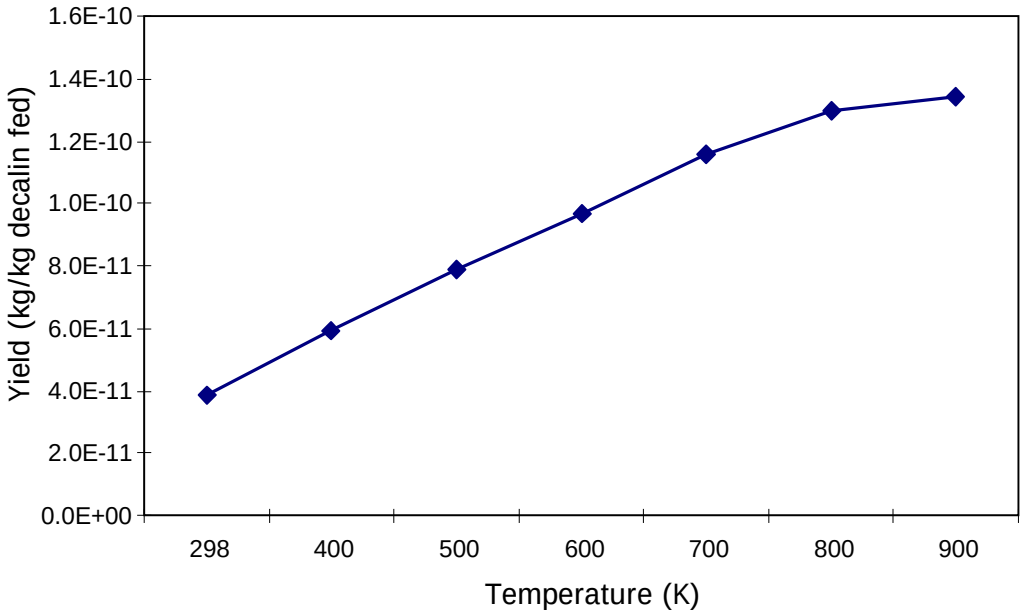

Figure 5.2.6: Yield of two-ring opening (TRO) products, as a function of temperature, obtained from thermodynamic equilibrium calculations.

5.2.4 Experimental observations

Kubicka et al. (2004a) studied ring opening of decalin over the proton-form zeolites – H-Beta-25, H-beta-75, H-modernite-20, and H-MCM-41. In their study the activity and deactivation of catalysts were correlated with acidity determined by FTIR pyridine adsorption, pore structure, and surface area changes. The effect of temperature and acid site concentration on ring opening of decalin was investigated without any interference of

pore-structure effects for H-Beta-25 (higher acidity) and H-Beta-70 (lower acidity), where the numbers 25 and 70 indicate SiO_2/Al_2O_3 ratios respectively. The authors indicated that the ring opening and cracking are the reaction steps most sensitive to catalyst acidity and temperature.

The effect of temperature on the concentration of ring opening products shows that the difference in concentration of ring opening products between the high- and low-acidity catalysts decreases as the temperature increases and the concentrations are almost the same for both catalysts at 553 K (Kubicka et al., 2004a). The increase in temperature favours the catalyst activity for both catalysts as this is evident from the increased formation of cracking products. However, when the temperature increases the lower acidity catalyst does not crack the ring opened products to the same extent as that of the higher acidity catalyst thus producing almost the same yield of ring opening products as that of the higher acidity catalyst at 553 K. The excessive cracking over the highly acidic H-Beta-25 converts the ring opening products into cracking products.

The thermodynamic equilibrium analysis of decalin carried out in the section 5.1 shows that the yield of total ring opening products increases with increasing temperature due to the fact that the formation of unsaturated compounds are favored at higher temperatures. The experimental evidence shows that the secondary cracking of ring opened products is reduced by reducing the acidity of the catalyst and the loss in activity due to the reduced acidity is compensated by increase in temperature. At higher temperatures the catalyst with lower acidity performs as good as the catalyst with higher acidity, which means yield of ring opening products can be increased by increasing the temperature while reducing the acidity of the catalyst.

Kubicka et al. (2004a, b) did not observe olefinic species in the product distribution. However, the hydrocracking experiments of decalin carried out by Mouli et al.(2007, 2009) showed that the yields of unsaturated ring opening products were observed consistently higher than the saturated ring opening products, but their yields reduced with increase in temperature due to excessive cracking.

It may be noted that the yield and selectivity values of the ring opening products calculated from the thermodynamic calculations are in the order of 10 to the power of (-10). In the present work, it was not attempted to compare the results from the thermodynamic calculations with the experiments but we have tried to show that the higher temperatures are preferred, from a thermodynamic perspective, to improve the yield and selectivity of ring opening products. This finding for the ring opening process has not been reported previously in the open literature. Comparison of the yields from the thermodynamic calculations with experimental observations should not be done in this case as the reaction system is not at equilibrium atleast with respect to the cracking reactions.

If lighter components such as methane and ethane are present in the reaction mixture that contains higher carbon number hydrocarbons too, the equilibrium composition will obviously favor the formation of smaller alkanes due to their lower standard Gibbs free energy values. This is the main reason behind the lower numbers (10 to the power of -10) for the yield values. The trend of increasing yields with respect to temperature is the important information for the experimental guidance but not their numerical values.

The key message from this work is that to improve yield and selectivity, the formation of unsaturated ring opening products must be promoted, which can be accomplished at higher operating temperatures. The implied guideline regarding the temperature and catalyst acidity is of fundamental importance to ring opening catalyst developers.

The choice of 1 bar pressure for thermodynamic calculations is far from reality. We have described the difficulties in incorporating the non-ideal phase behavior in our calculations. However, it must be pointed out that the conclusions we have derived from our calculations will remain the same because of the simple fact that thermodynamics favor dehydrogenation reactions at high temperatures, which facilitates the formation of unsaturated species. It must also be pointed out that the equilibrium calculations do not depend on the reaction mechanisms, and even if we restrict the type of the components based on the mechanistic considerations, the results will provide the same conclusions.

5.2.5 Summary

To understand the thermodynamic limitations on yield and selectivity of ring opening products, thermodynamic equilibrium calculations have been performed on a reaction mixture obtained from hydrocracking of decalin. A study of thermochemistry of single cracking reactions shows that the favorability of endocyclic cracking reactions of naphthenes increases over acyclic and exocyclic cracking reactions with increase in temperature. The equilibrium calculations performed on decalin reaction mixture show that the yield and selectivity of ring opening products increase with increasing temperature. This occurs because the increase in temperature favors the formation of unsaturated ring opening products as opposed to the formation of saturated ring opening

products. Secondary cracking and thermodynamic limitation of hydrogenation reaction cause the yield of saturated ring opening products reduce with increase in temperature.

Experimental evidence shows that by reducing the acidity of the catalyst and at the same time compensating the loss of activity by increasing the temperature leads to higher yield and selectivity. Based on these studies it is expected that lowering acidity of the catalyst to avoid excessive cracking and increasing the operating temperature to favor (i) the formation of unsaturated ring opening products and (ii) ring opening reaction over acyclic and exocyclic cracking reactions will improve the yield and selectivity of total ring opening products.

5.3 Comparison between ring opening of decalin on Ir-Pt and Ni-Mo carbide catalysts supported on zeolites.

This section gives a detailed description about the preparation, characterization and catalytic study of Ir-Pt noble metal catalysts supported on HY, H-Beta. Ni-Mo carbides supported on HY, H-Beta, Al-SBA-15 and Si-Al also will be studied for the ring opening of decalin. A comparison between the noble metal catalysts and carbide catalysts on the ring opening of decalin will be described in detail.

Group V111 noble metals (Platinum, Iridium, Osmium, Palladium, Rhodium and Ruthenium) are very active in hydrogenation and dehydrogenation reactions. Medium pore zeolites like HY and H-Beta have a pore size of 5 to 10 A and with high surface areas. These zeolites have a proven capability in providing acidic sites for isomerization and cracking reactions. Combination of metal and acid sites is required for the achievement of high ring opening yields. However these noble metals are costly and prone to the sulfur poisoning. On the other hand, carbide catalysts show good resistance to sulfur poisoning and also are cheap. Carbide catalysts are refractory in nature and they are resistant to sintering and attrition under reaction conditions. Ni and Mo composition is used based on the optimum composition used for the hydrotreating reactions. In this section an attempt is made to compare the ring opening activity between noble metal supported catalysts and Ni-Mo carbides supported on zeolites.

5.3.1 Catalyst Characterization

A detailed characterization of all the catalysts using XRD, TPR, TPD, CO chemisorption, ICP-MS, and CHNS analysis was carried out to see the physical and chemical characteristics of the catalysts.

5.3.1.1 Characterization of Ir-Pt supported on HY and H-Beta catalysts

The BET surface area, CO uptake and total acidity of HY, H-Beta supports and Ir-Pt catalysts supported on HY and H-Beta are shown in Table 5.3.1.

Table 5.3.1: Physicochemical properties of Ir-Pt catalysts.

Catalyst	SiO_2/Al_2O_3 Molar ratio	%Pt (wt.%)	%Ir (wt.%)	BET surface area, m^2/g	Pore volume, cc/g	Mesopore area, m^2/g	CO uptake µmol CO/g	Total Acid strength µmol NH_3/g
HY	11.60	-	-	763	0.47	140	-	583
H-Beta	25.00	-	-	581	0.43	100	-	326
Ir-Pt /HY	13.30	1.50	0.75	641	0.45	120	25.80	371
Ir-Pt /H-Beta	27.50	1.50	0.75	530	0.41	90	20.30	160

After impregnation of supports with Ir and Pt, the surface area decreased by 10-15%. This may be due to the pore filling by the Ir and Pt. The CO uptake of the Ir-Pt catalysts is also shown in Table 5.3.1. The total acidity of the supports as well as the Ir-Pt catalysts supported on HY and H-Beta are calculated from the NH_3-TPD curves shown in Figure 5.3.1. There is a 36 to 50% decrease in the total amount of acidic sites of the HY and H-Beta after impregnation.

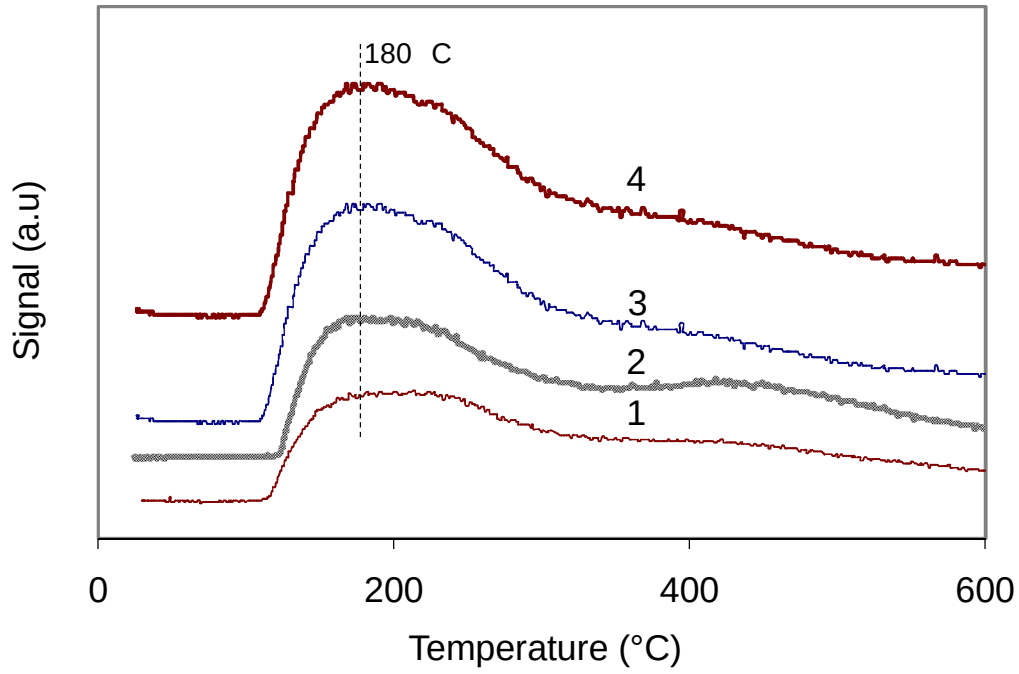

Figure 5.3.1: NH_3 TPD graphs of (1) Ir-Pt/H-Beta, (2) Ir-Pt/HY, (3) H-beta and (4) HY catalysts.

The decrease in the amount of acidic sites is due to the coverage of acid sites by the metals. From the TPD of ammonia, the acid sites are classified as weak, medium and strong (BorCave, 1997). In the TPD curve shown in Figures. 5.3.1 and 5.3.3, the NH_3 desorbed below 250 °C is due to weak acid sites. The NH_3 desorbed above 250 °C and below 400 °C is due to medium strength acid sites and the NH_3 desorbed above 400 °C is due to strong acid sites. In Figure 5.3.1, the presence of a small peak between 400 °C and 500 °C for the Ir-Pt/HY catalyst indicated higher acid strength than the Ir-Pt/H-Beta catalyst.

The TPR profiles of the Ir-Pt catalysts are displayed in Figure 5.3.2. The Ir-Pt catalysts displayed their H_2 consumption peak at 210 to 220 ℃ and one more shoulder peak at 260 ℃. The characteristic consumption peak at 210-220 ℃ with the Ir-Pt catalysts is attributed to reduction of iridium oxide (Nylén, 2004). The peak at 260 °C is assigned as the reduction of Pt^{2+} (Yoshioka, 2005).

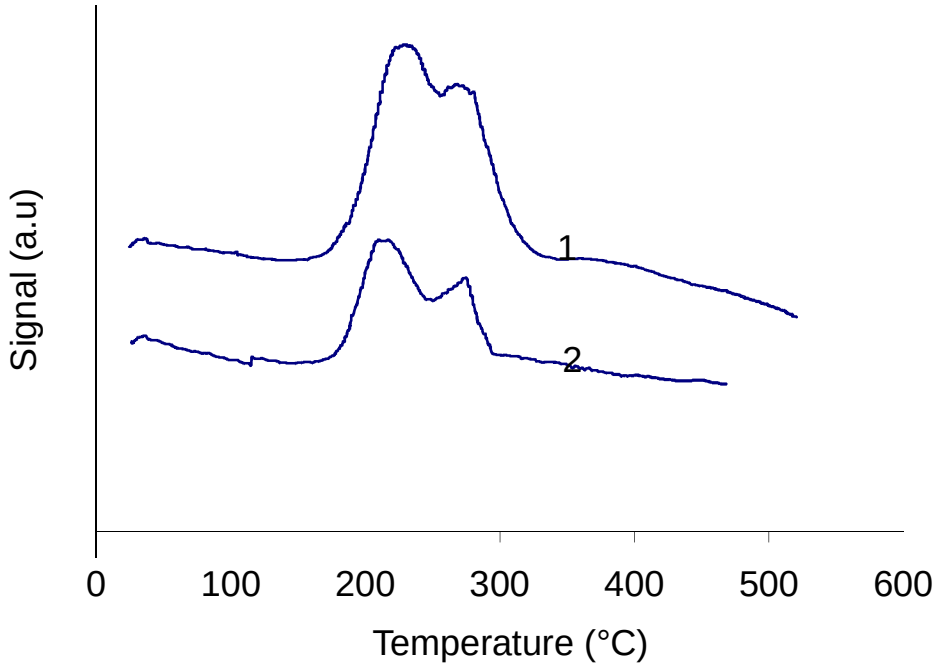

Figure 5.3.2: TPR patterns of the (1) Ir-Pt /HY and (2) Ir-Pt/H-Beta catalysts.

5.3.1.2 Characterization of Ni-Mo carbide catalysts.2.1.2

The elemental compositions, BET surface area and CO uptake of Ni-Mo carbide catalysts on HY, H-Beta, silica-alumina (Si-Al), Al-SBA-15 and γ-alumina supports are given in Table 5.3.2.

Table 5.3.2: Physicochemical properties of carbide catalysts.

Catalyst	Si/Al Ratio	%Ni (wt%)	%Mo (wt%)	BET surface area, m^2/g	CO uptake μmol CO/g	Total Acid strength μmol NH_3/g	Mo/C molar ratio
NiMoC / HY	13.5	2.25	11.3	492	69	189	2.0
NiMoC / H-Beta	22.9	2.25	11.2	395	66	116	1.9
NiMoC / Al-SBA15	55.7	2.45	12.0	391	37	31	2.2
NI-MoC / Si-Al	0.3	2.44	11.2	371	37	26	2.1
NiMoC / γ-Alumina	-	2.40	11.8	199	52	27	3.2

Elemental chemical analysis of carbide catalysts indicates that the Mo and Ni contents are equal to or slightly less than the corresponding targeted value of 12 and 2.5 wt% respectively. The BET surface area of the prepared carbide catalysts is slightly lower than that of the supports. This is apparently due to pore filling of supports by the Ni and Mo species. As shown in Table 5.3.2, the Mo/C ratio of the carbide catalysts supported on HY, Si-Al, Al-SBA15 and γ-alumina is equal or slightly greater than the

stoichiometric value of 2. Similar results were observed with supported carbide catalysts (Costa, 2004; Dhandapani, 1998; Costa, 2001). This higher Mo/C ratio indicates a strong interaction between support and molybdate (Wei, 1997). Carbon monoxide was used as a molecular probe to find out the number of accessible surface metal atoms on the carbide catalysts. As shown in Table 5.3.2, the CO uptakes of carbide catalysts supported on HY and H-Beta are higher than those of other carbide catalysts. This indicates uniform dispersion of metal sites on the surface of the HY and H-Beta supports. CO uptake of carbide catalysts is higher than that of Ir-Pt catalysts as expected due to higher metals loading. The total acidity of all carbide catalysts is shown in Table 5.3.2 and also in Figure 5.3.3. The carbide catalyst supported on HY shows more total acidic sites than other catalysts.

The comparison of TPD profile of HY and H-Beta supports shown in Figure 5.3.1 with those of corresponding carbide catalysts shown in Figure 5.3.3 indicates the presence of strong acid sites in the supported metals carbide catalysts. Literature (Diaz, 2003) showed the presence of coordinately unsaturated (CUS) Mo^{4+} sites on the surface of the support. These are well dispersed and not identified by XRD data. The strong acid sites on the carbide catalysts may be due to these CUS sites which are Lewis acid sites. According to the acid strength definition in the section 3.1.1, the γ-alumina, silica-alumina and SBA-15 catalysts show weak acid sites, whereas the HY and H-Beta-supported carbide catalysts show medium to strong acid sites.

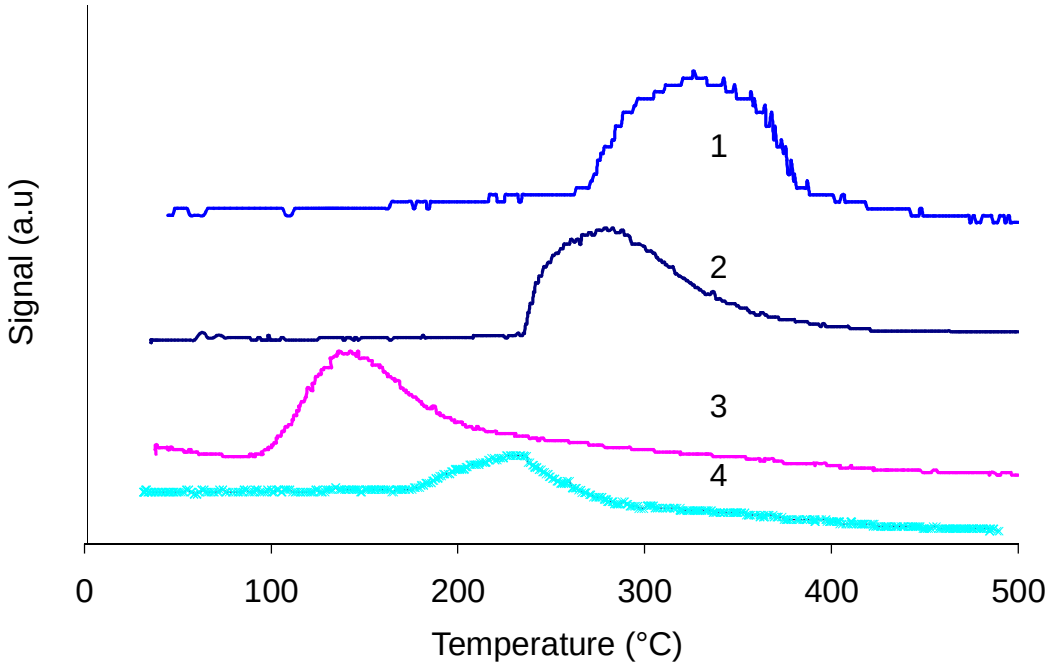

Figure 5.3.3: NH3 - TPD plots of Ni-Mo/carbide catalysts supported on (1) HY, (2) H-Beta, (3) Al-SBA-15, (4) Silica –Alumina.

H_2-TPR profiles of the passivated carbide catalysts are shown in Figure 5.3.4. All carbide catalysts showed a major H_2 consumption peak in the range of 220 to 280 °C. The peaks in this range are due to the reduction of surface oxygen bonded to Mo species of different states, which were formed during the passivation of the catalysts (Wei, 1997). The NiMo/γ-Al_2O_3 carbide catalyst exhibits a similar H_2 consumption peak at 255 °C, which was reported in our earlier publication (Sundaramurthy, 2007).

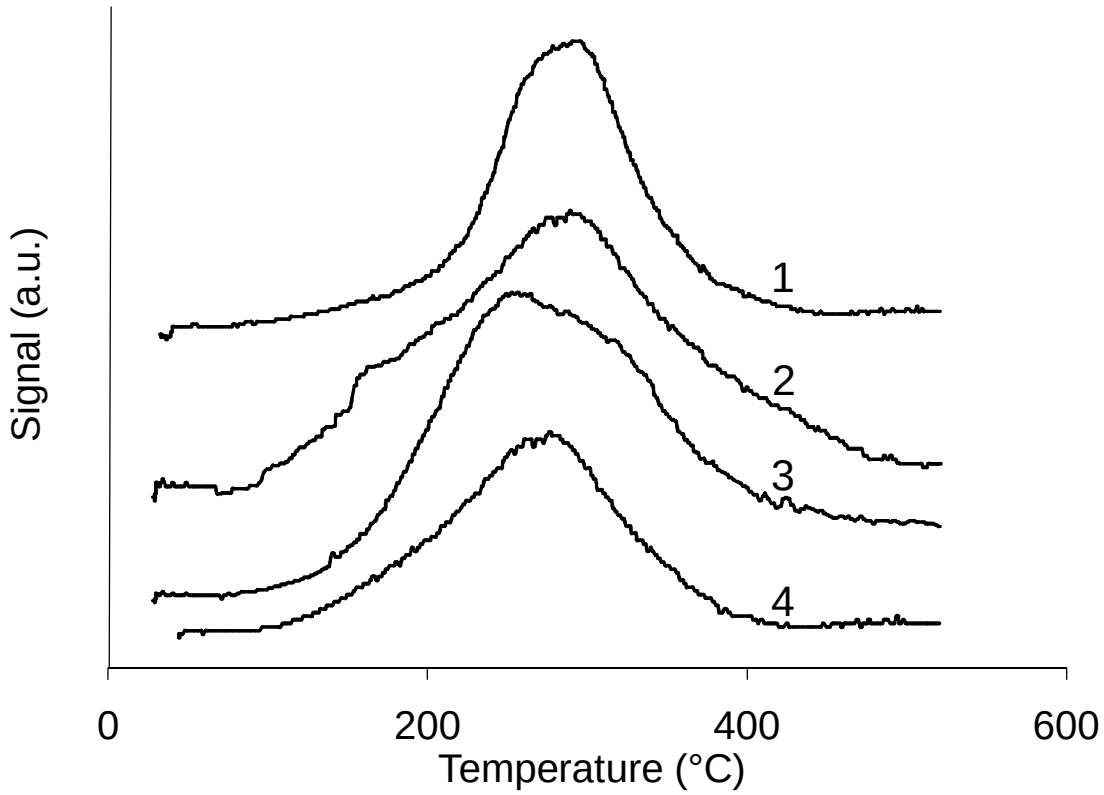

Figure 5.3.4: TPR patterns of the passivated Ni-Mo/Carbide catalysts supported on (1) HY, (2) H-Beta, (3) Al-SBA-15, (4)Silica-Alumina.

The XRD patterns of HY and H-Beta supports and all carbide catalysts are shown in Figure 5.3.5. HY and Ni-Mo carbide/HY catalysts show similar peaks in the diffractograms in agreement with the literature (Pedrosa, 2006). There is no peak representing Mo oxide or Mo carbide on the catalyst supported on HY. The characteristic peak shown by H-Beta at 2θ of 23° well matches with the literature (Zhang, 2007). The carbide catalyst supported on H-Beta showed extra peaks at 2θ of 26° and 38° which represent Mo oxide and β-Mo_2C respectively (Ardakani, 2007).

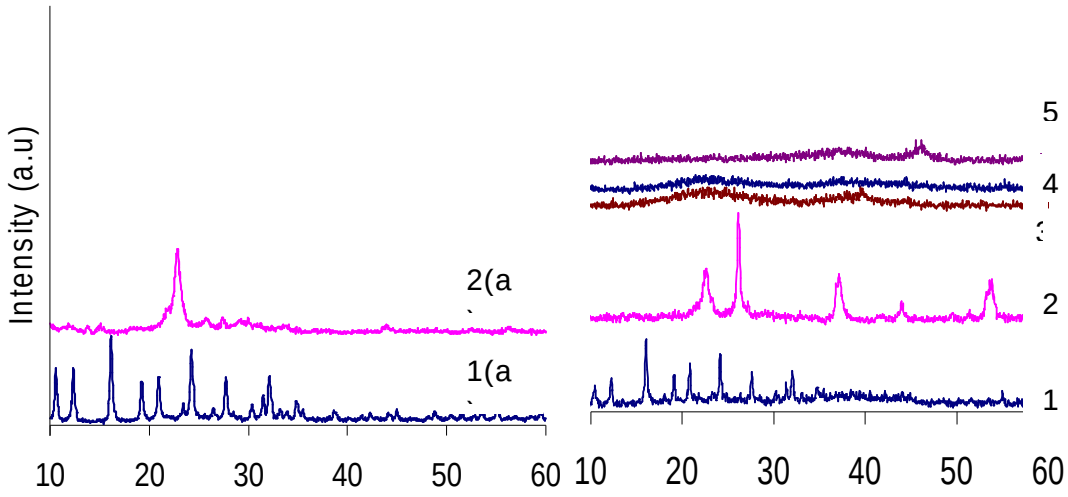

Figure 5.3.5: XRD patterns of the Ni-Mo carbide catalysts on various supports, (1) HY, (2) H-Beta, (3) Al-SBA -15, (4) Silica-Alumina and (5) γ-Alumina and on pure supports, (1a) HY and (2a) H-Beta.

The crystallinity of the zeolite does not change much because the intensity of the peaks in XRD is not decreased much in the Ni-Mo carbide catalysts during the carburization process. The difference in the BET surface area of the carbide catalysts before and after carburization is within 3-5%, which indicates no change in the structure of the zeolite. Further more; there is no apparent evidence for molybdenum carbide in the diffractograms of the carbide catalysts supported on HY, Al-Si and Al-SBA15, which indicates good dispersion of Mo_2C-like carbides on the surface of the supports. The Mo/C ratio of different catalysts varied from 1.9 to 3.2, and in most cases close to 2, as shown by elemental and CHNSO analyses (Table 5.3.2). Therefore, we assume the formation of Mo_2C-like carbides on the surface of the catalysts. However, Mo_2C peaks could not be identified by XRD data (Figure 5.3.5) indicating that they were well dispersed on the catalyst.

5.3.2 Catalytic activity

The products from the decalin ring- opening reaction are classified as follows:

(vi) Cracking products (CP): Methane, ethane, propane, isobutane, isopentane, methylcyclopentane, methyl cyclohexane, n-octane, 1-octene, n-nonane, 1-nonene, 1, 4-dimethylcyclohexane, propylcyclohexane, 1, 3, 5-trimethylcyclohexane, ethylbenzene, and ethylcyclohexane.

(vii) Ring-contraction products (RC): methylbicyclo[4.3.0]nonane, 3,7,7-trimethylbicylco[4.1.0]heptane, 3,7-dimethylbicyclo[3.3.0]octane, 1-methylbicyclo[3.3.1]nonane, 1,1-bicyclopentyl, spiro[4.5]decane.

(viii) Ring-opening products (RO): butylbenzene, pentenylcyclopentane, butenylcyclohexane, 4-methyl-1-(1-methylethyl)cyclohexene, 1-methyl-4-(1-methylethylidene) cyclohexane, 1-decene, pentylcyclopentane, butylcyclohexane, *n*-decane, 3,4,5-trimethylheptane, 3,5-dimethyloctane, 4-methylnonane, 3-ethyl-2-methyl heptane, and 4-ethyl-3-methyl heptane.

(ix) Dehydrogenation products (DH): Benzene, toluene, m-xylene, naphthalene, 1-methylindan, and tetralin.

The possible reaction scheme for decalin ring-opening reaction is shown in Figure 5.3.6.

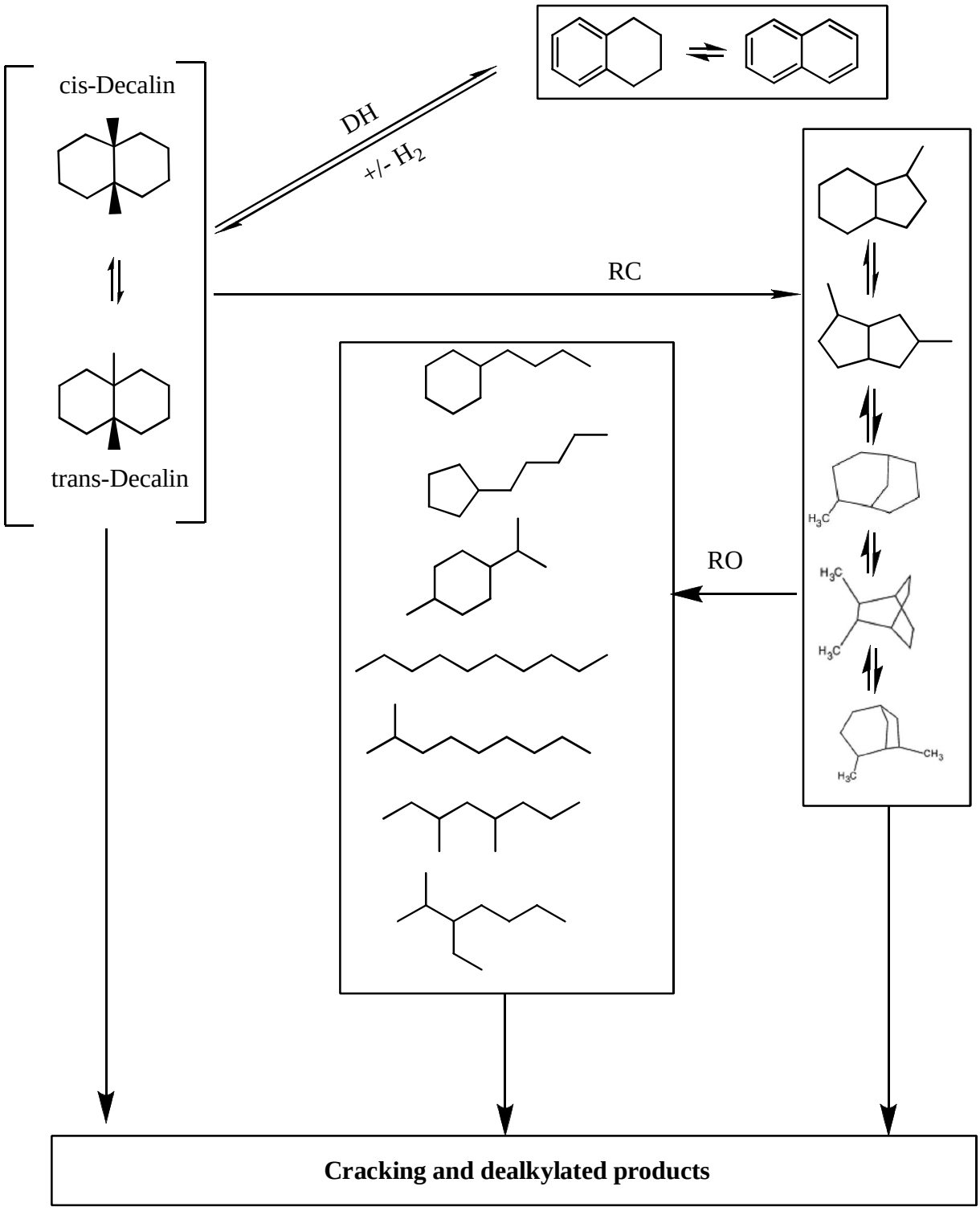

Figure 5.3.6: Reaction scheme of decalin ring-opening reaction

The metallic sites are responsible for hydrogenation and dehydrogenation reactions whereas the Brønsted acid sites are responsible for cracking and ring-opening reactions (Kubicka, 2004a; Santikunaporn, 2004; McVicker, 2002). The possible path toward the ring-opening products is through RC products as shown in Figure 5.3.6. These products have been identified by GC-MS analysis of decalin ring-opening reaction. The β-scission on the ring due to endocyclic cracking leads to RO products, whereas exocyclic cracking leads to dealkylation products. Secondary cracking of the RO products results in formation of the low molecular weight cracking products.

5.3.2.1 Ir-Pt catalysts supported on H-Y and H-beta

The effect of temperature on the conversion of decalin on Ir-Pt supported on HY and H-Beta is shown in Figure 5.3.7. The conversion of decalin was higher at all temperatures on the H-Y catalyst than on the H-Beta catalyst and reached almost 99% at 260 °C, as shown in Figure 5.3.7 and Table 5.3.3.

Table 5.3.3: Comparison of RO yield and selectivity on Ir-Pt and Ni-Mo carbide catalysts supported on HY.

Catalyst	Conversion (wt.%)			RO Yield (wt.%)			RO selectivity (%)		
	220°C	240°C	260°C	220°C	240°C	260°C	220°C	240°C	260°C
Ir-Pt/HY	82.8	92.4	99.4	31.7	11.7	0.3	65.1	14.9	0.3
Ni-Mo / HYcarbide	44.3	84.6	99.8	16.0	33.7	16.0	36.2	39.8	16.3

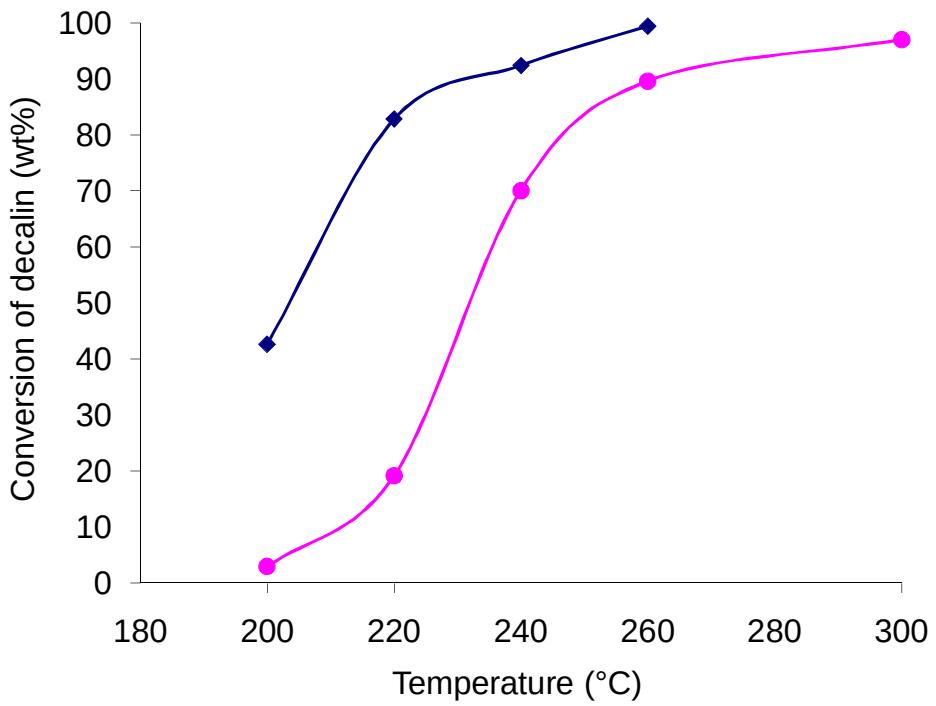

Figure 5.3.7: Conversions of decalin on catalyst (♦) Ir-Pt/HY and (●) Ir-Pt/H-Beta as a function of temperature at a pressure of 5 MPa and LHSV of 1.5 h^{-1}.

The effect of temperature on the yields of CP, RC, and DH products are given in Figure 5.3.8. At 200 °C the yield of RC products on Ir-Pt/HY is 10%, increased to 18% at 220 °C, and then decreases. In the case of Ir-Pt/H-Beta, the RC products increased with temperature up to 260 °C and then started converting to RO products. On Ir-Pt/HY, the yield of dehydrogenation products increased with an increase in temperature from 200 to 240 °C and then decreased with increasing temperature up to 260 °C possibly due to their conversion towards coke-forming precursors.

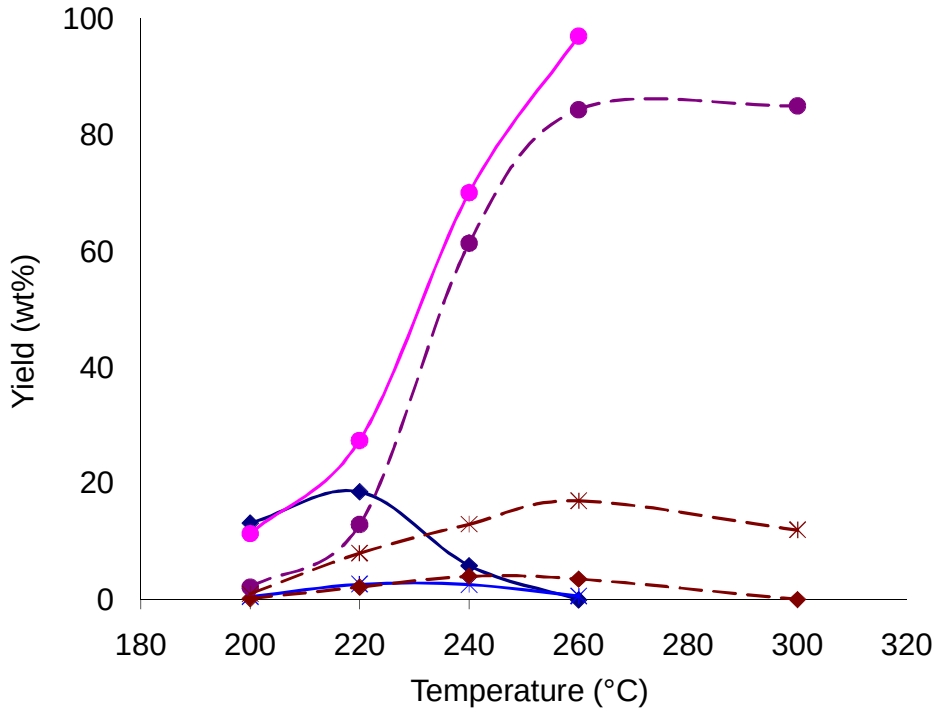

Figure 5.3.8: The yield of cracking (●), RC (♦) and DH (x) products as a function of temperature on catalysts Ir-Pt/H-Y (solid line) and Ir-Pt/H-Beta (dotted line). (Pressure of 5 MPa and LHSV of 1.5 h^{-1}).

The Ir-Pt/H-Beta catalyst gave a maximum of DH products yield of 10% at 260 °C and then converted to coke-forming precursors above 260 °C. The effects of temperature on the yield and selectivity of total ring-opening products are shown in Figure 5.3.9. The RO selectivity can be defined as the ratio of the wt.% of the RO products to the wt.% of the (RC+CP+DH) products. A maximum RO yield of 35% was obtained at 220 °C on Ir-Pt/HY, whereas Ir-Pt/H-Beta gave a maximum yield of 15% only at 260 °C.

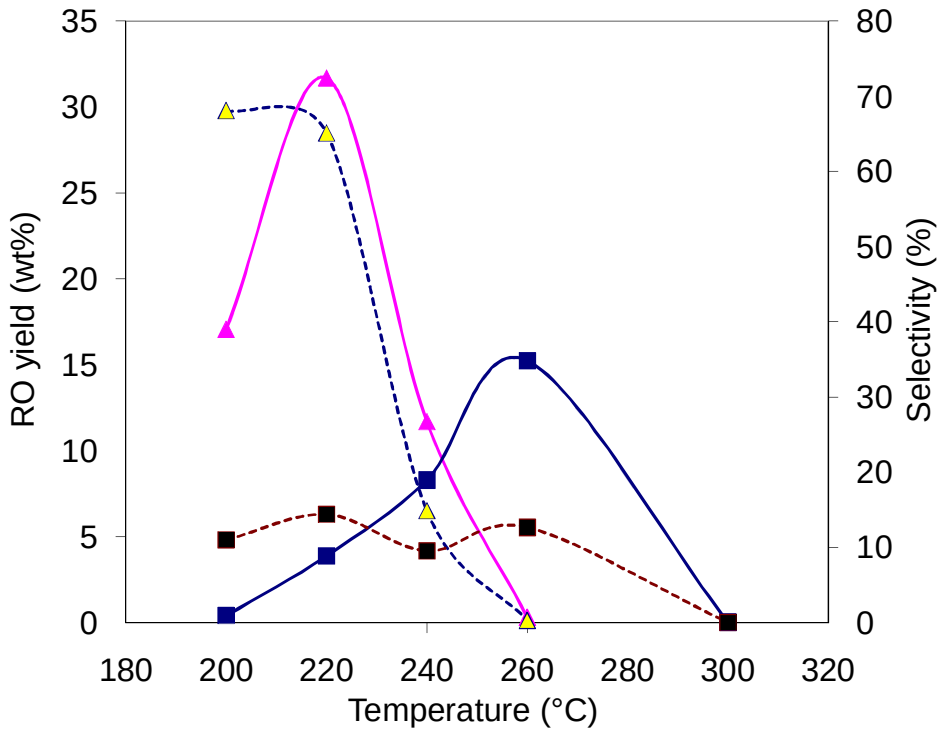

Figure 5.3.9: The RO yield (Solid line) and selectivity (dotted line) as a function of temperature on catalysts at a pressure of 5 MPa and LHSV of 1.5 h^{-1}. (Ir-Pt/ HY (▲); Ir-Pt/H-Beta (■)).

The Ir-Pt/HY catalysts show higher RO selectivity up to 220 °C compared to the Ir-Pt/H-Beta catalysts. A RO selectivity of 63% was achieved by the Ir-Pt/HY catalyst at 220 °C at which the RO yield was maximum, whereas the H-Beta-supported catalyst showed 12% RO selectivity at 260 °C, at which the RO yield was maximum. The effect of temperature on the yield and selectivity of saturated and unsaturated ring-opening products on Ir-Pt/HY is shown in Figure 5.3.10. They followed the same trend as that of total ring-opening products.

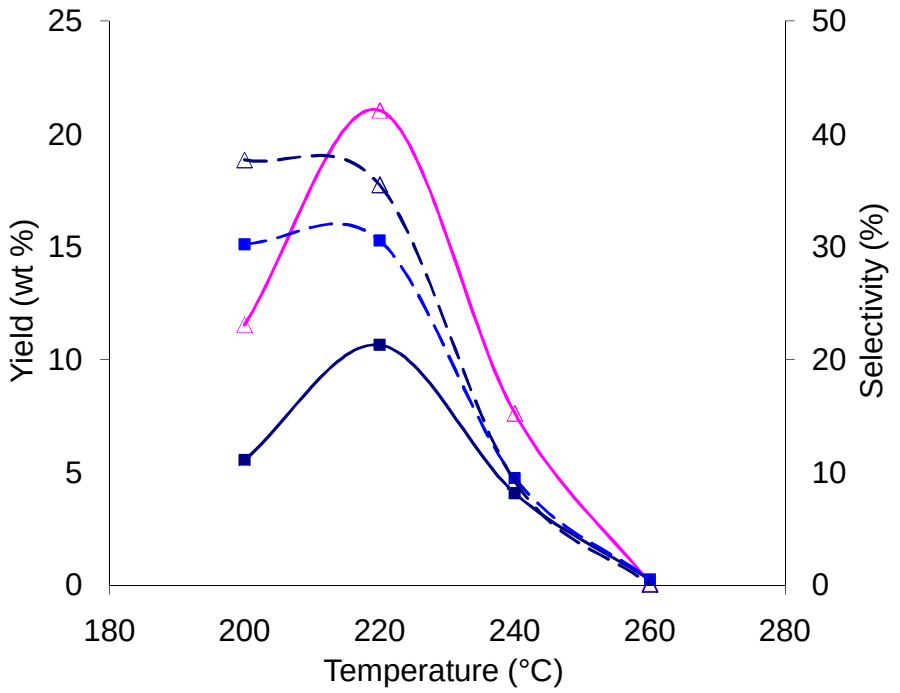

Figure 5.3.10: The saturated and unsaturated RO yield (Solid line) and selectivity (dotted line) as a function of temperature on catalyst Ir-Pt/ HY at a pressure of 5 MPa and LHSV of 1.5 h^{-1}. (Saturated RO products (■); Unsaturated RO products (Δ)).

The yield of unsaturated products increased with increasing temperature up to 220 °C because cracking (without hydrogenation) and dehydrogenation are favored with an increase in temperature. Above 220 °C, ring-opening products underwent further cracking to form C_1 to C_6 hydrocarbons. The subtle difference between the depletion of saturated and unsaturated ring-opening products can be used to think of ways to improve their yield. The conversion of decalin does not present a problem (Figure 5.3.7) for achieving higher RO yields but the excessive cracking eventually reduces the yield and

selectivity of ring-opening products (Figure 5.3.9). If the yield of cracking products is reduced by decreasing the acidity of the catalyst, reaction at high temperatures may favor better ring-opening products yields. However, high temperatures favor the formation of dehydrogenation products (Mouli, 2007) which might lead to coke-forming precursors.

Further, the opening of second ring in decalin is an important step in the view of cetane improvement. The effect of temperature on the yield and selectivity of two-ring-opening (TRO) products on Ir-Pt/HY is shown in Figure 5.3.11.

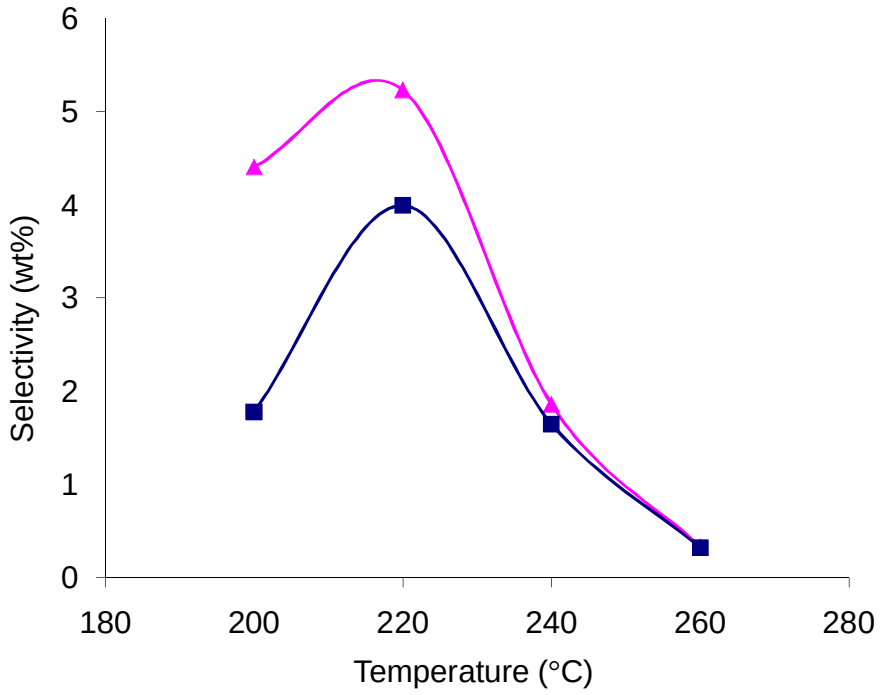

Figure 5.3.11: The yield (■) and selectivity (▲) of two-ring-opening (TRO) products as a function of temperature on catalyst Ir-Pt/H-Y at a pressure of 5 MPa and LHSV of 1.5 h^{-1}.

A maximum TRO selectivity of 5% at the yield of 4% was observed at 220 °C. The increase in the yield and selectivity from 200 to 220 °C is explained as follows. The

yield of saturated two-ring-opening products decreases with an increase in temperature. In contrast, the yield of unsaturated two-ring-opening products increases thus making the yield and selectivity increase with temperature. The yields of unsaturated species such as 2, 6-dimethyl-2-octene, 3-methyl-4-nonene increase with increase in temperature and beyond this temperature range excessive cracking causes the yield and selectivity to decrease. The ratio of two-ring-opening products to total ring-opening products increases with an increase in temperature which is observed in the present work and also reported in our earlier work (Mouli, 2007).

5.3.2.2 Ni-Mo carbide catalysts

The conversion of decalin on Ni-Mo carbide supported on HY, H-Beta, Al-SBA-15, silica-alumina and γ-alumina is shown in Figure 5.3.12. It was observed that the carbide catalysts supported on HY and H-Beta gave higher conversions (more than 80%), whereas carbides supported on other supports (SBA-15, silica-alumina and γ-alumina) showed negligible conversion. This is due to the weak acidity of latter sets of catalysts as evidenced by the NH_3-TPD. The Ni-Mo carbide catalysts supported on HY and H-Beta were chosen for optimization of process variables. Low temperatures (240-260 °C) favored higher conversion for the HY-supported carbide catalysts, whereas high temperatures (280-300 °C) favored higher conversion for the H-Beta-supported carbide catalysts. The deactivation behavior was observed continuously for 150 h.

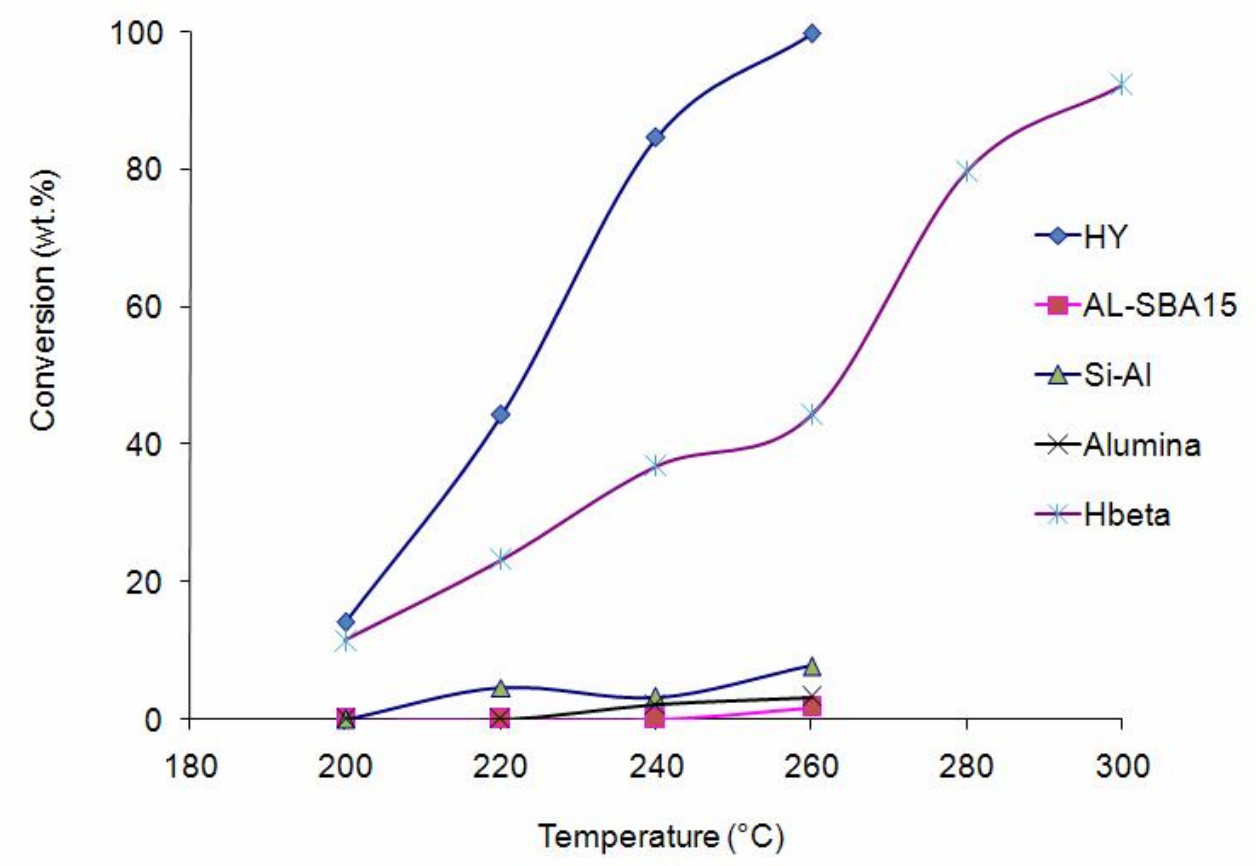

Figure 5.3.12: The conversions of decalin as a function of temperature on Ni-Mo/Carbide catalysts. Pressure = 5 MPa and LHSV = 1.5 h^{-1}.

The conversions at different times at temperature of 260 °C are shown in Figure 5.3.13. There was a 2% decrease in the conversion of decalin at the end of 150 h, which indicates the activity did not change much with the time period of 150 h. The products from decalin RO reaction are classified as RO, CP, RC and dehydrogenation products as discussed in the earlier section.

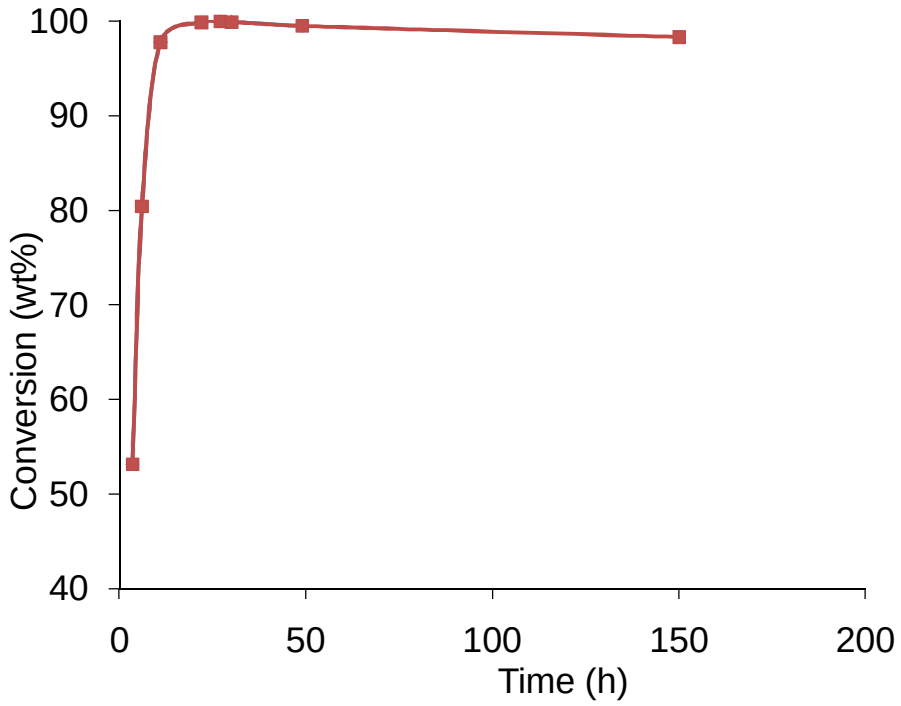

Figure 5.3.13: Conversion of decalin on Ni-Mo carbide/HY catalysts over time on stream at a temperature of 260 °C, pressure of 5 MPa and LHSV of 1.5 h^{-1}.

The ring-opening products yield with temperature on Ni-Mo carbides supported on HY and H-Beta is shown in Figure 5.3.14. A maximum ring-opening products yield of 33.7% was observed with the HY-supported carbide catalyst at 240 °C whereas the H-Beta-supported catalyst gave a maximum of 21.8% RO yield at 300 °C. The RO selectivity on both HY and H-beta supports are also shown in Figure 5.3.14. A maximum of 26% selectivity was observed on Ni-Mo carbide supported on H-Beta at 280 °C, whereas Ni-Mo carbide supported on HY showed a maximum selectivity of 40% at 240 °C. Observation of the products of decalin ring-opening reaction at 200 °C on Ni-Mo

carbide/HY and Ni-Mo carbide/H-Beta clearly indicates the effect of pore size on the product distribution. Even though the conversion is the same at this temperature on both the catalysts, HY gave higher yield and selectivity of ring-opening products. Due to large pore size, high mesoporous surface area and more amount of acid sites as shown in Table 5.3.2, Ni-Mo carbide supported on HY gave higher yield and selectivity of ring-opening products.

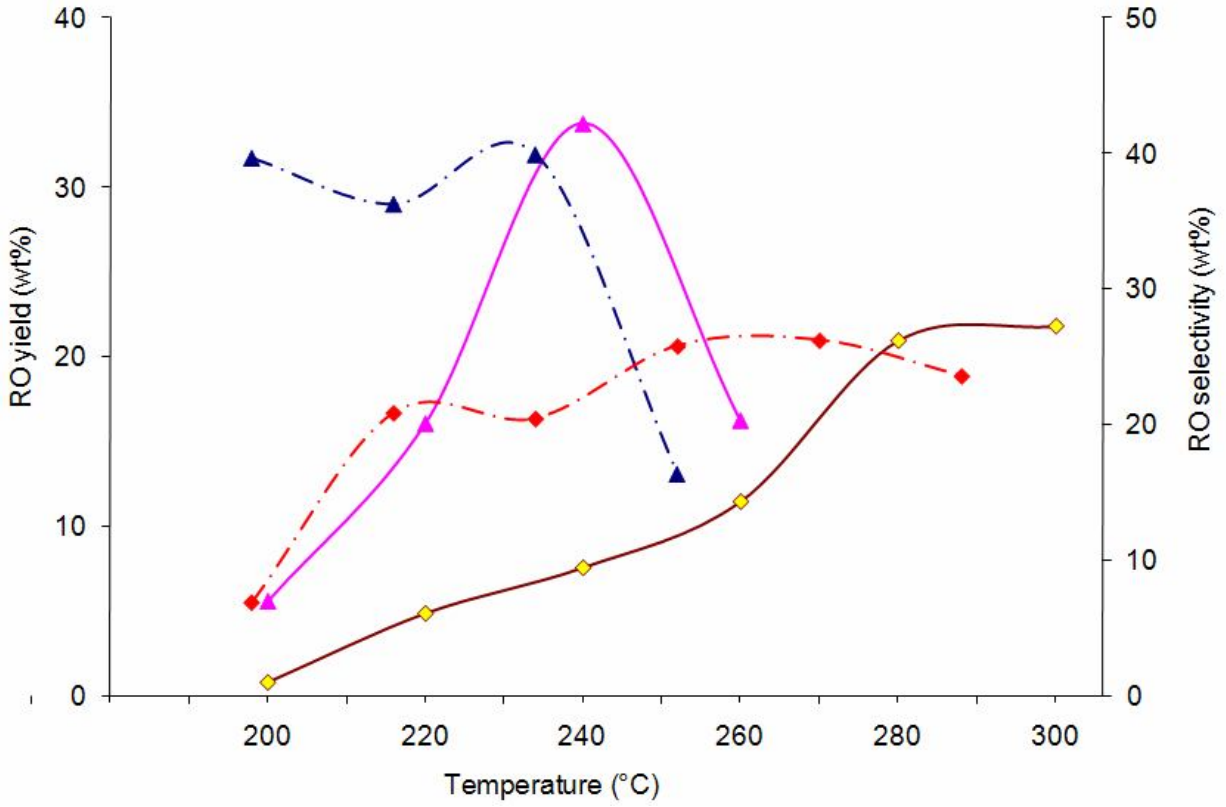

Figure 5.3.14: The RO product yield (solid line) and selectivity (dotted line) of decalin as a function of temperature on Ni-Mo/Carbide catalysts supported on HY (▲) and H-Beta (♦). (Pressure of 5 MPa and LHSV of 1.5 h^{-1}).

RC and cracking product yields with temperature changed on the Ni-Mo/carbide catalysts supported on HY and H-Beta are shown in Figure 5.3.15. The RC products yield

on the carbide/HY and carbide/H-Beta catalysts shows similar trends to that observed in the previous section with noble metals. The trends clearly show that the RC products are the intermediates before converting to ring-opening products.

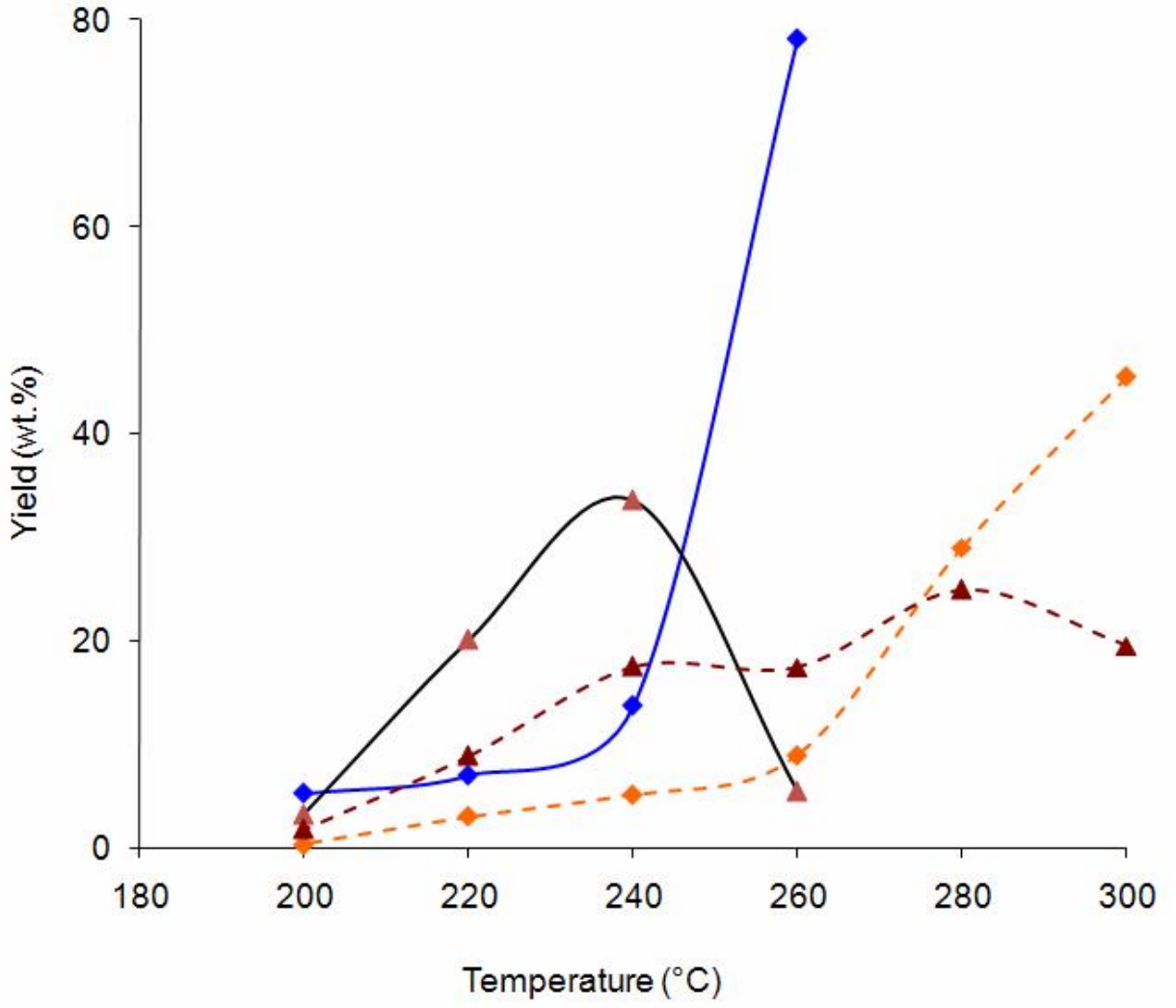

Figure 5.3.15: The Yield (wt.%) of RC (▲) and CP (♦)products as a function of temperature on Ni-Mo/Carbide catalysts supported on HY(solid lines) and H-Beta (dotted lines). (Pressure of 5 MPa and LHSV of 1.5 h^{-1}).

On the HY-supported carbide catalyst the cracking is dominant above 240 °C and behaved in the same way as that of Ir-Pt/HY. But in the case of H-Beta-supported carbide

catalysts, high cracking activity emerged above 260 °C. The cracking activity of H-Beta is low between 240 and 260 °C due to its low acidity, low mesopore area and small pore volume compared to HY as shown in Table 5.3.2; no access to high molecular weight molecules inside the pores is allowed. The RO yield and selectivity are compared for both Ir-Pt and Ni-Mo carbide catalysts supported on HY as shown in Table 5.3.3. At 220 °C, the maximum RO yield and selectivity are observed over the noble metal catalyst. The comparable RO yield with good RO selectivity is observed at 240 °C over the carbide catalyst. This should indicate that the Ni-Mo carbide catalyst can be an alternative to noble metal catalysts for the RO reaction.

5.3.3 Summary

The Ni-Mo carbide supported on HY, H-Beta, silica-alumina, γ-alumina and Al-SBA-15 catalysts were prepared for ring-opening reaction and the activity of the above catalysts are compared with noble metal catalysts. XRD patterns of the Ni-Mo carbide catalyst supported on H-Beta show the presence of β-Mo_2C, whereas with all other carbide catalysts, there is no β-Mo_2C peak in the diffractogram due to higher dispersion. CO chemisorptions show good dispersion of the metal on the support and that the available metal sites are large in number with the carbide catalysts. The total amount of acidic sites is higher for the noble metal catalysts and the acidity reduced to 30-35 % for the carbide catalysts. Selective ring opening of decalin over Ni-Mo carbide catalysts showed HY- and H-Beta-supported catalysts are the best among the carbide catalysts. These HY- and H-Beta-supported carbide catalysts were compared with the noble metals catalysts loaded on the same supports. The Ni-Mo carbide supported on HY showed a maximum yield of 33.5 % at 240 °C. The Ir-Pt/HY catalyst showed a 32 % RO yield at

220°C. The saturated and unsaturated ring-opening products yields follow the same trend as the total ring-opening products yield. It was observed that the Ni-Mo carbide catalyst can be successfully used to obtain the same level of ring-opening products yield that can be achievable with noble metals catalysts.

5.4 Ring opening and kinetics study of hydrotreated Light gas oil on Ni-Mo carbide supported on HY and H-Beta catalysts

This section discusses in detail about the activity of Ni-Mo carbide and Ir-Pt catalysts on HY and H-Beta supports on hydrotreated LGO. The fuel quality improvement was measured by cetane index and the conversion from aromatics and naphthenes to paraffins. Simulated distillation is used to measure the boiling point distribution and the proton NMR for estimation of percentage of aromatics, naphthenes and parrafins. This section also gives the details about the development of kinetics and estimation of kinetic parameters.

5.4.1 Catalyst characterization

The detailed characterization results of all the catalysts are reported in section 5.2.1. The BET surface area of the Ir-Pt/HY, Ni-Mo carbide/HY and Ni-Mo carbide/H-Beta catalysts are 641, 492 and 395 m^2/g respectively. Total acid strength of the catalysts are 379, 189, 116 μmol NH_3/g of catalyst respectively. The CO uptake is 26, 69 and 66 μmol CO/g of catalyst respectively. The H_2-TPR profiles on Ir-Pt/HY showed hydrogen consumption peaks at 215 and 260 °C, which are attributed as reduction of iridium oxide and Pt^{2+} respectively. NH_3-TPD of Ir-Pt/HY catalyst showed the presence of both medium and strong acid sites. Good dispersion of the metals on the supports was evidenced from the XRD and CO-chemisorption studies.

5.4.2 Reaction study

The properties of feed stock HLGO and products from the reaction were analyzed using simulated distillation for boiling point distribution, 1H NMR for wt.% of aromatics, naphthenes and aromatics. The amount of aromatics, naphthenes and paraffins were estimated by using the method described by Kapur et al. (2000). This method is applicable when considering the assumption that there are no unsaturated compounds present in the product. This assumption is satisfactory in the present case as the reaction was carried out under typical hydrotreating conditions in the presence of hydrogen.

Figure 5.4.1 shows a typical ^{1}H NMR spectrum of hydrotreated LGO recorded in $CDCl_3$. In the spectrum the region characteristic of aromatics is from 6.5 to 8.0 ppm. The region 2.5 to 3.2 represents the substituent groups of aromatics due to CH/CH2 protons and 2.05 to 2.5 ppm region represents the substituent groups of aromatics due to CH3 protons. The region between 0.5 to 2.05 ppm is highly overlapped and mainly represents the cycloalkanes, iso and normal paraffins. The signal intensity in the region 0.5 to 1.4 ppm is mainly due to normal and iso paraffins but some of the naphthenes also will overlap in this region. Similarly 1.4 to 2.05 signal intensity was due to naphthenes but is again overlapped with signals from isoparaffins. Therefore, in order to quantify the amount of aromatics, naphthenes and paraffins present in the mixture, standard naphthenic and isoparaffinic mixtures were used. The percentage of signal intensity was estimated in each region and equations were developed to estimate the individual weight percentages of aromatics, naphthenes and paraffins in the mixture (Kapur, 2000). In the present study, the authenticity of the method was verified by using the known mixture of

aromatics, naphthenes and paraffins and the calculated error was estimated to be with in 1%.

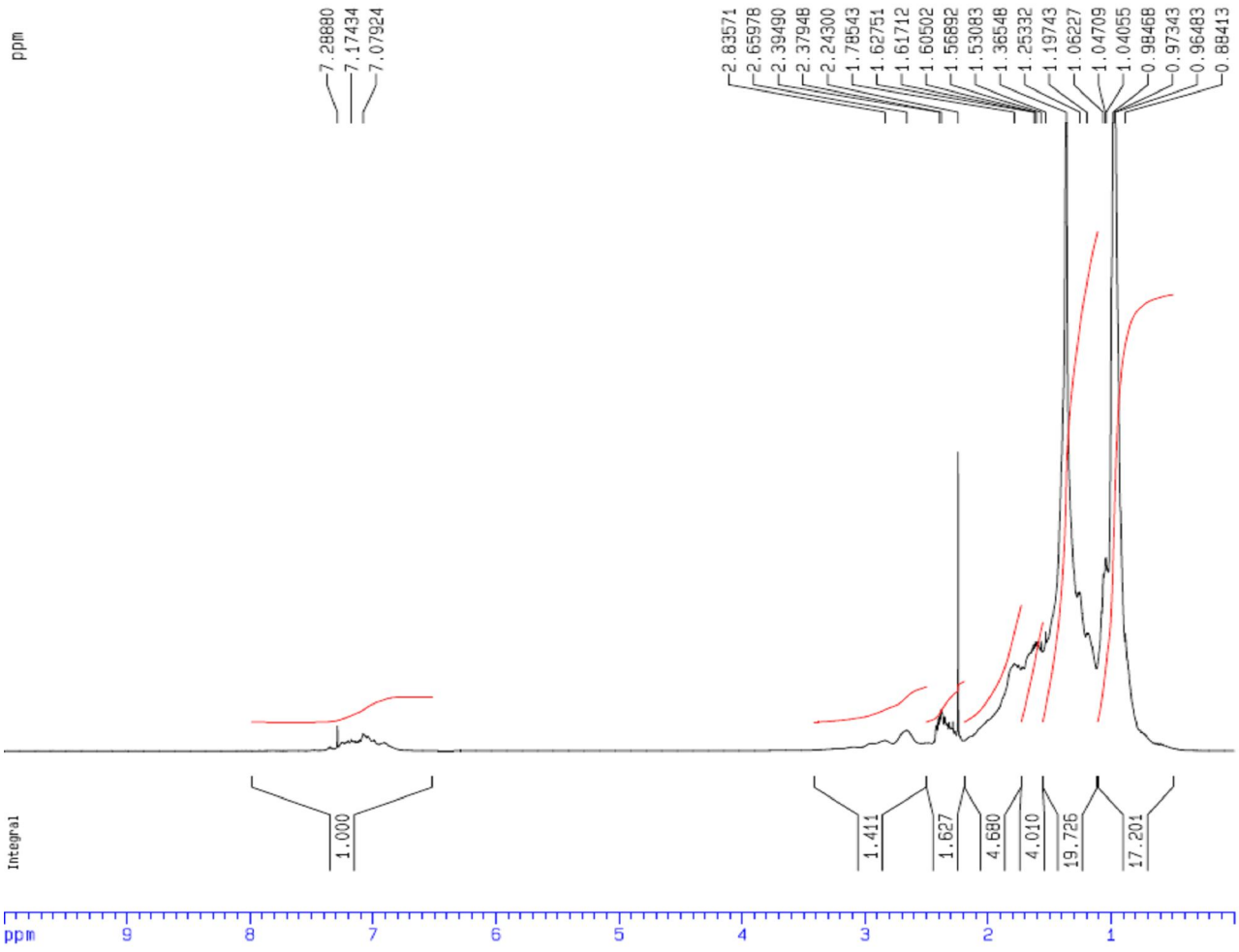

Figure 5.4.1: ^{1}H NMR spectrum of hydrotreated Light Gas Oil (HLGO).

Table 5.4.1 shows the properties of feed hydrotreated LGO. Based on the boiling point distribution, the feed is classified into naphtha, LGO and HGO fractions. The fraction boiled off below 177 °C is naphtha. The fraction distilled off above 177 and below 343 °C is called LGO. The fraction distilled off above 343 °C is HGO. Feed contains 6 wt% naphtha, 70 wt% LGO and 24 wt% HGO. The weight percentages of

aromatics, naphthenes and paraffins in the feed are 16.4, 38.8 and 44.8 respectively. Specific gravity and cetane index of the feed are 0.870 and 42.5 respectively. Total sulfur and nitrogen in the feed are 7149 ppm and 1773 ppm respectively. The activity of Ni-Mo carbide/HY catalysts on HLGO conversion was studied by varying the temperature from 200 to 375 °C. Pressure, LHSV and H_2/feed ratio were kept constant at 5 MPa, $1.5h^{-1}$ and 600 respectively.

Table 5.4.1: Properties of feed hydrotreated LGO.

Hydrotreated LGO					
Cetane Index = 42.5					
Specific gravity = 0.87					
Total sulfur = 7149 wppm					
Total Nitrogen = 1773 wppm					
Weight percentage					
Naphtha IBP-177 °C	LGO 177-343 °C	HGO 343 °C +	Aromatics	Naphthenes	Paraffins
6.0	70.0	24.0	16.4	38.8	44.8

The product boiling point distribution curve at different temperatures on catalyst Ni-Mo carbide/HY from the simulated distillation analysis was shown in Figure 5.4.2. It was clear from the figure that there is no change in the boiling point distribution of the product streams from 200 to 275 °C. The catalyst is not active upto 275 °C and there is a sharp change in the boiling point distribution at 300 °C.

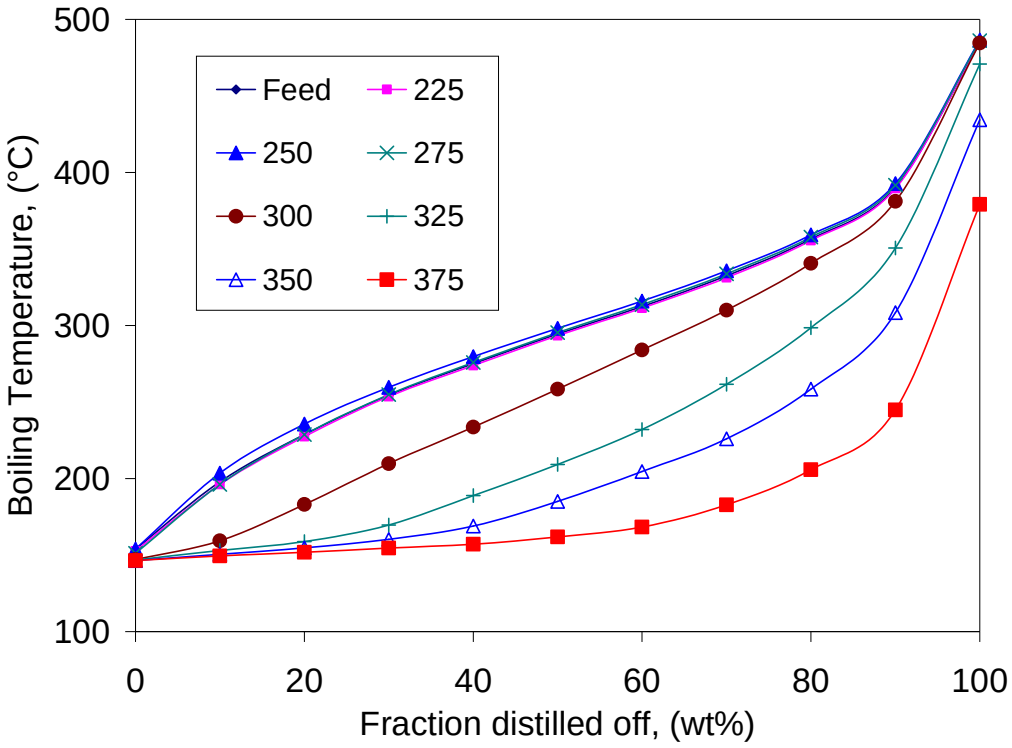

Figure 5.4.2: Boiling point distribution of product streams at different reaction temperatures on Ni-Mo carbide/HY catalyst at 5 MPa Pressure and LHSV of 1.5 h^{-1}.

The wt.% of naphtha, LGO and HGO fractions in the product streams at different temperatures on catalyst Ni-Mo carbide/HY is shown in Table 5.4.2. Different fractions are not affected much with temperature upto 275 °C but there is a 25% decrease in the HGO fraction and 200% increase in the naphtha fraction at 300 °C. At 325 °C the naphtha fraction increased further to 34 wt.% from 17.5 wt% at 300 °C. Further increase in temperature leads to increase in naphtha fraction and at 375 °C, it went upto 66 wt.%. This trend clearly shows the heavy cracking at higher temperatures. In the region 300 to °325 C, mild cracking took place whereas above 325 °C heavy cracking took place.

Table 5.4.2: Weight percentage of naphtha, LGO and HGO fractions present in product streams at different temperatures on different catalysts.

	Ni-Mo carbide/HY			Ni-Mo carbide/H-Beta			
	Naphtha	LGO	HGO	Naphtha	LGO	HGO	Naphtha
Raction Temp, ℃	IBP-177 ℃	177-343 ℃	343 ℃ +	IBP-177 ℃	177-343 ℃	343 ℃ +	IBP-177 ℃
200	5.5	69.5	25.0	5.0	69.0	26.0	-
225	6.0	69.0	25.0	5.0	70.0	25.0	-
250	5.0	68.0	27.0	6.0	70.0	24.0	-
275	6.0	68.0	26.0	4.5	67.5	28.0	5.0
300	17.5	63.5	19.0	7.0	70.0	23.0	12.0
325	34.0	55.0	11.0	13.0	63.0	24.0	24.0
350	45.0	49.0	6.0	-	-	-	-
375	66.0	32.5	1.5	-	-	-	

This was further confirmed from the weight percentages of aromatics, naphthenes and paraffins present in the product streams on Ni-Mo carbide/HY catalysts which is shown in Figure 5.4.3.Amount of aromatics increased with temperature above 300 ℃ as expected. This is due to the reversible nature of aromatic saturation reaction, where reversible reaction is favored with increase in temperature. Naphthenes are converted to both aromatics and paraffins at high temperatures. Therefore, low amount of naphthenes (27 wt.%) present in the product stream above 325 ℃.

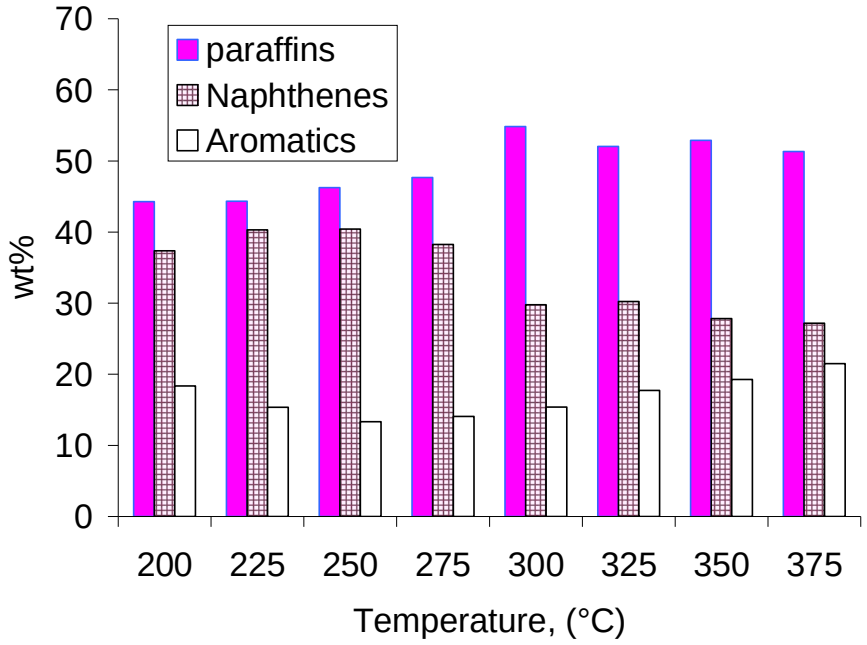

Figure 5.4.3: Amount (wt%) of paraffins, naphthenes and aromatics present in product streams at different reaction temperatures on Ni-Mo carbide/HY catalyst at 5 MPa Pressure and LHSV of 1.5 h^{-1}.

The quality of the fuel was assessed by calculating the cetane index. The cetane index of the product streams at different temperatures on different catalysts is shown in Figure 5.4.4. The cetane index was increased by 12 units at 325 °C temperature on Ni-Mo carbide/HY catalyst. At higher temperatures (>325 °C), cetane index was not improved comparing with the feed even though with the presence of high amount of paraffins. The reasons are 1) presence of higher amount of aromatics and 2) presence of secondary cracking products with low molecular weight. Aromatics and low molecular weight cracking products will greatly reduce the cetane number. The acidic nature of the catalyst was more active in forming secondary cracking products at temperatures above 325 °C.

Therefore, it is clear that higher cetane number products resulted from selective ring opening of the naphthenic compounds were formed at 300 to 325 °C on Ni-Mo carbide/HY catalyst in order to improve the cetane number.

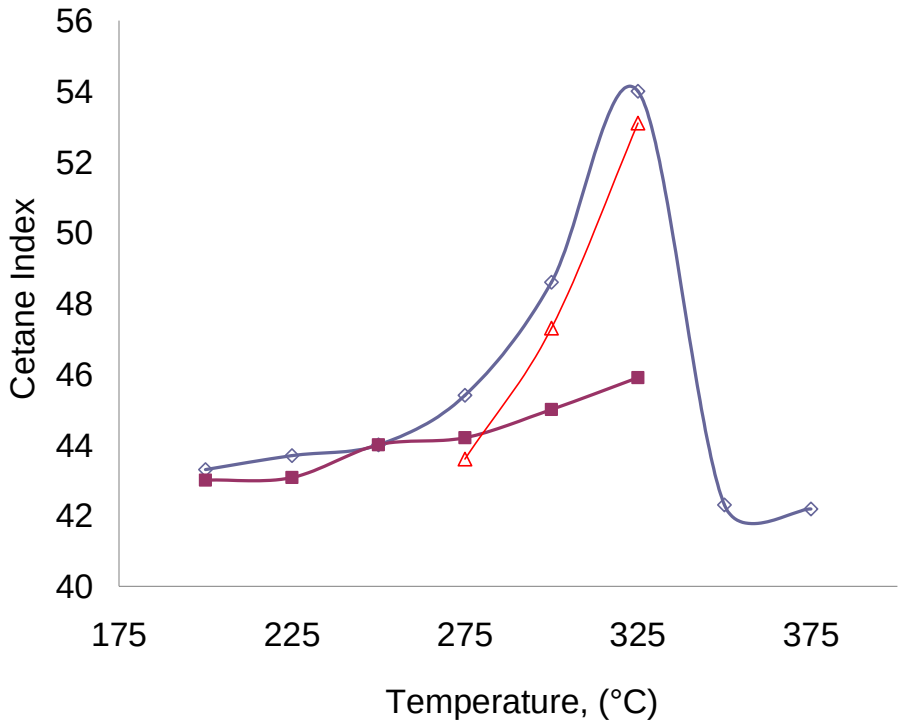

Figure 5.4.4: Cetane index of product streams at different reaction temperatures on Ni-Mo carbide/HY (◊), Ni-Mo carbide/H-Beta (■) and Ir-Pt/HY (Δ) catalysts at 5 MPa Pressure and LHSV of 1.5 h^{-1}.

In order to check the activity of other catalysts on the HLGO product quality, Ni-Mo carbide/H-Beta and Ir-Pt/HY catalysts are used for the catalytic study at 5 MPa and LHSV of 1.5 h^{-1}. The boiling point distribution of the products at different temperatures on Ni-Mo carbide/H-Beta catalyst is shown in Figure5.4.5. There is no change in the

boiling point distribution upto 300 °C. At 325 °C there is a change in the boiling point distribution.

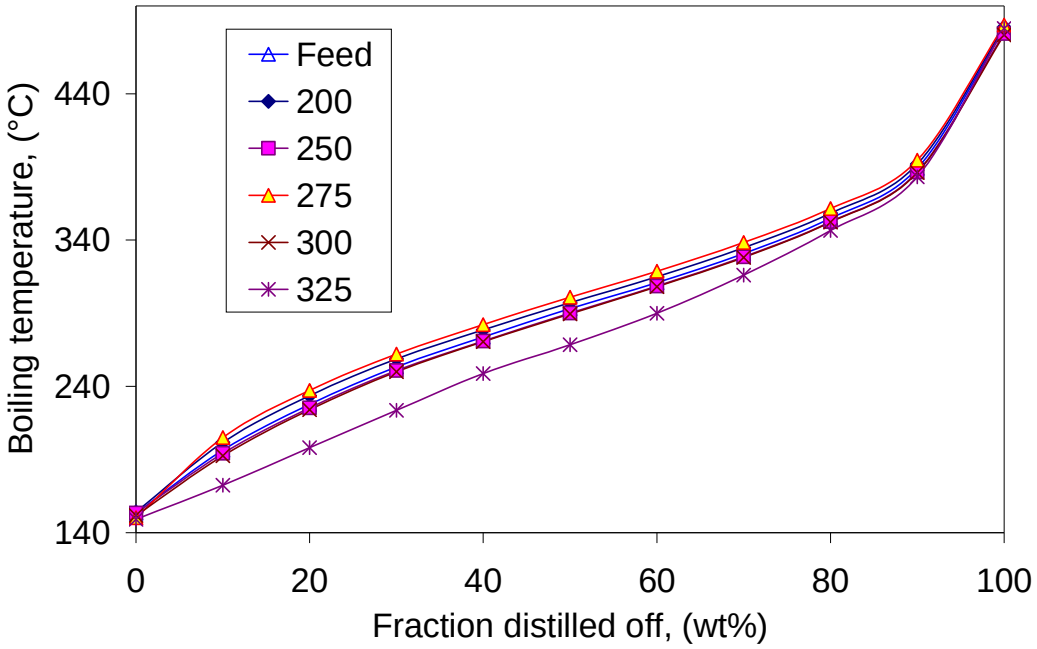

Figure 5.4.5: Boiling point distribution of product streams at different reaction temperatures on Ni-Mo carbide/H-Beta catalyst at 5 MPa Pressure and LHSV of 1.5 h^{-1}.

There is a 100% increase in the naphtha fraction and corresponding decrease in the LGO fraction is observed at 325 °C on Ni-Mo carbide/H-Beta catalyst as shown in Table 5.4.2. On this catalyst, improvement in the cetane index by 3 units is observed at 325 °C as shown in Figure 5.4.4. The low activity of the Ni-Mo carbide/H-Beta catalyst was due to its low pore diameter as observed from the BET surface area measurements. These pores are not accessible to the high molecular weight compounds thus making it less active. This was also supported from the amount of HGO fraction present at 325 °C

as shown in Table 5.4.2 as the decrease in the heavy oil fraction is less compared to the decrease in the LGO fraction.

The activity of Ir-Pt/HY catalyst is shown in figure 5.4.6. The conversion of naphthenes to paraffins is comparable with that of Ni-Mo carbide/HY catalyst. Improvement in the cetane number is 10 units on Ir-Pt/HY at 325 °C, which is in well comparison with NI-Mo carbide/HY catalyst.

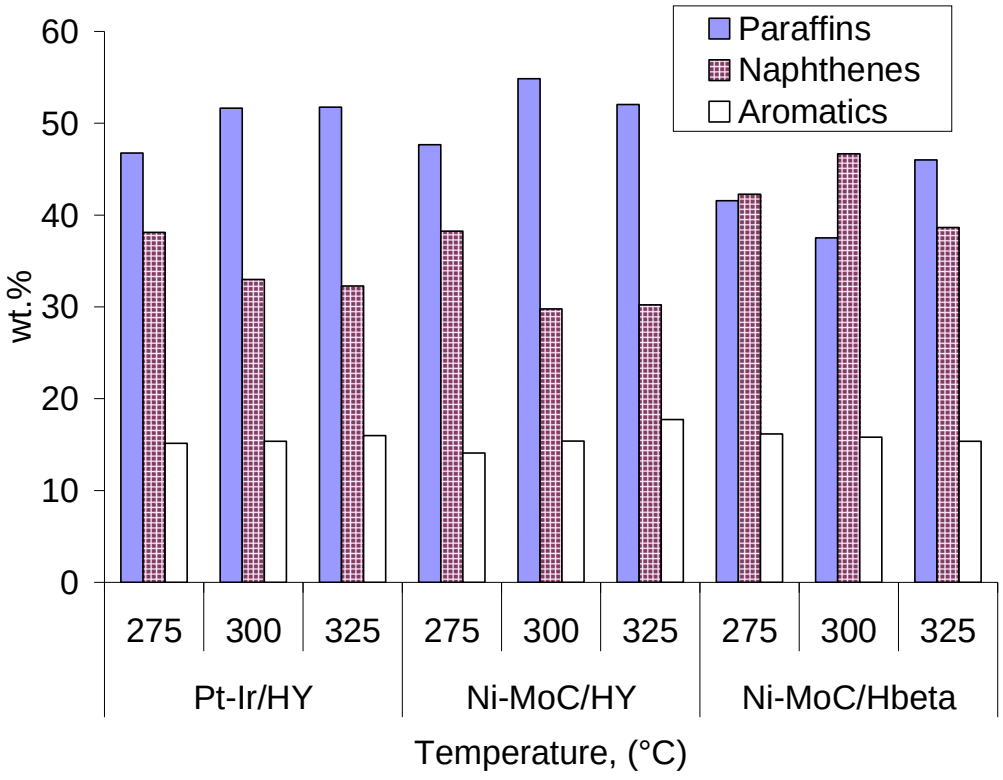

Figure 5.4.6: Amount (wt%) of paraffins, naphthenes and aromatics present in product streams at different reaction temperatures on different catalysts at 5 MPa Pressure and LHSV of 1.5 h^{-1}.

Even though the activity of the Ir-Pt/HY catalyst is in good comparison with Ni-Mo carbide catalyst, the deactivation of the earlier catalyst was fast. Ir-Pt/HY catalyst deactivated after 72 h, whereas Ni-Mo carbide/HY catalyst lasted for 168 h. In order to study the kinetics of the reaction, further experiments were conducted by choosing Ni-Mo carbide/HY as catalyst. Temperature and LHSV of the reaction were varied from 275 to 325 °C and 0.5 to 2 h^{-1}. The effects of LHSV on the product distribution at 300 and 325 °C are shown in Figure 5.4.7 and Figure 5.4.8 respectively.

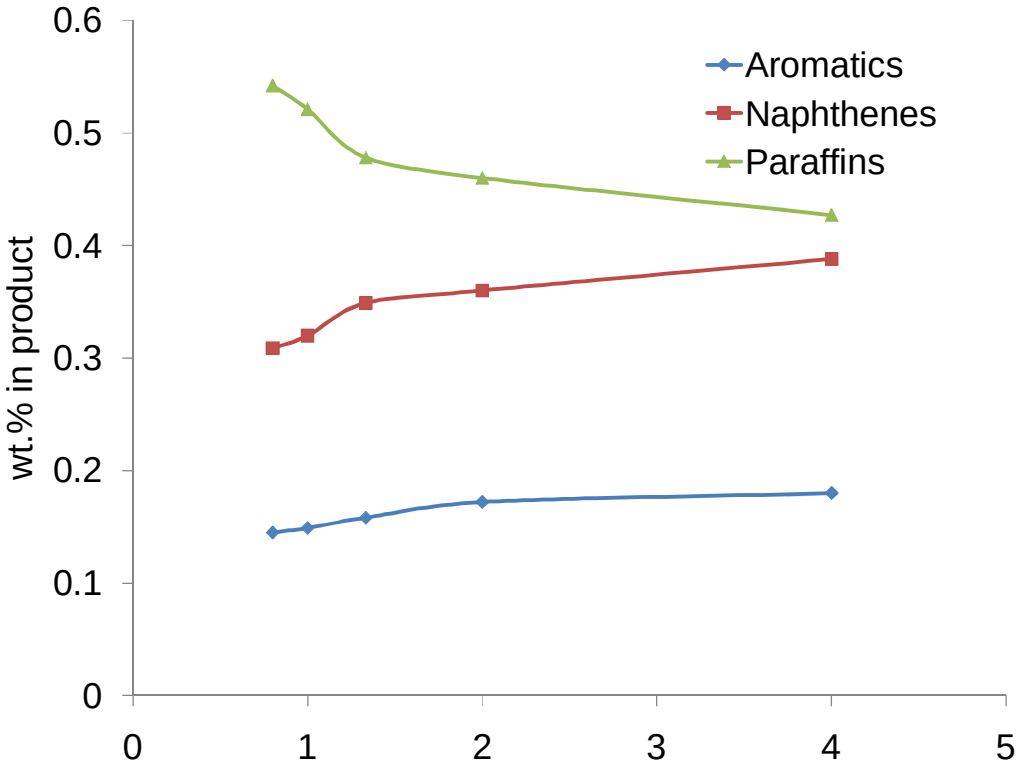

Figure 5.4.7: Amount (wt%) of paraffins, naphthenes and aromatics present in product streams as a function of LHSV on Ni-Mo carbide/HY catalyst at 5 MPa Pressure and 300 °C.

In both the cases, the amount of naphthenes increased with increase in LHSV, whereas, the amount of paraffins decreased with increase in temperature.

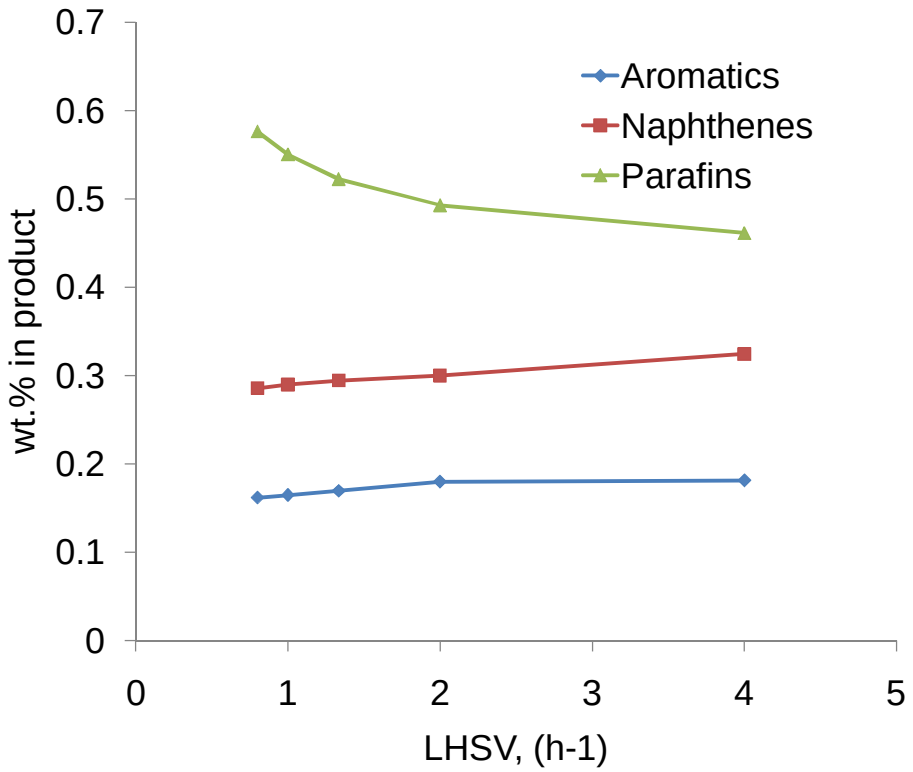

Figure 5.4.8: Amount (wt%) of paraffins, naphthenes and aromatics present in product streams as a function of LHSV on Ni-Mo carbide/HY catalyst at 5 MPa Pressure and 325 °C.

5.4.3 Kinetics study

The proposed kinetic model is shown below. Only aromatic, naphthenic and paraffinic lumps are considered in the model.

Aromatic saturation is a reversible reaction and k_1 and k_2 represent the rate constants for forward and reverse reactions. k_3 represents the rate constant for cracking

reaction where naphthenes are converted to paraffins. Methane formation from the aromatics was not evidenced from the experiments. Therefore, methane formation step was not included in the model.

Under typical dilution of catalyst in a trickle bed reactor, the L/d_p was maintained at 750, where the back mixing phenomena can be neglected (Bellos, 2003; Ramı´rez, 2004). Wetting phenomina is negligible under the studied conditions (Ramı´rez, 2004; Gierman, 1988) and the calculations are shown in Appendix B.1. Wall effects are negligible where the ratio of D_b to d_p is 60 (Ramı´rez, 2004,; Chu, 1989).

5.4.3.1 External mass transfer limitation

The order of the reaction is assumed to be 1 and the mass transfer coefficient is assumed according the the conditions of the reaction (Larachi, 2003). The required parameters and constants for the estimation of Mears criteria are calculated and are shown in Appendix B.2. All these calculations are based on the worst case in the reactor. According to the calculations the Mears criteria was estimated to be 0.00152 which is quiet lower than the value of 0.15. Therefore, the external mass transfer resistance can be neglected safely.

5.4.3.2 Internal mass transfer limitation

In order to see the effect of internal mass transfer limitations, the Weisz-Prater parameter was calculated and is shown in Appendix B.3. The Knudson diffusivity value is obtained from the literature (Larachi, 2003) according to the range of operating conditions. As shown in the Appendix B.3, Weisz-Prater parameter obtained is 0.066 and internal mass transfer resistance can be safely neglected.

5.4.3.3 Kinetic parameters estimation

The mass fractions of aromatics, naphthenes and paraffins are denoted as x_A, x_N and x_P and are taken as variables to fit the model. Pseudo first order rate expression for each step in the proposed model was assumed. The variation in the mass fraction of each lump along the reactor can be represented by the following differential equations.

$$\frac{dx_A}{dt} = -k_1 x_A + k_2 x_N \qquad \text{……..5.4.1}$$

$$\frac{dx_N}{dt} = k_1 x_A - k_2 x_N - k_3 x_N \qquad \text{…….5.4.2}$$

$$\frac{dx_P}{dt} = k_3 x_N \qquad \text{…….5.4.3}$$

The calculation has been carried out by reparameterization of Arrhenius equation in order to consider the effect of temperature in the kinetic constants. The differential equations are solved by using *ode45* routines in MATLAB and simultaneously the sum of the squares function was minimized by using *fminsearch*. The kinetic parameters were estimated by fitting the experimental values in the sum of the squares function and by minimizing the errors. The estimated kinetic parameters are shown in the Table 5.4.3. The residual error values obtained at 275, 300 and 325 °C are 0.00076945, 0.00030351 and 0.0041378 respectively. Arrhenius plots are drawn for obtaining activation energies and frequency factors, and the values are shown in Table 5.4.5.

Table 5.4.3: Arrhenius activation energies and frequency factor values for various reaction steps.

Reaction steps	Rate constants, h^{-1}			Frequency Factor, h^{-1}	Arrhenius Activation Energy, KJ/gmol
	275 ℃	300 ℃	325 ℃		
1	0.97	1.95	5.03	2.80E+08	89.2
2	0.36	0.86	2.81	1.39E+10	111.4
3	0.17	0.32	0.38	1.75E+03	41.6

Figure 5.4.9 shows the fit between experimental and predicted values from the model and a R^2 value of 0.988 shows a good fit by the model. Therefore in the studied range of conditions, first order can be assumed for all the steps. The apparent activation energy for the naphthenes cracking step is less compared to the aromatic hydrogenation or dehydrogenation reactions. Therefore, on Ni-Mo carbide/HY catalyst reduces the activation energy for the conversion of naphthenes to paraffins. But the studied conditions do not favor much for the aromatic saturation as confirmed by the activation energy values.

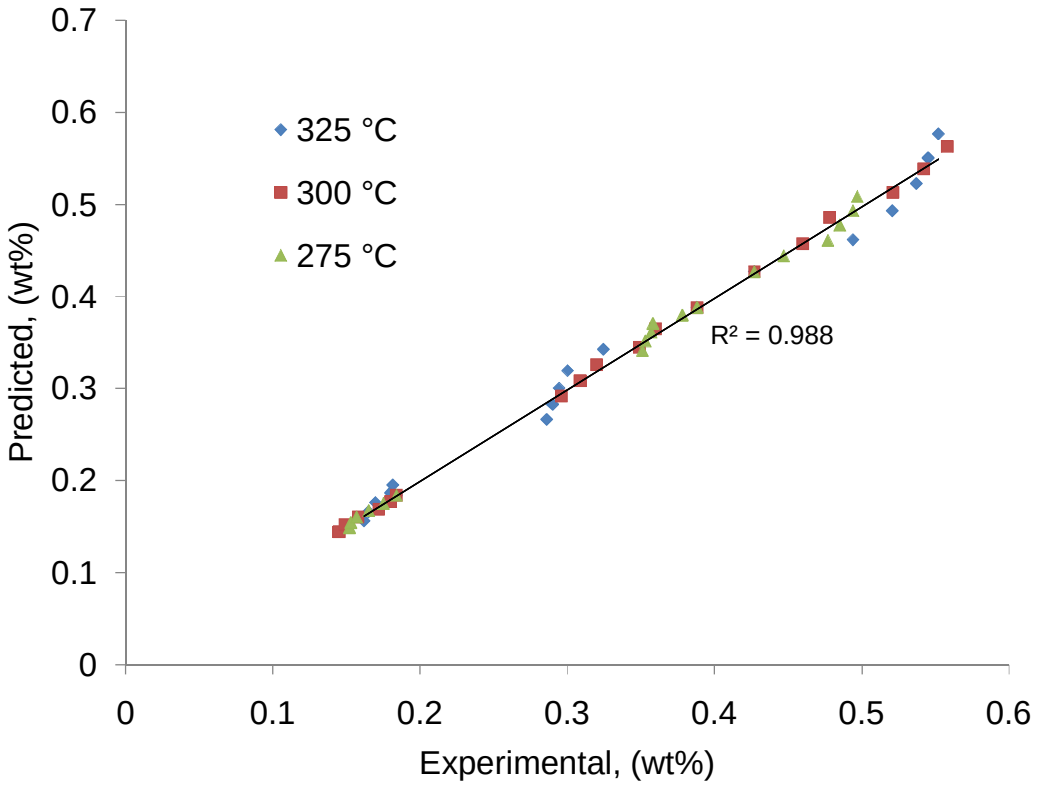

Figure 5.4.9: Amount (wt %) of paraffins, naphthenes and aromatics present in product streams from the predicted model and experiments at different temperatures and LHSV on Ni-Mo carbide/HY catalyst at 5 MPa Pressure.

5.4.4 Summary

Fuel quality improvement of hydrotreated LGO was studied on Ir-Pt/HY, Ni-Mo carbide/HY and Ni-Mo carbide/H-Beta catalysts. Screening of the catalysts revealed that Ni-Mo carbide/HY is an effective catalyst for the improvement in quality of the feed. A 12 unit increase in cetane number was observed on Ni-Mo carbide/HY at 325 °C, whereas Ni-Mo carbide/H-Beta could not improve the cetane index effectively. The activity of Ir-Pt/HY catalyst is comparable with that of Ni-Mo carbide/H-Beta, but the former catalyst deactivates fast. NMR analysis showed that the Ni-Mo carbide/HY

catalyst improves the cetane index of the fuel by selectively converting the naphthenes to paraffins in the temperature range of 300 to 325 °C. Dehydrogenation and secondary cracking are dominant above 325 °C, which leads to the reduction in cetane index. A first order kinetic model was proposed and the model was well fit with the experimental values. Arrhenius activation energies of 111, 89 and 42 KJ/gmol were observed for dehydrogenation, aromatic saturation and cracking reactions, respectively.

5.5 Ab initio calculations on dealkylation and ring opening of propylenecyclopentane

This chapter gives a detailed description about the energetics of deakylation and ring opening reactions of model molecule propylenecyclopentane. The calculations were performed in gas phase as well as on Brønsted acid sites. Different levels of theories were used to compare the results.

5.5.1 Gas phase reactions

Propenylcyclopentane is chosen as reactant, as the number of carbon atoms in the side chain required is three at least, to undergo β-scission on side chain which leads to dealkylation. The schematic representation of dealkylation and ring opening of propenylcyclopentane in gas phase is shown in the Figures 5.5.1(a) and 5.5.1(b) respectively.

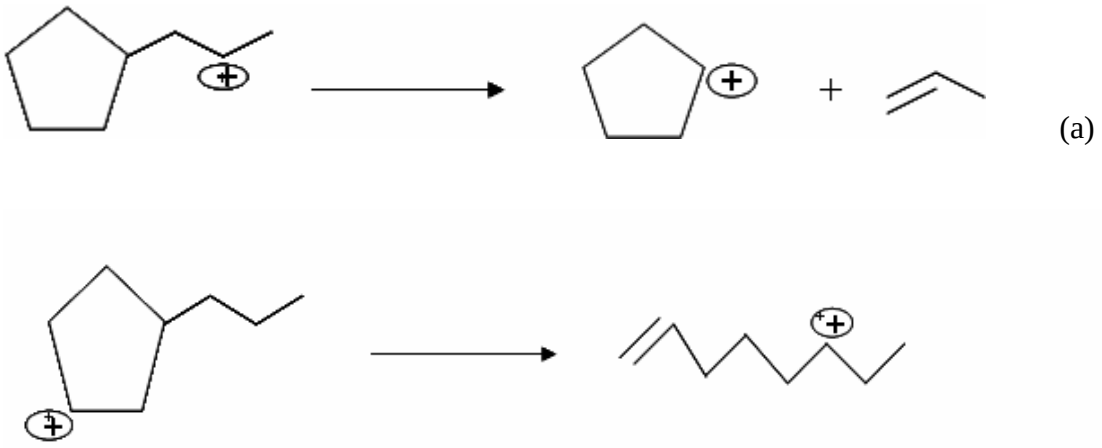

(a)

(b)

Figure 5.5.1: (a) β-scission dealkylation mechanism of propylene cyclopentane in gas phase. (b) β-scission ring opening mechanism of propylenecyclopentane ion.

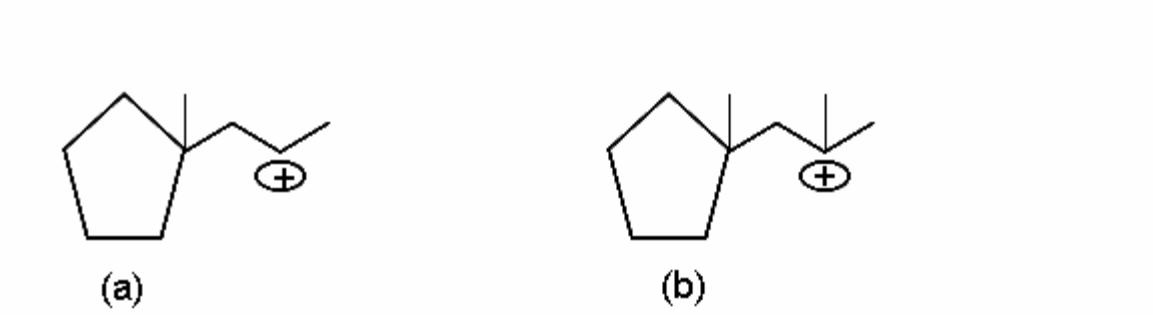

Figure 5.5.2: (a) 1, methyl-1, propylcyclopentane ion (b) 1, methyl-isopropylcyclopentane ion.

The position of the charge on 2nd carbon leads to β-scission and corresponding dealkylation from the cyclic structure takes place as shown in Figure 5.5.1.a. The position of the charge on the ring (3rd carbon from substituted group) leads to β-scission results in straight chain alkyl carbenium ion as shown in Figure 5.5.1.b. 1,methyl-isopropenylcyclopentane and 1,methyl-propenylcyclopentane are other structures on which dealkylation reaction was studied as shown in Figure 5.5.2. The activation barriers for the secondary and tertiary β-scission dealkylation reactions were shown in figure Figure 5.5.3. The differences in the energitics are compared for secondary and tertiary β-scission reactions by using 1,methyl-isopropylcyclopentane and 1,methyl-propylcyclopentane carbenium ions. The activation barrier for tertiary carbenium ion is nearly three times that of the secondarycarbenium ion as shown in Figure 5.5.3. The expected difference in the activation energies are due to the well known fact that tertiary β-scission is much faster than the secondary β-scission. The gas phase total energies and zeropoint energies are listed in Table 5.5.1 for dealkylation reaction of all the ions. The energetics calculations were carried out using HF and DFT levele theories.

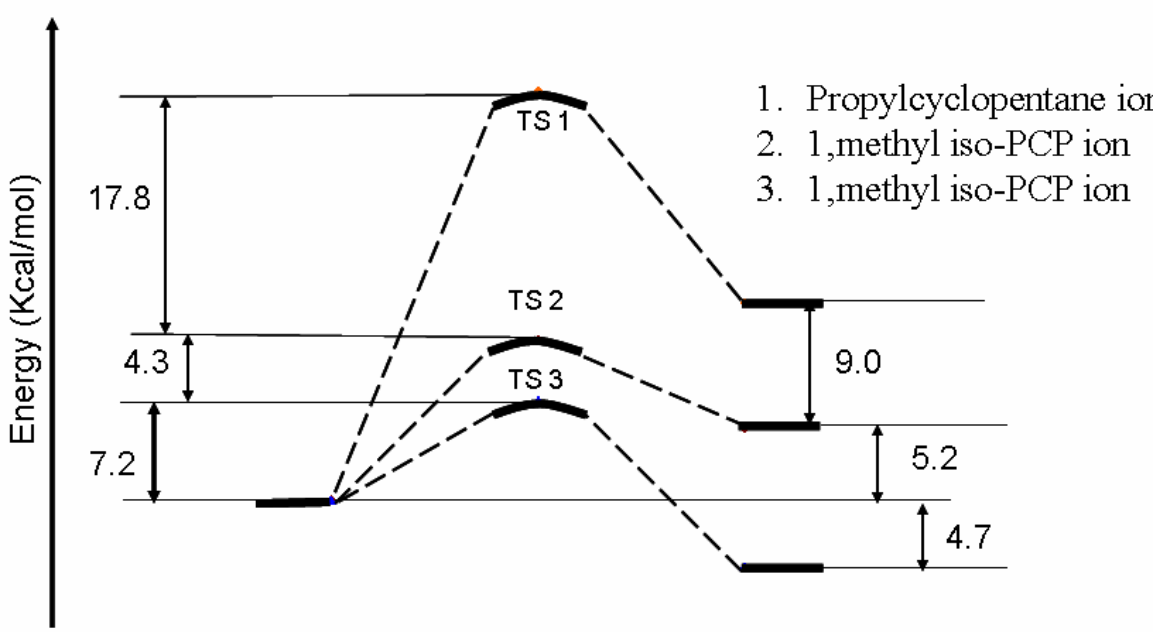

Figure 5.5.3: Gas phase dealkylation activation energies for different alkyl substituted cyclopentane ions.

Table 5.5.1: Total Energies (in AU) and Zero-Point Energies (ZPE, in kcal/mol) of the gas phase dealkylation reactions of alkylcyclopentanes.

Name	level	Reactant		TS		
		Total energy	ZPE	Total energy	ZPE	IF
PCP	HF-6-31G*	-311.64	141.71	-311.59	139.33	-532
	DFT-6-31G* PBEPBE	-313.39	129.65	-313.34	127.68	-317
1,methyl PCP	HF-6-31G*	-350.43	161.61	-350.42	160.57	-140
1,methyl, iso-PCP	HF-6-31G*	-389.49	180.57	-389.47	179.05	-210

6-31g(d) level basis set was used for HF and PBEPBE level approximations are used for DFT calculations. There is a difference in the energetics calculations using different level theories. Always DFT calculations gave less numbers than the HF calculations. The gas phase dealkylation and ring opening β-scission energetics are calculated using *ab initio* Hartree-Folk (HF) theory at 6-31g(d) basis set and DFT theory at PBEPBE level and are shown in Figure 5.5.4.

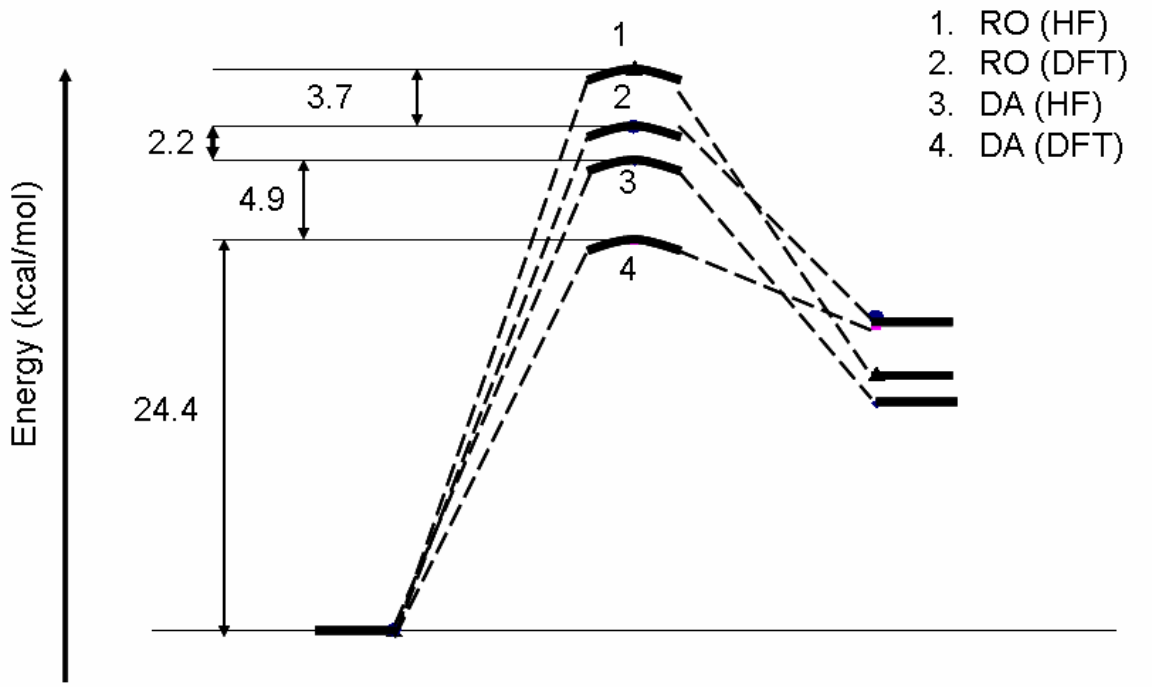

Figure 5.5.4: Gas phase activation energies for Ring opening (RO) and dealkylation (DA) of propylcyclopentane ion.molecule. All the transition states for three elementary steps.

Both DFT and HF studies give higher activation barriers for ring opening reactions. HF study showed a difference of 5.9 kcal/mol activation barrier between dealkylation and ring opening. Whereas, DFT studies gave a difference of 7.1 kcal/gmol activation barrier between dealkylation and riing opening reactions. Both the theories

concluded that the RO reaction is difficult compared to dealkylation due to its high activation energies as shown in the Figure 5.5.4.

5.5.2 Cluster simulations

The overall dealkylation reaction on Brønsted acid site is carried out through three elementary steps. 1) Protonation of the reactant molecule 2) Dealkylation at the surface and 3) Desorption of the product from the surface. The geometry of the various intermediates and transition states in β-scission which leads to dealkylation process of propylenecyclopentane are depicted in Fig. 5.5.5

In the diagram the Brønsted acid site was represented by a 1T cluster where T represents number of hetero atoms. The Pi-complex will be formed initially by weak interaction forces between the cluster and the reaction molecule. Formation of ∏-complex is an exothermic process with 4.4 kcal/mol energy and does not require any activation energy. The geometry of the reactant and cluster also does not change much in the ∏-complex formation. In the ∏-complex, the net positive charge on the alkylnaphthene is also quite small (+0.029e). It is mainly connected with the electron density transfer to the proton of the bridging hydroxyl, as observed by other investigators (Kazansky, 1996). The ∏-complex is then transformed into a stable alcoxy group through a carbenium ion like transition state as shown in Fig 5.5.5.

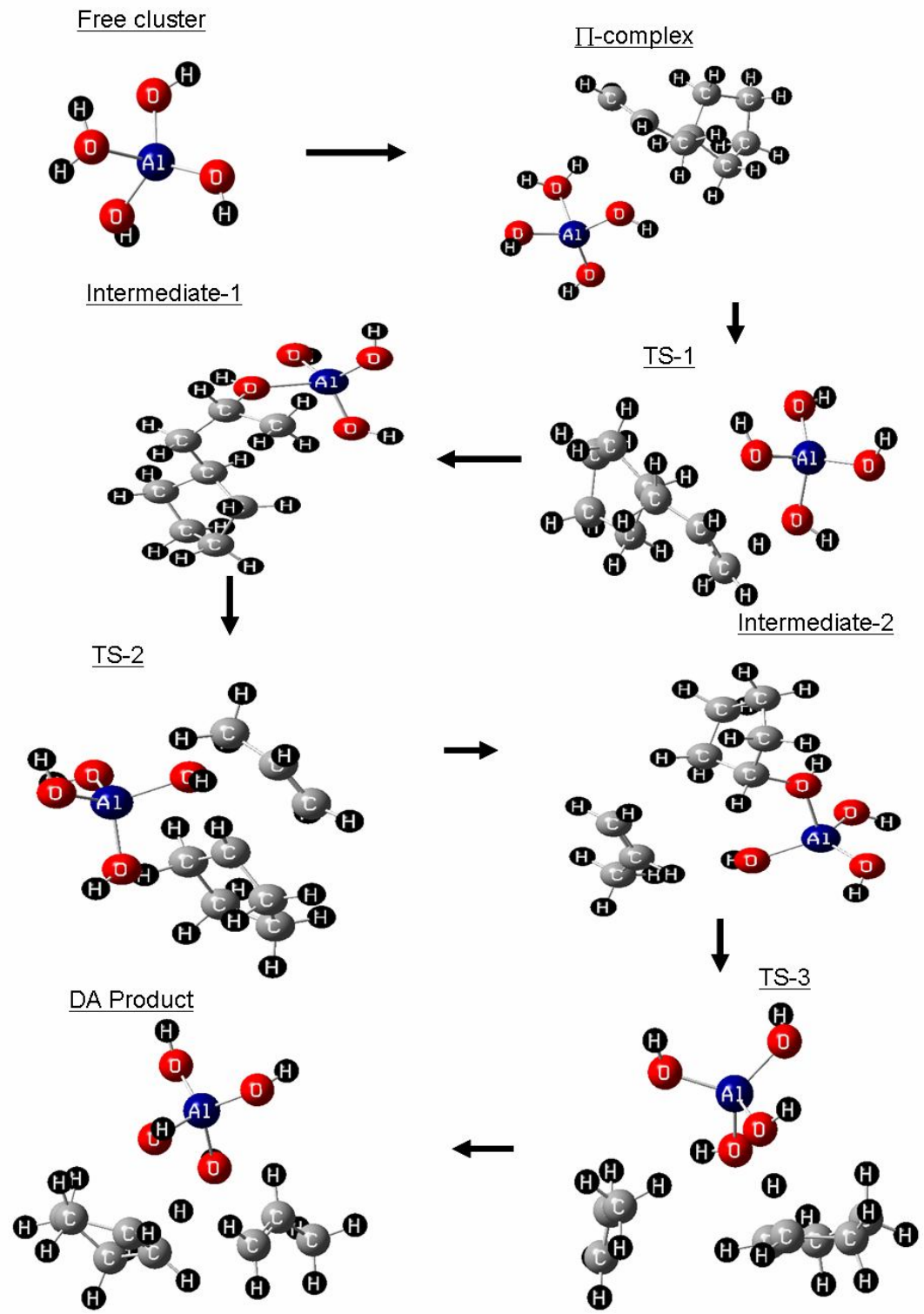

Figure 5.5.5: Geometry of different steps involved in dealkylation of propylenecyclopentane on a Brønsted acid site (1T-HF)

The C-O bond in alcoxy intermediate structure is covalent in nature as its distance is 1.447 Å, the angles are near tetrahedral at the tertiary carbon atom and the charge of the alkylcycloalkane is slightly positive (+0.462e). The energy diagram of the propenylcyclopentane interating with Brønsted acid site is depicted in Figure 5.5.6.

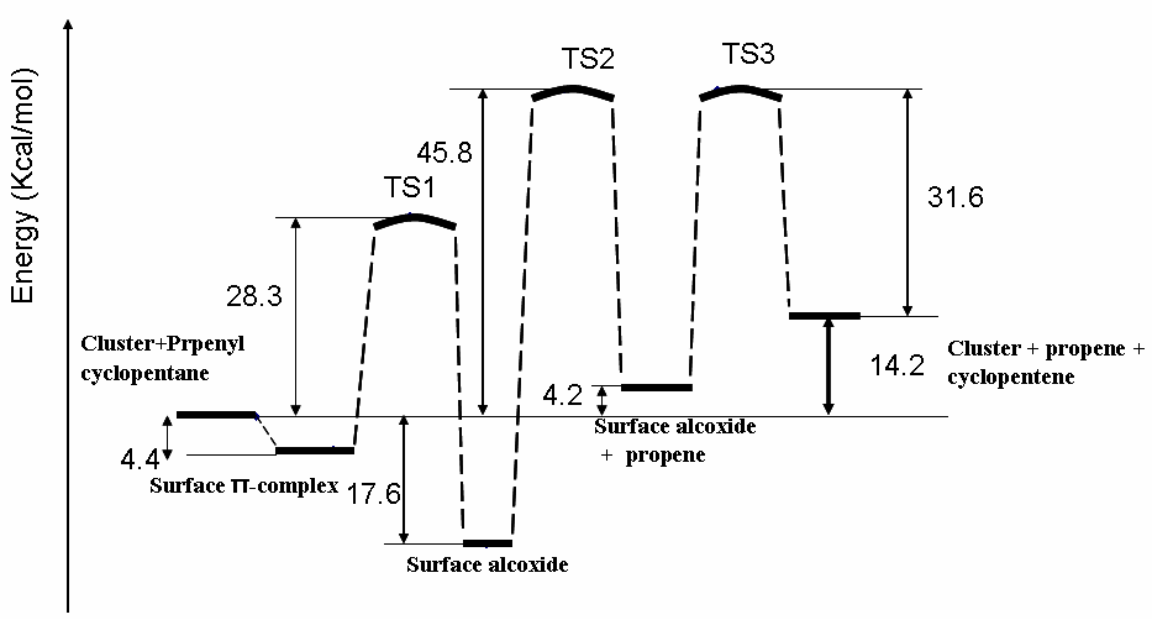

Figure 5.5.6: Reaction pathways for dealkylation of propylenecyclopentane on 1T zeolite, HF, 6-31g(d).

As shown in Figure 5.5.6, the alcoxide formation is exothermic reaction with an energy release of 13.3 kcal/mol. This energy is close to the protonation energy of isobutene on 1T cluster (Kazansky, 1996). In the first elementary step, in which the formation of alcoxide intermediate took place through TS1 with an activation barrier of 32.7 kcal/mol and is shown in Figure 5.5.6. The geometry of transition state resembles that of a carbenium ion but with more positive charge (+0.768e) on the alkyl group than that of the reactant or product.

The geometry transformation and general features of transformation from Π-complex to alcoxide are similar to the earlier observations on other molecules (Kazansky, 1996; Senchenya, 1991; Viruela-Martin, 1993). There is a clear change in the structure of the cluster at transition state than the initial and final structures. Al-O bond contraction from 1.957 to 1.81 Å took place in the transition state which indicates the bifunctional nature of the Brønsted acid site. Brønsted acid site protonates the adsorbed alkylnaphthene, whereas the neighboring oxygen interacts with the hydrocarbon to form the stable alcoxide. Corresponding β-scission on the C-C bond between cyclic and side chain carbons leads to dealkylation reaction. This β-scission reaction was achieved by stretching the C-C bond distance to 2.28 Å. The geometry of the transition state and the corresponding product is shown in Figure 5.5.5. To see the effect of cluster size on the energetics, a higher level cluster was used to study the dealkylation of propylenecyclopentane at HF and 6-31g(d) level theory. The cluster used was a 5T cluster which includes five hetero atoms and all the ends are terminated with hydrogens. Increasing the number of hetero atoms definitely increase the approximation of the zeolite structure and represents more accurate results.

The energetic of the dealkylation reaction on a 5T cluster is shown in Figure 5.5.7. There is a significant reduction in the activation barrier when using the 5T cluster for all the elementary steps. 10 kcal/mol reductions in activation barrier for the rate limiting surface reaction step were also observed. Even though there is areduction in the activation barriers in individual elementary steps, the trend of the activation barriers are similar in both 1T and 5T clusters.

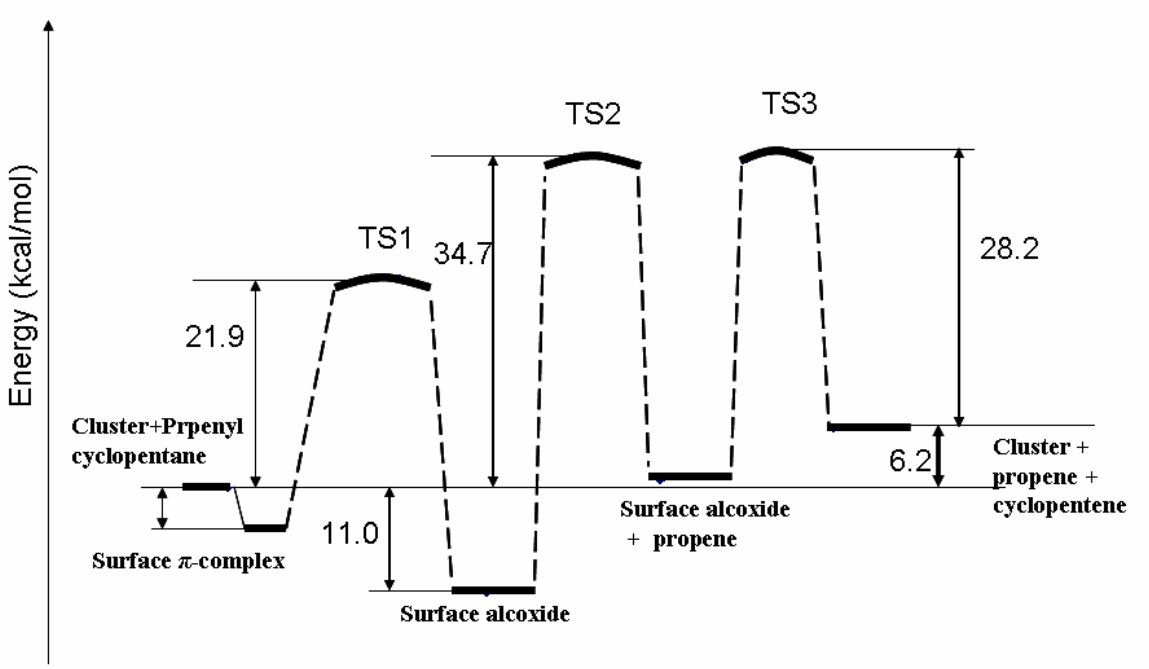

Figure 5.5.7: Reaction pathways of propylenecyclopentane on 5T zeolite cluster, HF, 6-31 g(d).

The energetic of the individual elementary steps are tabulated for both 1T and 5T cluster and shown in Table in 5.5.2. The imaginary frequencies are also added in the table for transition states. The dealkylation of propylenecyclopentane was also studied using DFT theory at PBEPBE level using 6.31g(d) basis set. The energetics of the corresponding elementary steps using DFT calculations are shown in the Figure 5.5.8. The geometry of the various ntermediates is similar to the geometries obtained by HF calculations with slight difference. DFT calculations are suggested the highest activation barrier of 33.8 kcal/mol for the surface reaction step. The trend of the activation barriers for different transition states is similar to the trend using HF calculations. DFT calculations also reduced the activation barriers for all the elementary steps. The

diffences in these numbers using different theories are mainly due to the usage of different approximation in solving the Schrodinger equation.

Table 5.5.2: Energetics of various dealkylation elementary structures at HF/6-31G with 1T and 5T clusters.

	1T cluster			5T Cluster		
Structure	Total energy	Zero point energy kcal/mol	IF	Total energy	Zero point energy kcal/mol	IF
Cluster	-544.44346	44.7	-	-1704.957500	88.3	-
Propenylcyclopentane	-311.07461	136.3	-	-311.074612	136.3	-
Π-complex	-855.52647	181.8	-			-
TS-1	-855.46936	178.7	-1109	-2015.992745	221.8	-869
Surface alcoxide	-855.55159	184.3	-	-2016.055594	228.3	-
TS2	-855.44187	179.0	-214	-2015.974717	223.3	-183
surface alcoxide	-855.52420	180.8	-	-2016.031679	225.1	-
TS3	-855.44890	15.2	-956	-2015.968352	219.0	-156
product	-855.50461	178.5	-	-2016.018264	222.1	-

Ring opening of propylenecyclopentane reaction was studied on a Brønsted acid site to see the difference between the deakylation and ring opening energetics. The geometry of the various intermediates in the ring opening reactions is shown in Figure 5.5.9. The scission on the ring leads to opening of the ring and a ring opening product. The attack on the substituted C-C bond on the ring results in ring opening with out losing the carbon number. The final product in the geometry diagram represents a straight chain

carbon compound with eight carbons which is having higher cetane number compared to a dealkylation product.

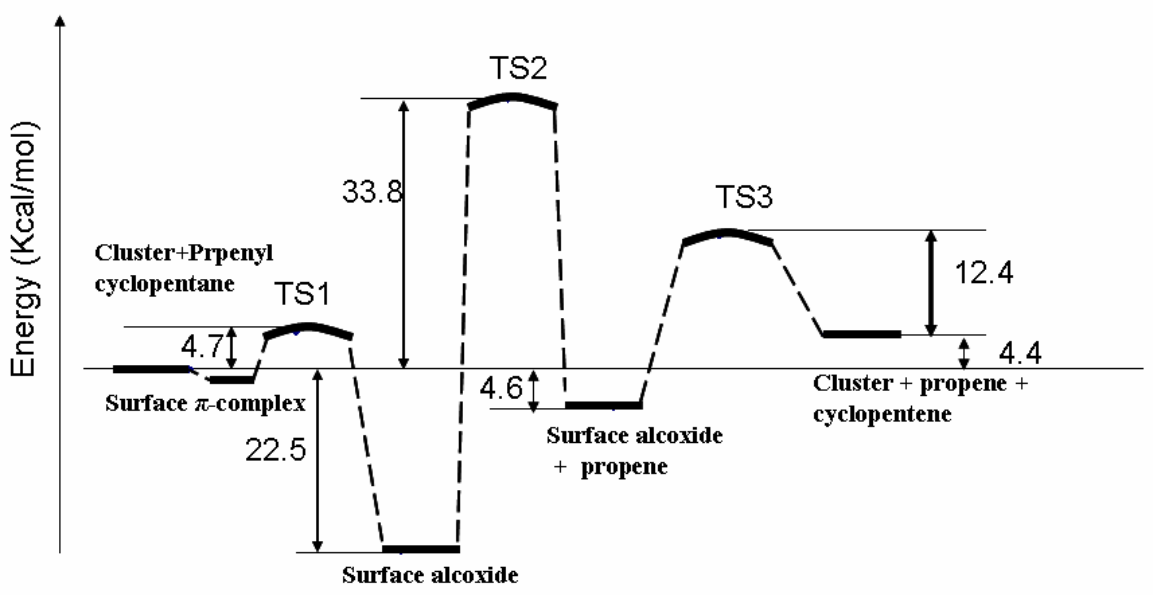

Figure 5.5.8: Reaction pathways for dealkylation of propylenecyclopentane on 1T zeolite, DFT, PBEPBE, 6-31g(d).

Energetics of the ring opening of peopylenecylopentane reaction is shown in Fgure 5.5.10. The calculations were carried out at 6-31g(d) basis set using HF theory. Highest activation abarrier of 50.1 kcal/gmol was required by the TS2 that is surface reaction step. All the elementary steps in the ring opening reaction require higher activation energies than the dealkylation reaction.

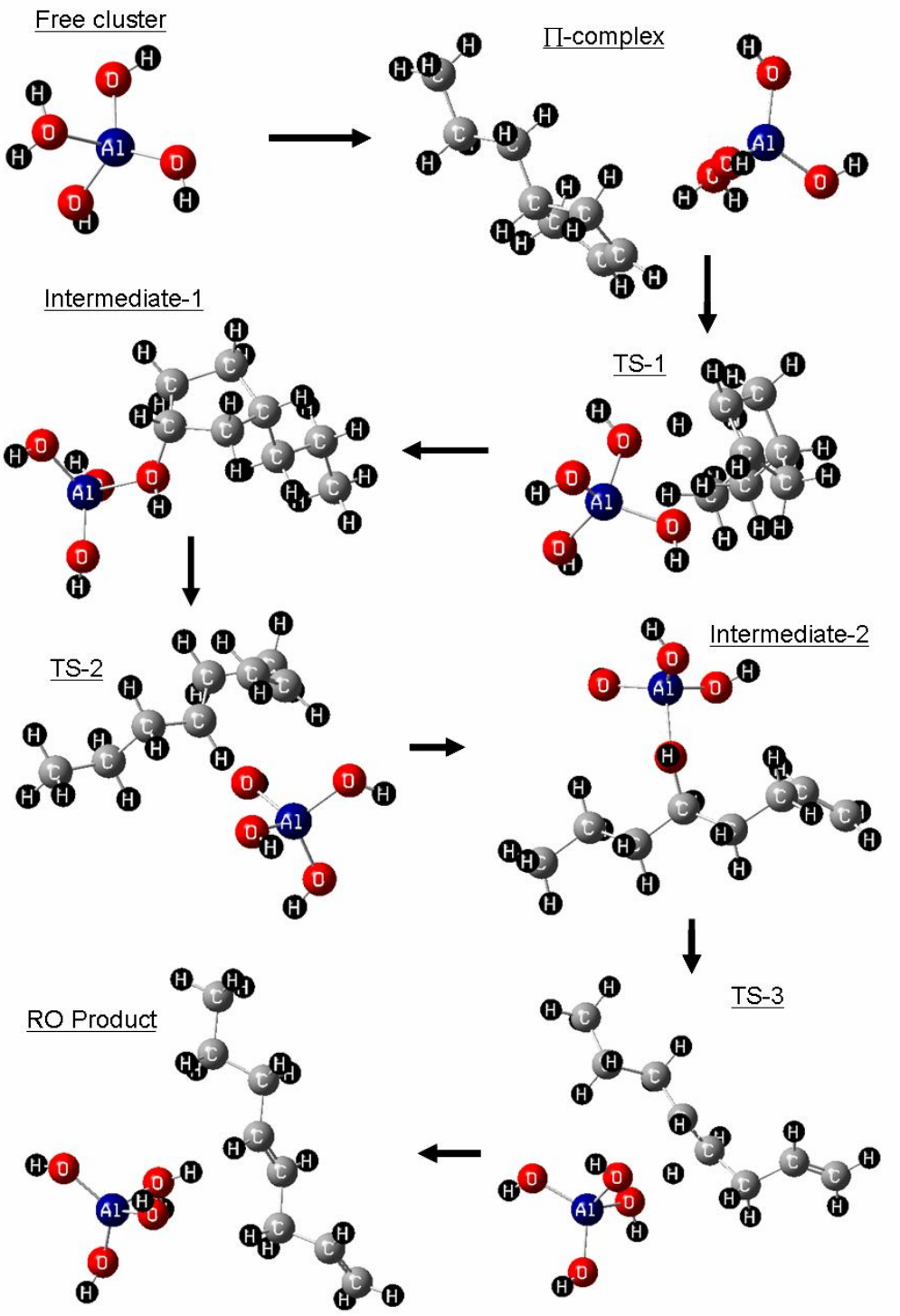

Figure 5.5.9: Geometry of different steps involved in ring opening of propylenecyclopentane on a Brønsted acid site (1T-HF).

There is a activation barrier difference of 4.3 kcal/gmol between the ring opening and dealkylation reactions. The activation barrier diagram clearly shows that ring opening reaction and dealkylation reactions are more competitive in nature.

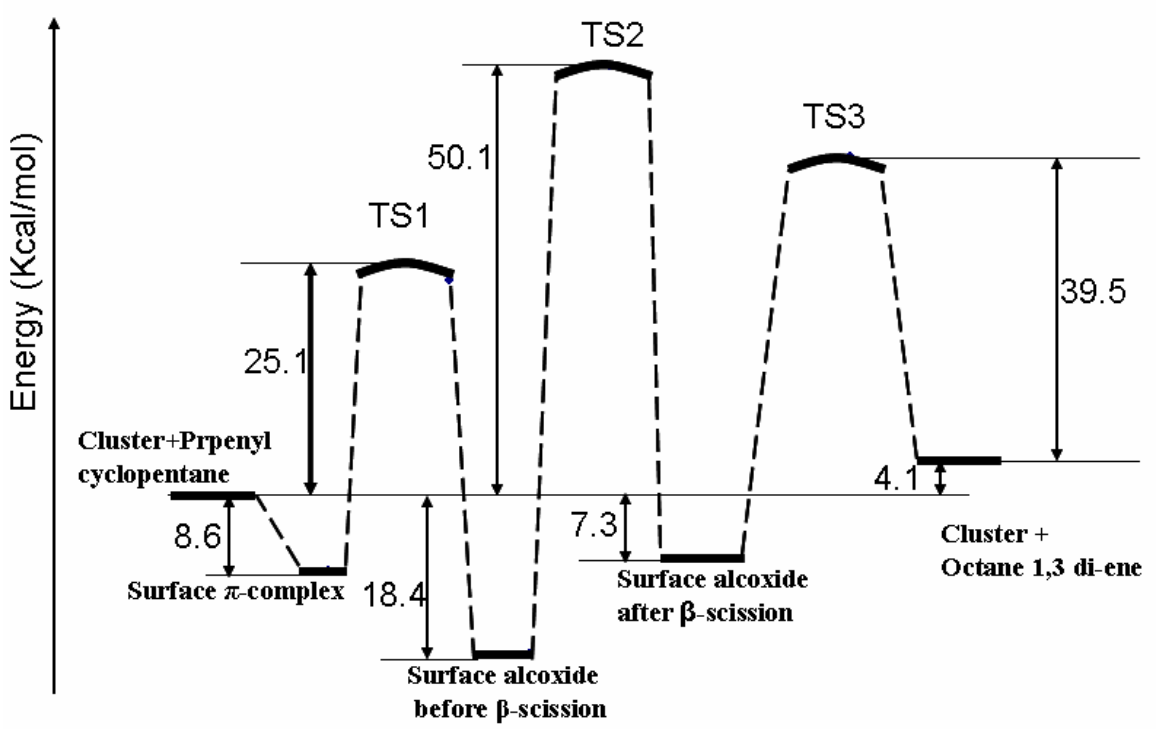

Figure 5.5.10: Reaction pathways for ring opening of propylenecyclopentane on 1T zeolite, HF, 6-31g(d).

5.5.3 Summary

Molecular level simulations were carried out successfully on the propenylcyclopentane molecule to see the energetics of the ring opening and deaakylation reactions. Gas phase calculation shows that ring opening reaction require high activation barrier compared to dealkylation reaction at both HF and DFT theories. Compared to dealkylation reaction, 5.9 and 7.1 kcal/gmol of more activation energy is needed for ring

opening reaction when using HF and DFT calculations respectively. The Arrhenius activation energies and frequency factors also indicated that RO and DA reactions are very competitive due to their similar range of activation energies. The dealkylation reaction on Brønsted acid sites is carried out using 1T and 5T clusters. The overall reaction is carried out through three elementary steps: 1) proton transfer between the catalyst surface and the reactant molecule, 2) dealkylation, and 3) desorption of the proton from the product molecule. All the transition states for three elementary steps are identified and both 1T and 5T cluster energetics clearly show that surface reaction step requires high activation energy and is the rate limiting step. There is a decrease in the activation energies when we move from 1T to 5T. Study of the energetics of ring opening and dealkylation reactions on 1T cluster showed that ring opening reaction requires higher activation barrier than the dealkylation reaction. Therefore it can be concluded that ring opening and dealkylation reactions are more competitive in nature.

6 CONCLUSIONS SUMMARY AND RECOMMENDATIONS

6.1 Conclusions and Summary

In phase 1, selective ring opening of model compound decalin was studied on catalysts Ir-Pt/Zr-MCM-41. The Pt and Ir concentrations were varied from 0-1.75% by weight. Zr-MCM-41support with hexagonal nature was prepared and moderate acidity was observed through NH_3-TPD and NH_3 drift sperctra. Impregnation of Pt and Ir were carried out on Zr-MCM-41 support. All the catalysts are well characterized using TPD, DRIFTS of CO and NH_3, BET, and CO-chemisorption. DRIFTS of CO adsorption on Ir-Pt/Zr-MCM-41 catalysts indicated that Pt was in Pt^0 and Pt^1 states and there was interaction between Ir and Pt metallic phases on the support. Brønsted and Lewis acid sites were observed on all the catalysts fron DRIFTS of NH_3.

Selective ring opening of decalin was studied at 300 to 400 °C over the synthesized catalysts. All the catalysts activity was stable after 24 hours. The optimum temperature for the ring opening yield and selectivity in the studied conditions is 350 °C. Optimization of metal loading was resulted in maximum ring opening yield of 16 wt.% and selectivity of 26 wt.% from decalin at 350 °C when the metal loading is 1.5% Ir and 0.75% Pt. Temperature above 350 °C was not favoured for ring opening products as dehydrogenation was a dominant reaction at high temperatures. At low temperatures only cis- to trans-decalin conversion was dominant. It was also observed that temperatures above 350 °C are favored for the high cetane number products. Pt presence caused an increase in the trans-decalin reactivity. The Ir-Pt/Zr-MCM-41 showed considerable thioresistance in the studied temperature and time range.

In phase 2, to understand the thermodynamic limitations on the yield and selectivity of ring opening products, thermodynamic equilibrium calculations have been performed

on a reaction mixture obtained from hydrocracking of decalin from phase 1. Ring opening of naphthenes under hydrocracking environment differs from hydrocracking of alkanes mainly in entropic contribution. The adverse entropy change is due to hydrogenation. Thermodynamically controlled hydrogenation reactions severely hinder the formation of saturated ring opening products. The same limitation, although exists in alkane hydrocracking, is much more severe in ring opening due to entropy consideration.

To overcome this limitation, the operating temperature need to be increased to promote dehydrogenation reactions and the formation of unsaturated species as the same philosophy is followed in fluidized catalytic cracking systems. The idea of increasing temperature is also encouraged by analyzing different types of cracking reactions that show that ring opening reactions are favorable over exocyclic and alkane cracking reactions at higher temperatures. These findings are confirmed by equilibrium calculations for a reaction mixture having 46 components identified from the experiments.

The selectivity of ring opening products increases with increasing temperature because of increase in production of unsaturated ring opening products, which is confirmed in the literature that the higher temperatures favor dehydrogenation reactions and the formation of unsaturated species.

As methane and naphthalene are the highly favorable compounds at equilibrium, the comparison between the numerical (at equilibrium) and experimental results (at real conditions) is not justifiable. Our main objective in this theoretical work is to study the effect of temperature on the ring opening (RO) yield and selectivities at equilibrium but

not to compare with experimental results, as it is quite difficult to generate experimental data on RO reaction production yields at equilibrium. No such data is available in the open literature.

Experimental evidence shows that by reducing the acidity of the catalyst and at the same time compensating the loss of activity by increasing the temperature produces better yield and selectivity. Based on these studies it is expected that lowering acidity of the catalyst to avoid excessive cracking and increasing the operating temperature to favor (i) the formation of unsaturated ring opening products and (ii) ring opening reaction over acyclic and exocyclic cracking reactions will improve the yield and selectivity of total ring opening products. In addition, our results clearly demonstrate that the systematic procedure developed by Smith and Missen (1968) for obtaining initial guesses for equilibrium calculation works extremely well for a large system.

In phase 3, deaclin ring-opening reaction was studied over Ni-Mo carbide catalysts supported on HY, H-Beta, silica-alumina, γ-alumina and Al-SBA-15. The catalytic activity of the above said catalysts are compared with Ir-Pt catalysts supported on HY and H-Beta. All the catalysts are well characterized using NH_3-TPD, H_2-TPR, XRD, BET and CO chemisorption. XRD patterns of the Ni-Mo carbide catalysts supported on H-Beta showed the presence of β-Mo_2C, whereas all other carbide catalysts did not displayed any β-Mo_2C peak in the diffractogram which indicated higher dispersion of metal on the catalysts. CO chemisorptions show good dispersion of the metal on the support and that the available metal sites are large in number with the carbide catalysts. 30-35 % reduction in the total acid sites was observed from TPD of ammonia for the carbide catalysts. The total amount of acidic sites is higher for the noble

metal catalysts. Selective ring opening of decalin over Ni-Mo carbide catalysts showed HY- and H-Beta-supported catalysts are the best among the carbide catalysts.

Comparision of HY- and H-Beta-supported carbide catalysts with the noble metals catalysts was studied. The Ni-Mo carbide supported on HY showed a maximum yield of 33.5 % at 240 °C, whereas, the Ir-Pt/HY catalyst showed a 32 % RO yield at 220°C. Further classification of ring opening products as saturated and unsaturated ring-opening products leads to the conclusion that yields of total, sastrated and unsaturated ring opening products follow the same trend. It was observed that the same level of ring-opening products yield can be successfully achieved by using Ni-Mo carbide catalyst when compared with noble metals catalysts.

In phase 4, Fuel quality improvement of hydrotreated LGO was studied on the best catalysts observed from the model compound studies. Ir-Pt/HY, Ni-Mo carbide/HY and Ni-Mo carbide/H-Beta catalysts are chosen for the study of real feed. Screening of the Ni-Mo carbide/HY catalyst revealed that 275 to 325 °C is the best operating temperature for the for the improvement in quality of the feed. A 12 unit increase in cetane number was observed on Ni-Mo carbide/HY at 325 °C, whereas Ni-Mo carbide/H-Beta could not improve the cetane index effectively. Simulated distillation results also supported this information by observing the ring opening capability of these catalysts. The fuel quality improvement activity of Ir-Pt/HY catalyst is comparable with that of Ni-Mo carbide/H-Beta, but the former catalyst deactivates fast. NMR, cetane index and boiling point distribution analysis of the products showed that the Ni-Mo carbide/HY catalyst improves the cetane index of the fuel by selectively converting the naphthenes to paraffins in the temperature range of 300 to 325 °C. Dehydrogenation and secondary

cracking are dominant above 325 °C, which leads to the reduction in cetane index and forming low carbon number products. For the development of kinetic model on Ni-Mo carbide/HY catalyst, the further experiments were conducted by varying temperature and space velocity. A first order kinetic model was proposed and the model was well fit with the experimental values. Arrhenius activation energies of 111, 89 and 42 KJ/gmol were observed for dehydrogenation, aromatic saturation and cracking reactions, respectively.

In phase 5, molecular level simulations were carried out on the propenylcyclopentane molecule to see the energetics of the ring opening and deaakylation reactions. Gas phase calculations were carried out at both HF and DFT level theories. Gas phase calculation show that ring opening reaction require high activation barrier compared to dealkylation reaction. HF and DFT calculations show 5.9 and 7.1 kcal/gmol of more activation energy needed for ring opening reaction than dealkylation reaction. The Arrhenius activation energies and frequency factors also indicated that RO and DA reactions are very competitive due to their similar range of activation energies. 1T and 5T cluster models were used to model the dealkylation and ring opening reactions on Brønsted acid sites. The overall reaction is carried out through the elementary steps 1) Proton transfer between the catalyst surface and the reactant molecule 2) surface reaction and 3) Desorption of the proton from the product molecule. All the transition states for three elementary steps are identified and both 1T and 5T cluster energetics clearly show that surface reaction step requires high activation energy and is the rate limiting step. Always higher level cluster gave low activation barriers. Study of the energetics of ring opening and dealkylation reactions on 1T cluster showed that ring opening reaction

requires higher activation barrier than the dealkylation reaction. Therefore, it can be concluded that ring opening and dealkylation reactions are more competitive in nature.

6.2 Recommendations

1) Another route of selective ring opening reaction is through partial oxidation. The catalysts tried in this study can be further used for the selective ring opening of model compound through partial oxidation step and comparision of the results can be made.

2) Thermodynamic equilibrium calculations for the decalin cracking can be carried out considering non ideal behaviour and phase equilibrium problem using HYSYS.

3) Energetics of ring opening reactions can be studied using true catalyst model.

4) A high sulfur resistant and ring opening catalyst development to study the HGO.

7 REFERENCES

Siegell, Jeffrey H., “Control valve fugitive emissions”, Hydrocarb. Process 76 (1997) p.45-48.

Ancheyta, S. Sanchez, M.A. Rodriguez, “Kinetic modeling of hydrocracking of heavy oil fractions: A review”, Catal. Today 109 (2005) p.76-92

Ardakani, S. J., X. Liu, K. J. Smith, “Hydrogenation and ring opening of naphthalene on bulk and supported Mo_2C catalysts”, Appl. Catal. A: General 324 (2007) p.9–19

Anderson, J. R., “Metal Catalyzed Skeletal Reactions of Hydrocarbons”, Adv. Catal. 23 (1973) p.1-90.

Albertazzi, S., Enrique Rodriguez-Castellon, Massimiliano Livi, Antonio Jimenez-Lopez, Angelo Vaccari,. J. Catal. 0 (2004) p.1.

Albertazzi, S., G. Busca, E. Finocchio, R. Glockler, and A.Vaccari, “New Pd/Pt on Mg/Al basic mixed oxides for the hydrogenation and hydrogenolysis of naphthalene”, J. Catal. 223 (2004) p.372-381.

Alvarez, W.E., D.E.Resasco, “Methylcyclopentane Ring Opening as a Reaction Test for Pt Catalysts Supported on Non-acidic Materials”, J. Catal.164 (1996) p.467-476.

Arbuznikov, A. V.; Zhidomirov, G. M., “Selective oxidation of methane by dinitrogen monoxide on FeZSM-5 zeolites. Ab initio quantum chemical analysis”, *Catal. Lett. 40* (1996) p.17-23.

Arribas, M. A., A. Mart´ınez, “The influence of zeolite acidity for the coupled hydrogenation and ring opening of 1-methylnaphthalene on Pt/USY catalysts”, Appl. Catal. A: General 230 (2002) p.203-217

Arribas, M. A., P. Concepción, A. Mart´ınez, “The role of metal sites during the coupled hydrogenation and ring opening of tetralin on bifunctional Pt(Ir)/USY catalysts”, Appl. Catal. A: General 267 (2004) p.111-119.

Bai, X.L., W.H.M. Sachtler, “Methylcyclopentane conversion catalysis by zeolite encaged palladium clusters and palladium-proton adducts”, J. Catal. 129 (1991) p.121-129.

Bars, J.L., J. C. Vedrine, A. Auroux, S. Trautmann, M. Baerns, “Role of surface acidity on vanadia/silica catalysts used in the oxidative dehydrogenation of ethane”, Appl. Catal. A 88 (1992) p.179-195.

Beck, L. W.; Xu, T.; Nicholas, J. B.; Haw, J. F., “Kinetic NMR and Density Functional Study of Benzene H/D Exchange in Zeolites, the Most Simple Aromatic Substitution”, *J. Am. Chem. Soc. 117* (1995) p.11594-11595.

Becke, A. D., “Density-functional thermochemistry. III. The role of exact exchange”, *J. Chem. Phys. , 98 (*1993) p.5648.

Bellos, G. P. and Papayammokas, N. G., “The use of a three phase microreactor to investigate HDS kinetics”, Catalysis Today 79-80 (2003) p.349-355.

Blaszkowski, S. R.; van Santen, R. A., “Quantum chemical studies of zeolite proton catalyzed reactions”, *Top. Catal. 4* (1997) p.145-156.

Blaszkowski, S. R.; van Santen, R. A., “The Mechanism of Dimethyl Ether Formation from Methanol Catalyzed by Zeolitic Protons”, *J. Am. Chem. Soc. 118* (1996) *p.*5152-5153.

BorCave, A., A. Auroux, C. Guimon, “Nature and strength of acid sites in HY zeolites: a multitechnical approach”, Microporous Materials 11 (1997) p.275-291.

Brandenberger, S. G., W. L. Callender, W. K. Meerbott, “Mechanisms of methylcyclopentane ring opening over platinum-alumina catalysts”, J. Catal. 42 (1976) p.282-287

Broclawik, E.; Himei, H.; Yamadaya, M.; Kubo, M.; Miyamoto, A.; Vetrivel, R., “Density functional theory calculations of the reaction pathway for methane activation on a gallium site in metal exchanged ZSM-5”, *J. Chem. Phys. 103* (1995) p.2102-2109.

Brouwer, D. M., H. Hogeveen, RECUEIL, 89 (1970) p.211-224.

Capitan, M. J.; Odriozola, J. A.; Marquez, A.; Fernandez Sanz, J., “Ab Initio SCF-Mo Study of the Chemisorption of Methane on Al and La Oxide Surfaces”, *J. Catal. 156* (1995) p.273-278.

Caray, F.A., R.J. Sundberg, “Advanced organic chemistry”, third ed., Plenum, New York, 1990.

Carri´on, M.C., B.R. Manzano, F.A. Jal´on, P. Maireles-Torres, E. Rodr´ıguez-Castell´on, A. Jim´enez-L´opez, “Hydrogenation of tetralin over mixed PtMo supported on zirconium doped mesoporous silica: Use of polynuclear organometallic precursors”, J. Mol. Catal A: Chemical 252 (2006) p.31-39.

Carri´on, M.C., B.R. Manzano, F.A. Jal´on, D. Eliche-Quesada, P.Maireles-Torres, E. Rodr´ıguez-Castell´on, A. Jim´enez-L´opez, “Influence of the metallic precursor in the hydrogenation of tetralin over Pd–Pt supported zirconium doped mesoporous silica”, Green Chem. 7 (2005) p.793-799.

Chu, C. P. and Ng, K. M., "Flow in packed tubes with a small tube to particle diameter ratio", *AICHE J*. 35 (1989) p.148-158.

Chiou, J. F., Y. L. Huang, T. B. Lin, and J. R. Chang, "Aromatics Reduction over Supported Platinum Catalysts. 1. Effect of Sulfur on the Catalyst Deactivation of Tetralin Hydrogenation", *Ind. Eng. Chem. Res.* 34 (1995) p.4277-4283.

Clarke, J. K., J. J. Rooney, "Stereochemical Approaches to Mechanisms of Hydrocarbon Reactions on Metal Catalysts", Adv.Catal. 25 (1976) p.125-183

CNEB (Canada National Energy Board), "Canada's oil sands. An update on opportunities and challenges to 2015", 2006.

Corma, A., V.Gonzalez-Alfaro, and A.V.Orchilles, "Decalin and Tetralin as Probe Molecules for Cracking and Hydrotreating the Light Cycle Oil", J. Catal. 200 (2001) p.34-44.

Costa, P. D., C. Potvin, J. M. Manoli, B. Genin, G. D. Mariadassou, "Deep hydrodesulphurization and hydrogenation of diesel fuels on alumina-supported and bulk molybdenum carbide catalysts", Fuel 83 (2004) p.1717-1726.

Costa, P. D., C. Potvin, J. M. Manoli, M. Breysse, G. Djega-Mariadassou, "Novel phosphorus-doped alumina-supported molybdenum and tungsten carbides: synthesis, characterization and hydrogenation properties", Catal. Lett. 72 (2001) p.91-97.

Curtiss, L. A., P. Redfern, K. Raghavachari, V. Rassolov, J. A. Pople, "Gaussian-3 theory using reduced Møller-Plesset order", J. Chem. Phys. 110, 10 (1999) p.4703-4709.

De Jong, K. P., "Deposition Precipitation Onto Pre-Shaped Carrier Bodies. Possibilities and Limitations", Stud. Surf. Sci. Catal. 63 (1991) p.19-36.

Dhandapani, B., S. Ramanathan, C.C. Yu, B. Fruhberger, J.G. Chen, S.T. Oyama, "Synthesis, Characterization, and Reactivity Studies of Supported Mo_2C with Phosphorus Additive", J. Catal. 176 (1998) p.61-67.

Diaz, B., S. J. Sawhill, D. H. Bale, R. Main, D. C. Phillips, S. Korlann, R. Self, M. E. Bussell, "Hydrodesulfurization over supported monometallic, bimetallic and promoted carbide and nitride catalysts", Catal. Today 86 (2003) p.191-209.

Du, H., C. Fairbridge, H. Yang, Z. Ring, "Review-The chemistry of selective ring-opening catalysts" , Appl. Catal. A: General 294 (2005) p.1–21.

Duprez, D., and Mendez, M., "The Effect of Partial Reduction on the Thioresistance of Ni/Al_2O_3 Catalysts", Stud. Surf. Sci. Catal. 34 (1987) p .523-534

Egan, C. J., G. E. Langlois, R. J. White, "Selective Hydrocracking of C_9- to C_{12}-Alkylcyclohexanes on Acidic Catalysts. Evidence for the Paring Reaction", J. Am. Chem. Soc. 84 (1962) p.1204-1212.

Eliche-Quesada, D., J.Merida-Robles, P.Maireles-Torres, E.Rodriguez-Castellon, G.Busca, E.Finocchio, and A.Jimenez-Lopez, "Effects of preparation method and sulfur poisoning on the hydrogenation and ring opening of tetralin on NiW/zirconium-doped mesoporous silica catalysts", J. Catal. 220 (2003) p.457-467.

Erdohelyi, A., K.Fodor, G.Suru, "Reaction of carbon monoxide with water on supported iridium catalysts", Appl. Catal. A:General 139 (1996) p.131-147.

Evleth, E. M.; Kassab, E.; Jessri, H.; Allavena, M.; Montero, L.; Sierra, L. R., "Calculation of the Reaction of Ethylene, Propene, and Acetylene on Zeolite Models", *J. Phys. Chem. 100 (*1996) *p.*11368-11374.

Fenoglio, R.J., G.M.Nunez, D.E.Resasco, "Selectivity changes in the ring-opening reaction of methylcyclopentane over rhodium catalysts caused by the addition of silver and metal—support interactions", Appl. Catal. 63(1990) p.319-332.

Forni, L., "Laboratory reactors", Catal. Today 34 (1997) 353-367.

Fujikawa, T., K.Idei, T.Ebihara, H.Mizuguchi, K.Usui, "Aromatic hydrogenation of distillates over SiO_2-Al_2O_3-supported noble metal catalysts", Appl. Catal.A 192 (2000) p.253-261.

Galperin, L.B., J.C. Bricker, J.R. Holmgren, "Effect of support acid–basic properties on activity and selectivity of Pt catalysts in reaction of methylcyclopentane ring opening", Applied Catalysis A: General 239 (2003) p.297–304.

Frisch, M. J., Gaussian 03, Revision B. 5, Gaussian Inc., Pittsburgh, PA , 2003.

Gault, F. G., "Mechanisms of Skeletal Isomerization of Hydrocarbons on Metals", Adv.Catal. 30 (1981) p.1-95.

Gierman, H., "Design of laboratory hydrotreating reactors: Scaling Down of Trickle-flow Reactors", Applied Catalysis, 43 (1988) p.277-286.

Gopal, S., and Panagiotis G.S., "Deactivation Behavior of Bifunctional Pt/H-Zeolite Catalysts during Cyclopentane Hydroconversion", J. Catal. 205 (2002) p.231-243.

Haase, F.; Sauer, J., "Interaction of methanol with Broensted acid sites of zeolite catalysts: an ab initio study", *J. Am. Chem. Soc. 117* (1995) p.3780-3789

Hayek, K., R.Kramer, Z.Paal, "Metal-support boundary sites in catalysis", Appl. Catal. A: General 162 (1997) p.1-15.

Hendershot, R. J., Snively, C.M., Lauterbach, J. "High-Throughput Heterogeneous Catalytic Science", Chem. Eur. J. 11 (2005) 806-814.

Himei, H.; Yamadaya, M.; Kubo, M.; Vetrivel, R.; Broclawik, E.; Miyamoto, A., Study of the Activity of Ga-ZSM-5 in the de-NOx Process by a Combination of Quantum Chemistry, Molecular Dynamics, and Computer Graphics Methods, J. Phys. Chem. *99 (*1995) p.12461-12467.

Jacquin, M., D. J. Jones, J. Rozière, S. Albertazzi, A Vaccari, M. Lenarda, L. Storaro, R. Ganzerla, "Novel supported Rh, Pt, Ir and Ru mesoporous aluminosilicates as catalysts for the hydrogenation of naphthalene", Appl. Catal. A: General 251 (2003) p.131-141.

Jacquin, M., D. J. Jones, J. Rozière, A. J. López, E. Rodríguez-Castellón, J. Manuel, T. Menayo, M. Lenarda, L. Storaro, A. Vaccari, S. Albertazzi, "Cetane improvement of diesel with a novel bimetallic catalyst", J. Catal. 228 (2004) p.447-459.

Kapteijn, F., J.A. Moulijn, in: G. Ertl, H. Knözinger, J.Weitkamp (Eds.), "Handbook of Heterogeneous Catalysis", Vol.3, VCH, Weinheim, (1996) p.1359.

Kapteijn, F., J.A. Moulijn, in: G. Ertl, H. Knözinger, J.Weitkamp (Eds.), Handbook of Heterogeneous Catalysis, Vol.3, VCH, and Weinheim, (1996) p.1189.

Kapur, G.S., A.P. Singh, A.S. Sarpal, "Determination of aromatics and naphthenes in straight run gasoline by ^{1}H NMR spectroscopy", Part I, Fuel, 79 (2000) p.1023-1029.

Kjarstad, J., F. Johnsson, “Resources and future supply of oil”, Energy Policy 37 (2009) p.441–464

Kramer, G. J.; van Santen, R. A. *Chem. Re*V.,” Reactivity Theory of Zeolitic Broensted Acidic Sites”, 95 (1995) p.637-660.

Kresge, C.T., M.E.Leonowicz, W.J.Roth, J.C.Vartuli and J.S.Beck, letters to nature, Nature 359 (1992) p.22.

Krossner, M.; Sauer, J., “Interaction of Water with Brønsted Acidic Sites of Zeolite Catalysts. Ab Initio Study of 1:1 and 2:1 Surface Complexes”, *J. Phys. Chem. 100*, (1996) p.6199-6211.

Kubicka, D., N. Kumar, P. Maki-Arvela, M. Tiitta, V. Niemi, H. Karhu, T. Salmi, D.Y. Murzin, “Ring opening of decalin over zeolites II. Activity and selectivity of platinum-modified zeolites”, J. Catal. 227 (2004a) p.313-327.

Kubicka, D, N. Kumar, P. Maki-Arvela, M. Tiitta, V. Niemi, T. Salmi, D.Y. Murzin, “Ring opening of decalin over zeolites I. Activity and selectivity of proton-form zeolites”, J. Catal. 222 (2004b)p.65-79.

Laherrere, J. “Forecast of oil and Gas Supply to 2050, Petrotech 2003”, New Delhi (2003).

Larachi, F., Alix,C., Grandjean, B. P. A., and Bernis, A., “*Nu*=*Sh* CORRELATION FOR PARTICLE±LIQUID HEAT AND MASS TRANSFER COEFFICIENTS IN TRICKLE BEDS BASED ON PEÂ CLET SIMILARITY”, Trans IChemE, Vol 81, Part A, July 2003

Li, X., W. Zhang, S. Liu, L. Xu, X. Han, X. Bao, “The role of alumina in the supported Mo/H-Beta–Al_2O_3 catalyst for olefin metathesis: A high-resolution solid-state NMR and electron microscopy study”, J. Catal. 250 (2007) p.55-66.

Lin, T. B., C. A. Jan, and J. R. Chang, “Aromatics reduction over supported platinum catalysts. 2. Improvement in sulfur resistance by addition of palladium to supported platinum catalysts”, *Ind. Eng. Chem. Res.* 34 (1995) p.4284-4289.

Matsubayashi, N., H.Yasuda, M. Imamura and Y. Yoshimura, “EXAFS study on Pd–Pt catalyst supported on USY zeolite”, *Catal. Today* 45 (1998) p.375-380.

Mc Vicker, M. daage, G.B, Touvelle, M.S, Hudson, D.P Klein, W. C Baird, Jr., B.R Cook, J.G.Chen, S.Hantzer, D.E.W.Vaughan, E.S Ellis, and O.C. Feeley, “Selective Ring Opening of Naphthenic Molecules”, J. Catal. 210 (2002) p.137-148.

McVicker, G.B, Touvelle, M.S, Hudson, C.W, Vaughan,D.E.W, Daage, M, Hantzer, S.Klein, D.P, Ellis, E.S,Cook, B.R, Feeley, O.C, and, Baumgartener, J.E, *U.S.Patent* 5,763,731, (1998).

Mihut, C., C. Descorme, D. Duprez, M.D. Amiridis, “Kinetic and Spectroscopic Characterization of Cluster-Derived Supported Pt–Au Catalysts”, J. Catal. 212 (2002) p.125-135.

Mills, G.A., H. Heinemann, T.H. Milliken, A.G. Oblad, Ind. Eng. Chem. 45 (1953) p.134.

Mota, C. J. A.; Esteves, P. M.; de Amorin, M. B., “Theoretical Studies of Carbocations Adsorbed over a Large Zeolite Cluster. Implications on Hydride Transfer Reactions”, *J. Phys. Chem. 100 (*1996) p.12418-12423.

Mouli, K. C., V. Sundaramurthy, A. K. Dalai, Z. Ring, "Selective Ring Opening of Decalin with Ir-Pt on Zr Modified MCM-41", Appl. Catal. A: General 321 (2007) p.17-26.

Mouli, K. C., V. Sundaramurthy, A.K. Dalai, "A comparison between ring-opening of decalin on Ir-Pt and Ni-Mo carbide catalysts supported on zeolites", *J. Mol. Catal. A: Chemical*, *304, 1-2,* (*2009)* p.*77-84.*

Nylen, U., Barbara Pawelec, Magali Boutonnet, J.L.G. Fierro, "Catalytic ring opening of naphthenic structures: Part I. From laboratory catalyst screening via pilot unit testing to industrial application for upgrading LCO into a high-quality diesel-blending component", Appl. Catal. A: General 299 (2006) p.1-13.

Nylen, U., L. Sassu, S. Melis, S. Ja¨ra°s, M. Boutonnet, "Catalytic ring opening of naphthenic structures: Part II. In-depth characterization of catalysts aimed at upgrading LCO into a high-quality diesel-blending component", Appl. Catal. A: General 299 (2006) p.14-29.

Nylén, U., Juana Frontela Delgado, Sven Järås, Magali Boutonnet, "Low and high-pressure ring opening of indan over 2 wt.% Pt, Ir and bi-metallic $Pt_{25}Ir_{75}$/boehmite catalysts prepared from microemulsion systems", Appl. Catal. A 262 (2004) p.189-200.

Ochterski J. W., "Thermochemistry in Gaussian", help@gaussian.com, Gaussan Inc., June 2, 2000.

Otten, M. M., M.J. Clayton, H.H. Lamb, "Platinum-Mordenite Catalysts for *n*-Hexane Isomerization: Characterization by X-Ray Absorption Spectroscopy and Chemical Probes", J. Catal. 149 (1994) p.211-222.

Paal, Z., and P.Tetenyi, Nature 267 (1997) p.234.

Pedrosa, A. M. G., M. J. B. Souza, D. M. A. Melo, A. S. Araujo, “Cobalt and nickel supported on HY zeolite: Synthesis, characterization and catalytic properties”, Mater. Res. Bull. 41 (2006) p.1105–1111

Qiu, P., J. H. Lunsford, M. P. Rosynek, “Steady-state conversion of methane to aromatics in high yields using an integrated recycle reaction system”, Catal. Lett. 48 (1997) p.11-15.

Ramı´rez, L. F., J. Escobar, E. Galvan, H. Vaca, F. R. Murrieta, and M. R. S. Luna, “Evaluation of Diluted and Undiluted Trickle-Bed Hydrotreating Reactor with Different Catalyst Volume”, Petro. Sci. Tech. (22) (2004) p.157-175.

Rodr´iguez-Castellón, E., Josefa Mérida-Robles, Lourdes D´iaz, Pedro Maireles-Torres, Deborah J. Jones, Jacques Rozière, Antonio Jiménez- López, “Hydrogenation and ring opening of tetralin on noble metal supported on zirconium doped mesoporous silica catalysts”, Appl. Catal. A 260 (2004) p.9-18.

Rodr´iguez-Castellón, E., Lourdes D´iaz, Pilar Braos-Garcia, Josefa Mérida-Robles, Pedro Maireles-Torres, ntonio Jiménez-López, Angelo Vaccari, “Nickel-impregnated zirconium-doped mesoporous molecular sieves as catalysts for the hydrogenation and ring-opening of tetralin”, Appl. Catal. A 240 (2003) p.83-94.

Rousset, J.L., L. Stievano, F.J. Cadete Santos Aires, C. Geantet, A.J.Renouprrez, M.Pellarin, “Hydrogenation of Tetralin in the Presence of Sulfur over γ-Al_2O_3-Supported Pt, Pd, and Pd–Pt Model Catalysts”, J. Catal. 202 (2001) p.163-168.

Sanchez, S., M.A. Rodriguez, J. Ancheyta, “Kinetic Model for Moderate Hydrocracking of Heavy Oils”, Ind. Eng. Chem. Res. 44 (2005) p.9409-9413

Santikunaporn, M., J.E. Herrera, S. Jongpatiwut, D.E. Resasco, W.E. Alvarez, E.L. Sughrue, "Ring opening of decalin and tetralin on HY and Pt/HY zeolite catalysts", J. Catal. 228 (2004) p.100-113.

Santikunaporn, M., W. E. Alvarez , D. E. Resasco, "Ring contraction and selective ring opening of naphthenic molecules for octane number improvement", Appl. Catal. A: General 325 (2007) p.175-187.

Sauer, J.; Ugliengo, P.; Garrone, E.; Saunders, V. R., "Theoretical Study of van der Waals Complexes at Surface Sites in Comparison with the Experiment", *Chem. Re*V. *94 (* 1994) p.2095-2160.

Schmal, M., M.M.V.M. Souza, N.S. Resende, A.L. Guimarães, C.A. Perez, J.G. Eon, D.A.G. Aranda and L.C. Dieguez, "Interpretation of kinetic data with selected characterizations of active sites", Catal. Today 100 (2005) p.145-150.

Sepulveda, J., and Figoli, N.S., "Ni/SiO_2 catalysts, effect of Ni reduction on activity and thiotolerance during ethylbenzene hydrogenation", React. Kinet. Catal. Lett. 55, (1995) p.383-389

Sheppard, N. and C. D. L. Cruz, "The reliability of vibrational spectroscopy as a means of identification of the structures of chemisorbed species on metal surfaces: the cases of CO, NO and C_2 hydrocarbon surface species", Catal. Today 70 (2001) p.3-13.

Sinclair, P. E.; Catlow, C. R. A., "Generation of Carbenes during Methanol Conversion over Brönsted Acidic Aluminosilicates. A Computational Study", *J. Phys. Chem. B 101 (*1997) p.295-298.

Simon, L.J., J.G. van Omnen, A. Jentys and J.A. Lercher, "Sulfur tolerance of Pt/mordenites for benzene hydrogenation: Do Brønsted acid sites participate in hydrogenation?", *Catal. Today* 73 (2002), p.105-112.

Skutil, K. and Taniewski, M., "Some technological aspects of methane aromatization (direct and via oxidative coupling)", *Fuel Processing Technology*, 87, 6 (2006) p.511-521

Smith, J. M., H. C. Van Ness, M. M. Abbott, "Introduction to Chemical Engineering Thermodynamics", 7th edition, McGraw-Hill, (2005) p.525-526

Smith, W. R., R. W. Missen, Can. J. Chem. Eng. 46 (1968) p.269-272.

Smith, W. R., R. W. Missen, Chem. Eng. Edu. 13 (1979) p.26-32.

Solymosi, F., J. Rasko, "An infrared study of CO and NO adsorption on alumina-supported iridium catalyst", J. Catal. 62 (1980) 253-263.

Solymosi, F., J. Rasko, "An infrared study on the formation of isocyanate in the NO + CO reaction on supported Ir catalyst", J. Catal. 63 (1980) p.217-225.

Stanislus, A., B. H. Cooper, "Aromatic Hydrogenation Catalysis: A Review", Catal. Rev. Sci. Eng. 36 (1994) p.75-123.

Stringham Greg, "The Canadian oil sands: Opportunities and challenges", CAPP, Feb 2006.

Stull, D. R., E. F. Westrum, Jr., G. C. Sinke, "The Chemical Thermodynamics of Organic Compounds", John Wiley & sons, New York, 1969.

Sundaramurthy, V., I. Eswaramoorthi, A.K. Dalai, J. Adjaye, Hydrotreating of gas oil on SBA-15 supported NiMo catalysts, Micro. Meso. Mater. 111 (2008) p.560-568.

Sundaramurthy, V., A.K. Dalai , J. Adjaye, "Effect of phosphorus addition on the hydrotreating activity of $NiMo/Al_2O_3$ carbide catalyst", Catal.Today 125 (2007) p.239-247.

Teschner, D., K. Matusek, and Z. Paal, "Ring opening of methylcyclopentane on alumina-supported Rh catalysts of different metal loadings", J. Catal. 192 (2000) p.335-343.

The Refiner, Newsletter of the NCUT, #8, Spring/summer 2003, (www.ncut.com/refiner.htm)

Ugliengo, P.; Ferrari, A. M.; Zecchina, A.; Garrone, E., "Structure and Vibrational Features of Complexes between Unsaturated Hydrocarbons and Acidic Sites in Silica and Zeolites: An ab Initio Study", *J. Phys. Chem. 100 (*1996) p.3632-3645.

Upgrading & Catalyst Development Network (UCDN) workshop, Devon, 16 June, 2005

Vaarkamp, M., P.Dijkstra, J. van Grodelle, J.T.Miller, F.S.Modica, D.C.Koningsberger, and R.A.van Santen, "The Effect of Hydrogen Partial-Pressure on Methylcyclopentane Ring-Opening", J. Catal. 151 (1995) p.330-337.

Vaarkamp, M., J.T.Miller, F.S.Modica,D.C.Koningsberger, "On the Relation between Particle Morphology, Structure of the Metal-Support Interface, and Catalytic Properties of $Pt/\gamma\text{-}Al_2O_3$", J. Catal. 163 (1996) p.294-305.

Wang, X., F.Lefebvre, J.Patarin and J.Basset, "Synthesis and characterization of zirconium containing mesoporous silicas: I. Hydrothermal synthesis of Zr-MCM-41-type materials", Micro. Meso. Mat., 42 (2001) p.269-276.

Wei, Z., Q. Xin, P. Grange, B. Delmon, "TPD and TPR Studies of Molybdenum Nitride" J. Catal. 168 (1997) p.176-182.

Weisz, P.B., Swegler, E.W., "Stepwise Reaction on Separate Catalytic Centers: Isomerization of Saturated Hydrocarbons", Science 126 (1957) p.31-32.

Weitkemp, J., and Ernst, S., "Large pore molecular sieves : Chapter 5 Catalytic test reactions for probing the pore width of large and super-large pore molecular sieves", Catal. Today 19 (1994) p.107-149.

Weitkamp, J., S. Ernst, Proc. Intern. Symposium on catalysis by acids and bases, Sept. 25-27 (1984) p.419-426

Weitkamp, J., S. Ernst, H. g. Karge, Erdol und Kohle Erdgas 37 (1984) p.457-462.

Yasuda, H. and Y. Yoshimura, "Hydrogenation of tetralin over zeolite-supported Pd-Pt catalysts in the presence of dibenzothiophene", *Catal. Lett.* 46 (1997) p. 43-48.

Yasuda, H., N. Matsubayashi, T. Sato and Y. Yoshimura., "Confirmation of sulfur tolerance of bimetallic Pd–Pt supported on highly acidic USY zeolite by EXAFS", *Catal. Lett.* 54 (1998), p. 23-27.

Yasuda, H., T.Sato, Y.Yoshimura, "Influence of the acidity of USY zeolite on the sulfur tolerance of Pd–Pt catalysts for aromatic hydrogenation", Catal.Today 50 (1999) p.63-71.

Yoshioka, C. M. N., T. Garetto, D. Cardoso, "*n*-Hexane isomerization on Ni-Pt catalysts/supported on HUSY zeolite: The influence from a metal content", Catalysis Today 107–108 (2005) p.693-698.

Zimmer, H. and Zoltán Paál, "Reactions of alkylcyclopentanes over pt catalysts", J. Mol. Catal., 51, 3 (1989), p.261-278

APPENDIX

Appendix A: Experimental calibrations

This section gives the details about the calibration of different instruments and reactors used in the experimental work.

A.1 Reactor temperature calibration

The reactor was temperature calibrated using the pressurized and nonpressurized reactors. Temperature was varied from 150 to 400 °C while maintaining the reaction pressure at 5 MPa. The corresponding reactor temperature was measured using a single thermocouple inserted just below the catalyst bed.

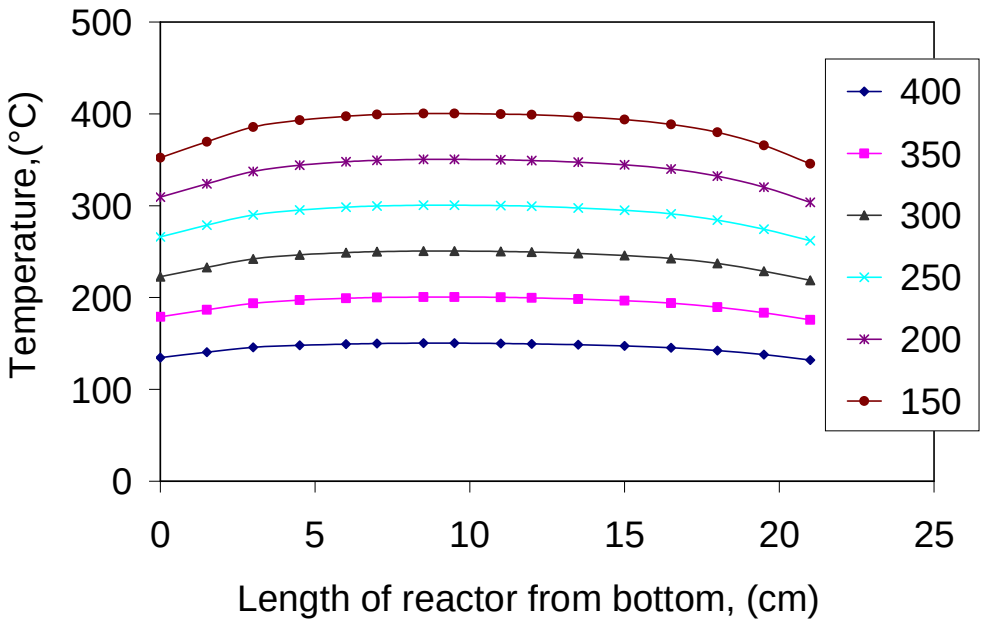

Figure A.1: Temperature distribution along the axial length of the reactor (without pressure)

The thermocouple was then moved every 1 cm up the catalyst bed to measure the temperature along the reactor bed. Temperature distribution profile along axial length of

the reactor bed for unpressurized and pressurized systems is shown in Figure A.1 and Figure A.2 respectively.

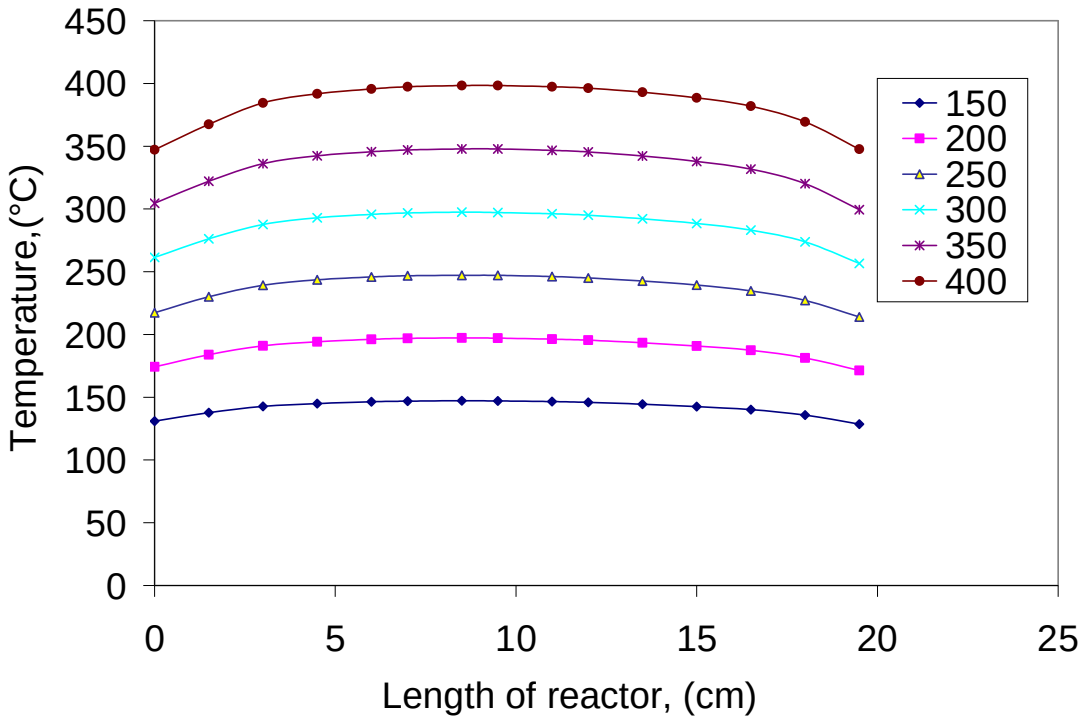

Figure A.2: Temperature distribution along the axial length of the reactor (with pressure)

Figure A.3 shows the calibration curve for the temperature controller when the system is under pressure.

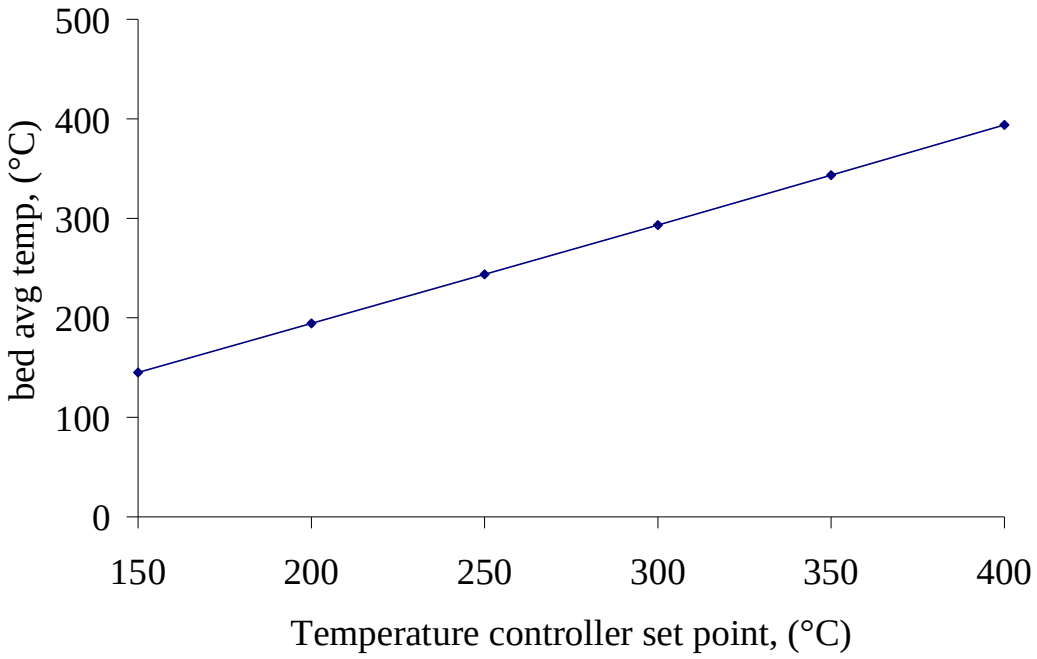

Figure A.3: Calibration of Temperature controller

A.2 Mass flow controller calibration

The mass flow controller was calibrated for hydrogen flow at the experimental operating conditions using a bubble flow meter connected to the exit of the back pressure regulator. All the flow rates were measured at atmospheric conditions. The following equation was used to calculate the flw rates at standard conditions.

$$V^s = \left[\frac{P^n}{P^s}\right]\left[\frac{T^s}{T^n}\right]V^v$$

Where V is the flow rate in ml/hr, T is temperature, P is pressure, the superscripts ‘s’ and ‘n’ represent standard conditions normal operating conditions, respectively. Figure A.4 shows the calibration curve of the mass flow controller.

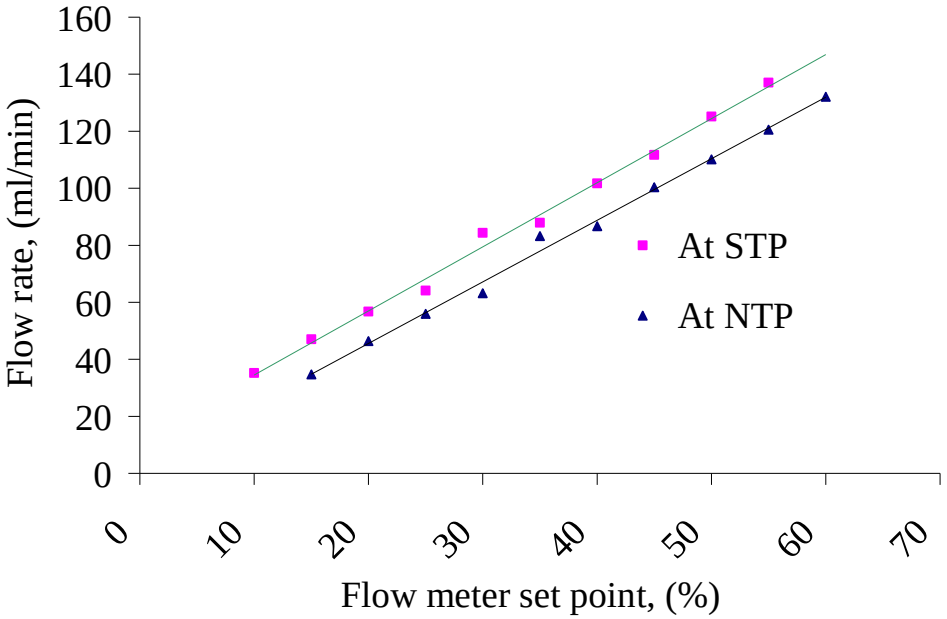

Figure A.4: Calibration of mass flow controller

A.3 TPD calibration

Known volume of ammonia was injected in the U-tube with the helium flow and the corresponding peak area was calculated. A plot is drawn between the peak area and the amount of ammonia adsorbed on the surface of the catalyst. The fit is leniar and the actal point are extended to get the exact amount of ammonia adsorbed got from the equation.

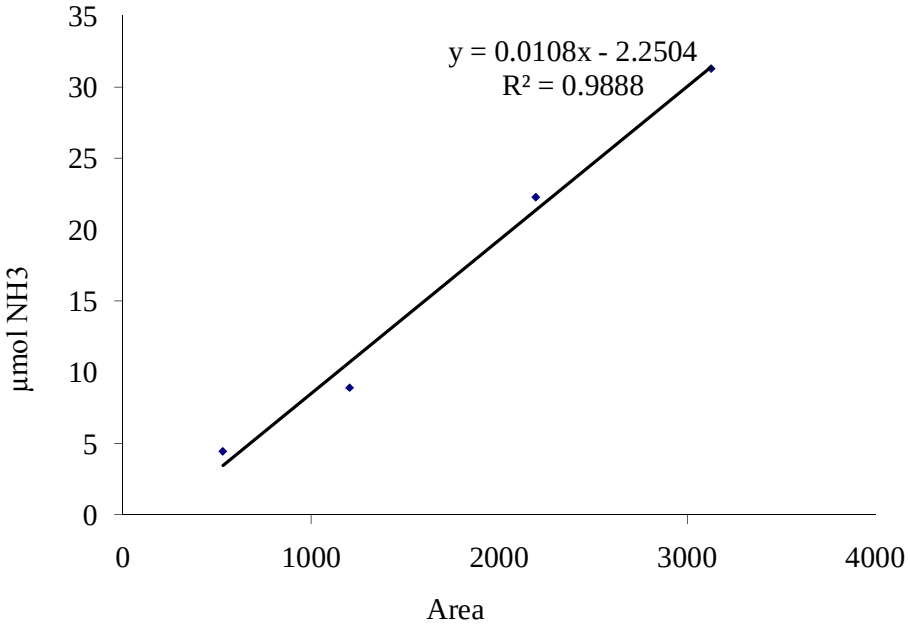

Figure A.5:Calibration plot of TPD

Appendix B: External and Internal mass transfer calculations

B.1 Wetting Phenomina

Wetting phenomina is calculated based on W (Ramı´rez, 2004; Gierman, 1988).

$$W = \frac{\eta_L u_L}{\rho_L d^2{}_p g} = 600 > 5*10^{-6}$$

ρ_L density of liquid (g cm^{-3}),

η_L dynamic viscosity of liquid, (g cm^{-1} s^{-1}),

d_p diameter of the particle (m),

u_L Liquid superficial velocity (cm s^{-1}).

B.2 External mass transfer limitation

The mass transfer parameters and constants for the estimation of Mears criteria are calculated and are shown in Table B.1.

Table B.1: External mass transfer calculations

n, reaction order	1
rate, $-r_A$, kmol/kg-s	-1.16E-08
R,Catalyst particle radius, m	0.0001
$\rho_b = (1 - \varepsilon)\ \rho c$, kg/m3	550
ρ_c, kg/m3	1200
Awg. Mol. Wt. of LGO	250
C_{ab},bulk conc., kmol/m3	0.00064032
k_c, mass transfer coeff., m/s	6.53E-04
$C_m = (-r_A\ r_b Rn)/k_c C_{Ab} < 0.15$	1.52E-03

B.3 Internal mass transfer limitation

Weisz-Prater parameter was calculated for internal mass transfer limitation and the results are tabulated in Table B.2.

Table B.2: Internal mass transfer calculations

ρc, kg/m^3	R ,m	C_{As},kmol/m^3	De,m^2/s	rA, kmol/kg-s	C_{WP}
1200	0.0001	0.00064	3.29E-09	1.16E-08	0.066